STRUCTURAL IDENTIFICATION OF A FULL-SCALE TIED ARCH BRIDGE SPAN USING GENETIC ALGORITHMS

by

Neal Heber Salas Zamudio

A thesis submitted to the faculty of
The University of North Carolina at Charlotte
in partial fulfillment of the requirements
for the degree of Master of Science in
Civil Engineering

Charlotte

2016

Approved by:

Dr. Matthew J. Whelan

Dr. David C. Weggel

Dr. Brett Q. Tempest

ABSTRACT

NEAL HEBER SALAS ZAMUDIO. Structural identification of a full-scale tied arch bridge span using genetic algorithms. (Under the direction of DR. MATTHEW J. WHELAN)

Fostered by advancements in computational capabilities and the development of low-cost structural health monitoring systems, structural identification has emerged as a promising experimental technique offering contributions to several applications in performance-based civil engineering. Fundamentally, the methodology provides a framework for determining the mechanical properties of in-service civil structures by leveraging experimental measurements to update a physics-based model of the structure. Use of these calibrated high-fidelity finite elements models, and the parameters identified in the analysis, has been proposed for numerous applications in condition assessment, structural health monitoring, vibration-based damage detection, and other areas supporting decision-making support in infrastructure management. In this thesis, structural identification of a full-scale tied arch bridge span is performed using genetic algorithms to solve the optimization problem. The study leverages ambient vibration monitoring test data acquired by a wireless sensor network consisting of 48 accelerometers distributed across the tie girders of the span. Stochastic subspace state-space system identification is used to experimentally estimate a set of twenty mode shapes of the bridge with their undamped natural frequencies and damping ratios. An idealized finite element model of the span is developed to analytically predict these dynamic properties, and this idealized model is correlated to the measured response to indicate discrepancies. A parametric sensitivity analysis is then

performed to identify the most meaningful uncertain parameters within the finite element model for subsequent model updating. Optimization of the model correlation through tuning uncertain parameters is achieved by minimizing an objective function using a parallel implementation of the genetic algorithm capable of exploring large population sizes. In total, sixteen different scenarios of model updating using the genetic algorithm are explored to identify the effects of varying the number of modes included in the objective function as well as the number of uncertain parameters included in the model updating routine. The results indicate that the identified parameter assignments may be highly sensitive to these factors, especially the number of modes included in the objective function. The strongest model correlation is achieved using all 20 modes in the objective function and the largest number of uncertain parameters in the model. The improvement in model correlation relative to the idealized finite element model is presented to contribute a real-world case study to the field of structural identification.

DEDICATION

To my wife Anna and professor Dr. Whelan both of whom played a major role in my life.

ACKNOWLEDGMENTS

This thesis could not have been completed without the guidance, contribution, and support of many people including my faculty advisor, faculty professors, graduate student and fellow lab research assistant, and my wife. I would like to express my deep gratitude to my faculty advisor Dr. Matthew J. Whelan, whose devoted guidance, assistance, and patience led to a more comprehensive thesis. Dr. Whelan not only served as my advisor but he also served as my professor for multiple classes and as an inspiring role model whose passion for the structural engineering field inspired me to continue dedicated research efforts. His conceptual explanations, corrections, and valuable suggestions are greatly appreciated. I would also like to express my extended appreciation to Dr. David C. Weggel and Dr. Brett Q. Tempest for their revisions, and constructive feedback. I would also like to thank graduate student Timothy P. Kernicky, whose knowledge about MATLAB coding and Genetic Algorithms, helped me clarify multiple questions throughout the research process. Finally, I wish to thank my wife Anna B. Salas whose endless love, guidance, and support have greatly inspired me and encouraged me to continue learning and become a better engineer.

TABLE OF CONTENTS

LIST OF TABLES

LIST OF FIGURES

CHAPTER 1: INTRODUCTION

1.1 Introduction

The challenge of sustaining the current transportation infrastructure in the United States through replacing, rehabilitating, and maintaining bridges not only is costly but also requires the development of effective strategies to allocate financial resources to critical structures in the greatest need of repairs. Conventionally, quantitative feedback on the assessment and performance of in-service bridges has been provided by the visual inspection program. However, visual inspections are subjective and lack the ability to characterize deterioration that is not visible and might affect the bridge's overall performance. Among the vibration-based methods that have been proposed to complement visual inspections, structural identification has emerged as a promising technique for monitoring the structural health of civil structures. By calibrating a preliminary idealized finite element model, the in-service behavior of structures can be simulated and used within structural health monitoring and vibration-based damage detection routines to support decision-making. This thesis promotes and evaluates the implementation of structural identification by presenting a case study for a steel tied arch bridge using application of genetic algorithms with ambient vibration test data.

Bridges that are compromised by either natural or event-driven deterioration to

the extent that the load carrying capacity is reduced are referred to as structurally deficient bridges. Although structurally deficient bridges are still considered safe for operation, inspections need to be scheduled at least once a year until deficiencies have been corrected and, in many cases, load postings are introduced that negatively impact freight mobility. In the United States, over 600,000 bridges connect more than 4 million miles of public transportation (U.S. Department of Transportation, Federal Highway Administration and Federal Transit Administration, 2014). In 2013, the U.S. Federal Highway Administration (FHWA) rated over 10% of these bridges as structurally deficient, resulting in at least 60,000 structurally deficient bridges in the United States (FHWA, 2013). Moreover, the FHWA reported an estimated total replacement cost for these structurally deficient bridges of almost $52 billion in 2012 (FHWA, 2013). Rehabilitation of these structures as an alternative to replacement also presents a significant cost at an estimated $34 billion. The effect of this significant need, coupled with the inadequate funding and resources to address it, is reflected in the 2013 Report Card for America's Infrastructure issued by the American Society of Civil Engineers (ASCE), which provided the overall bridge system in the United States a C+ grade (ASCE, 2013). In addition to the current needs, an increasing number of structurally deficient bridges are estimated to reach the end of their expected service life within the next decade and will require additional resources to maintain, rehabilitate, and replace them. Figure 1 presents the age distribution of the current US bridges classified as structurally deficient, where the average age of a structurally deficient bridge is found to be 63 years (FHWA, 2013).

An increased interest in reducing bridge maintenance costs by improving needs-

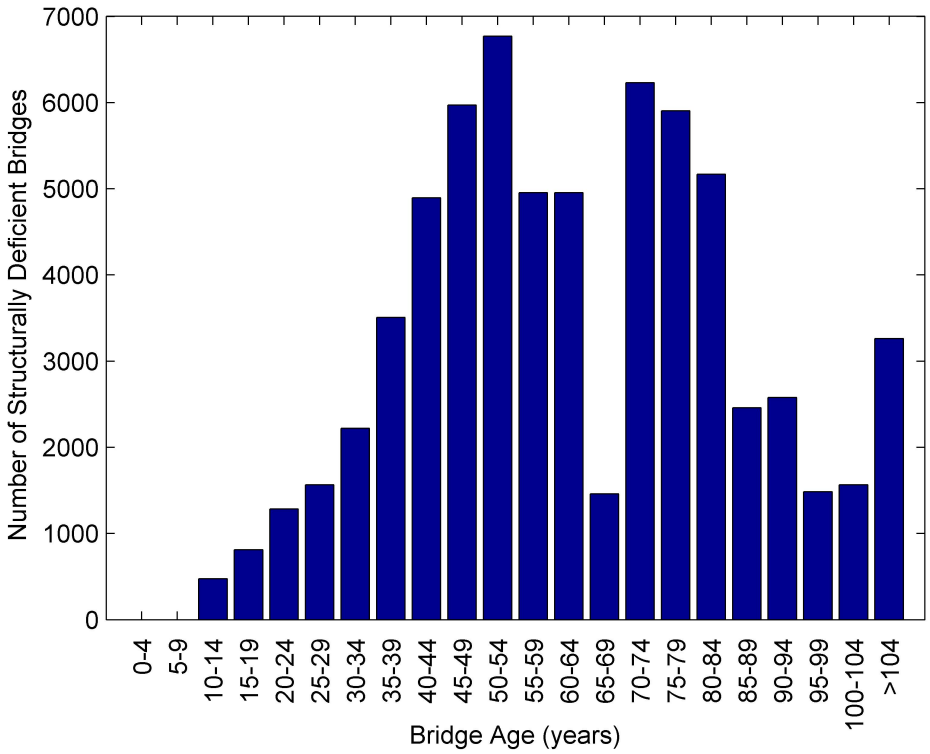

Figure 1: Age distribution of structurally deficient bridges in the United States

based scheduling of actions, as well as safely extending the service life of bridges, has encouraged the development of non-destructive methods for monitoring and assessing the health of bridges using sensor technologies. A variety of systems and approaches have been explored to address this need, although particularly active areas of research have been vibration-based methods for structural health monitoring and damage detection (Fritzen, 2005; Doebling et al., 1998). Vibration-based methods attribute changes in the dynamic behavior to structural damage although the dynamic properties of a structure can also be significantly affected by changes in temperature and humidity. Numerous vibration-based methods have been proposed using both data-driven and physics-based methods and can be classified by the capability of structural damage identification and quantification. Four levels of vibration-based

structural damage classification have been established (Rytter, 1993). Level 1 classification is simply identifying the presence of damage, while level 2 is associated with not only detecting damage but also localizing it. In level 3, the severity of damage is quantified in addition to detecting its locations. Lastly, in level 4, the remaining service life of a damaged structure is assessed in addition to all the capabilities of level 3. Vibration-based methods can also be further classified as data-driven or physics-based methods. Data-driven methods are based on a statistical approach to model the measured response and associating changes in the statistical properties of prediction errors from these models with structural damage. Although data-driven methods have been successful at localizing damage (Whelan and Janoyan, 2010), they lack the ability to quantify the severity of damage in direct engineering measures, such as stiffness, since they are constructed on statistical models. Consequently, physics-based methods that provide a theoretical basis for quantifying damage severity have emerged as a key area of structural health monitoring research. Physics-based methods rely on the utilization of mathematical models that are governed by the laws of physics and generally involve the development of a finite element model in order to perform structural identification of uncertain parameters within the model to evaluate the presence, location, and severity of damage. The approach attempts to correct parameters in an analytical model of the structure using experimental measurements of the structural behavior. When applied for condition assessment, the assignments of the corrected parameters are compared to baseline parameter assignments obtained by prior application of structural identification to gain insight into the health and performance of the structure. However, this technique remains relatively unproved in

real-world implementation and there are many technical challenges to effectively and reliably implementing it on large civil structures.

1.2 Overview of Research Effort

This thesis seeks to complement the growing database of full-scale case studies applying structural identification to bridges and the limited database of studies using genetic algorithms for global optimization of uncertain parameters in the model. Furthermore, by applying structural identification on numerous subsets of the experimental data and with different sets of uncertain parameters in the model, this study will explore the effects of decisions made in forming the optimization problem used to implement structural identification. Specifically, the effect of incrementing the number of uncertain parameters calibrated in the model, coupled with the effects of increasing the number of experimentally estimated natural frequencies and mode shapes incorporated in the objective function are examined. Consequently, the study provides insight into the richness of experimental modal parameter sets needed for reliable parameter identification and the performance of genetic algorithms in calibrating large finite element models with relatively large sets of uncertain parameters.

The various stages encompassing the structural identification framework are conceptually presented in Figure 2 and described in detail throughout this thesis as summarized in the following synopsis. The Marquette-Joliet Bridge, a 140.8m span steel tied arch bridge, for which ambient vibration monitoring test data was available from an in-service field monitoring effort, serves as the case study structure for this thesis. Using operational modal analysis, the experimental data was processed and fit to a

stochastic state-space model using the stochastic subspace state-space system identification algorithm. Strategies for extracting modal parameter estimates, including natural frequencies, damping ratios, and mode shapes, and approaches for averaging and verifying the plausibility of estimates are presented using the case study data. In parallel, an idealized finite element model was developed from the as-built bridge drawings using assumed material properties, boundary conditions, and element connectivity conditions. Modal analysis of the idealized finite element model was used to produce analytical modal parameter estimates for the structure and model correlation with the experimental modal parameter estimates was performed. Discrepancies between the experimental and analytical modal parameter estimates suggested inaccuracies in the model and particularly highlighted opportunities to correct torsional behavior in the model that was not in strong agreement with the experimental measurements.

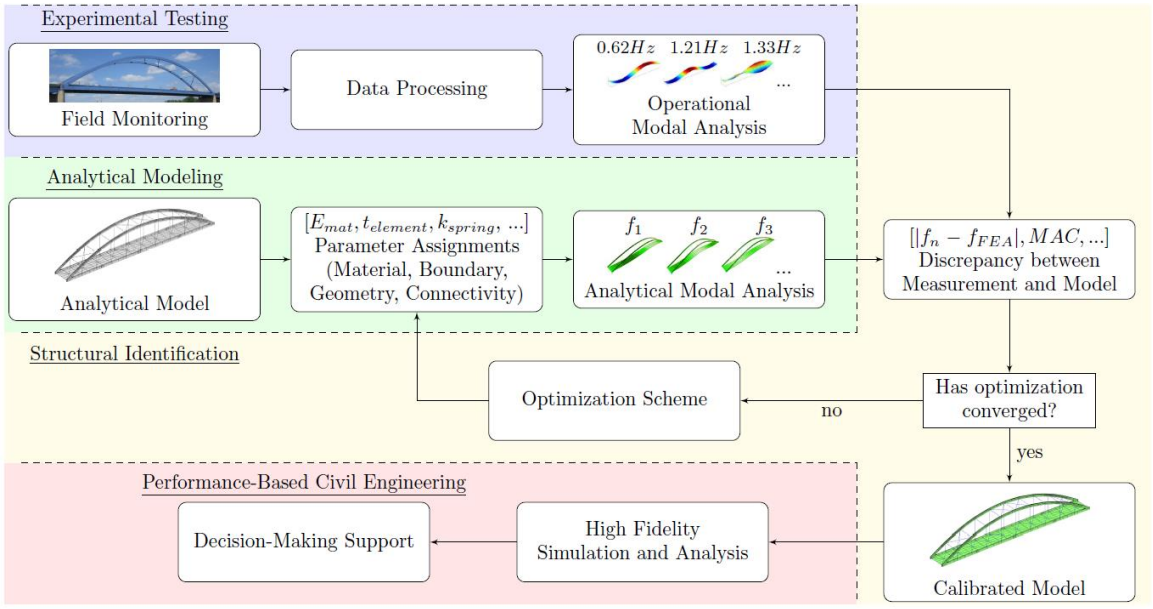

Figure 2: Schematic of the general structural identification process

Finite element model updating was performed using a genetic algorithm to optimize an objective function developed using the residuals between paired estimates of natural frequencies and residuals between paired mode shapes obtained from the model and measurements. A sensitivity analysis was first conducted to identify the set of parameters in the model that have the greatest impact on the natural frequencies of the lowest frequency modes in the model. Then, using sets of either the 3, 6, 9, or 12 uncertain parameters that the dynamic properties of the model are most sensitive to, the global optimization was performed to calibrate the model under different conditions. This calibration routine was repeated using sets of the first 5, 10, 15, or 20 experimentally measured modes to examine the effect of limited measurement data on the correlation between the calibrated model and experimental data as well as on the values of the uncertain parameters assigned to the calibrated models. An in-depth comparison between the experimental modal parameters and those of the calibrated model was performed to quantify the improvement in agreement produced by the optimization scheme to serve as a case study for structural identification on a full-scale bridge. In terms of the broader use of this technique, these high-fidelity finite element models can then be used to assess the performance of the structure, and ultimately the goal is to use such calibrated models to support decision-making related to maintenance actions.

1.3 Thesis Outline

A summary of each chapter of this thesis follows:

- Chapter 2 provides a literature review on the framework and challenges of struc-

tural identification as well as several case study applications. Three different optimization approaches used for calibrating finite element models with experimental vibration measurements are introduced and referenced for further exploration. The principles of global optimization using genetic algorithms and challenges associated with the implementation of this method on large models are discussed.

- Chapter 3 details the case study structure and the instrumentation used for ambient vibration testing. Operational modal analysis is explained and the vibration theory associated with the state-space representation used for data regression is described. Lastly, output-only system identification is performed using stochastic subspace identification for the extraction of experimental modal parameter estimates, including the natural frequencies, relative damping factors, and mode shapes.

- Chapter 4 introduces a preliminary, idealized finite element model of the case study structure and the results obtained from performing linear modal analysis of this idealized model. Comparison between idealized and experimental modal parameter estimates is presented using conventional measures for model correlation. The technique for parameterizing the analytical model for finite element model updating using a scripted routine is described. Lastly, a sensitivity analysis is presented to identify the most meaningful uncertain parameters within the FE model to be included in the model updating and establish their upper and lower bounds.

- Chapter 5 details the genetic algorithm used as well as the objective function constructed to distill the model correlation into a single function suitable for optimization. Results from the application of the genetic algorithm over 16 different case scenarios are summarized and compared. Furthermore, variability in the identified uncertain parameter assignments obtained from each scenario of structural identification is presented. Analysis of the modal parameters from the calibrated finite element model exhibiting the best correlation with the experimental data is provided to document the improvement in the model correlation with the experimentally measured response relative to the idealized finite element model for this real-world case study.

- Chapter 6 concludes with a summary of the contributions of the study as well as recommendations for future research.

CHAPTER 2: LITERATURE REVIEW

Driven by the desire to complement visual inspection routines currently used for condition assessment of large civil structures, structural identification has emerged as an active area of research in performance-based civil engineering by providing a framework to assess the in-service behavior of civil structures based on physical measurements. Defined as a state-of-the-art technique due to its complexity and the numerous approaches available, structural identification operates on the basis of calibrating and validating a preliminary idealized FE model to ensure consistency of the model predictions with the actual measured response. Such calibrated models can immediately serve within high-fidelity simulations and analyses used to support decision-making (E. Aktan, N. Çatbaş, A. Türer, and Z. Zhang, 1998). Furthermore, the process of calibrating the model, which identifies parameter assignments for structural elements within the model, may serve as a means for structural health monitoring and damage detection of in-service structures. The use of structural identification for this application has been particularly active as a research topic because it may address the increased demand for safely extending the service life of aging structures that have exceeded the life-cycle for which they were originally designed.

Structural identification is an applied technique that seeks to determine structural properties of civil structures by calibrating a representative idealized finite element model of the structure using experimental measurements. In this sense, structural

identification builds on FE model updating by emphasizing identification of structural properties from the model rather than seeking to simply improve the correlation of the model with experimental measurements. In the process of FE model updating used within structural identification, correlations between predictions from the physics-based model and the actual, measured in-service behavior of large civil structures, such as buildings and bridges, are improved through optimization techniques that seek to minimize the errors associated with modeling assumptions and uncertainties in material properties or geometries assigned in the model (Ribeiro et al., 2012). Structural identification has proven to be a powerful technique, although the challenges associated with its successful implementation have attracted numerous researchers. This state-of-the-art technique has opened up multiple areas of research, and its applications include vibration-based damage detection, structural health monitoring, and condition assessment of civil structures among others.

2.1 Overview of the Structural Identification Framework

The American Society of Civil Engineers (ASCE) Committee on Structural Identification of Constructed Systems identifies the application of structural identification as a six step process. Successful application involves defining the motivation to perform structural identification, development of a preliminary idealized FE model, acquiring experimental data on the system performance, data processing and interpretation of these measurements, calibration of the finite element model, and finally, utilization of the model for decision-support (ASCE SEI, 2011). As for the first step, there are many reasons that motivate the use of structural identification, including con-

struction quality control, identifying maintenance needs, and general assessment of complex structures. While the development of a high-fidelity FE model calibrated to experimental data can be used to verify modeling assumptions and predict static and dynamic behavior of the structure, extension of the model can be used to simulate the response of the structure to new occupational conditions or with structural modifications. Additionally, baseline dynamic properties of in-service structures can be used to monitor long-term performance to assess the operational health over the life-cycle.

Development of a preliminary idealized FE model is the second step within structural identification. If available, as-built drawings are usually used to accurately estimate and model geometric dimensions, member section properties, and connection details. This preliminary model is physics-based and is built by using engineering judgment to idealize the boundary conditions, connectivity (continuity) conditions, and material properties for each element. Commercial FE software packages can be used to develop the idealized FE model, and beam, plate, cable, and link elements are the most frequently used elements. The idealized model then serves as a baseline model and provides a way to validate the reasonableness of experimentally estimated modal parameters by comparing them to the analytical modal parameters extracted from the model using linear modal analysis. This baseline model is later formally calibrated to best match the measured response of the experimental structure within the process of identifying the uncertain structural parameters (Zhou et al., 2012).

The third step in structural identification encompasses instrumentation and vibration testing of the structure. Structural identification is most commonly based on

vibration measurements that are processed using system identification, which is the process of identifying and estimating the dynamic properties or modal parameters of a structure using experimental measurements. These modal parameters include the undamped natural frequencies, f_n, relative damping factors, ξ, and mode shapes, ϕ. There are two types of experimental measurements that are conventionally used to develop estimates of the dynamic properties of a structure. The first is the input force, or driving excitation, which is a measurement of the external dynamic forces that cause a structure to vibrate. The second type of measurement is the output response, which is a record of the dynamic response of the structure under the driving excitation and is typically acquired with distributed arrays of either accelerometers or velocity transducers. In experimental modal analysis (EMA), both the input and the output are measured in order to estimate modal parameters by performing regression on a mathematical model of the transfer function of the system (Ren et al., 2004). EMA is generally the preferred method for testing structures due to the advantages associated with controlled and measurable input. However, when testing large and complex civil structures, applying controlled input (by shaker, weights, etc) and suppressing ambient excitation is often impossible and strategies using only response measurements are applied within a technique known as operational modal analysis (OMA). The most common form of OMA is ambient vibration testing due to the low costs and convenience associated with in-service vibration monitoring, and its application includes structural health monitoring of large in-service civil structures under natural environmental and service loads (Wenzel and Pichler, 2005). In ambient vibration testing, the input force is not measured, although enough input

force is still required to physically perturb the structure in order to induce vibrations with adequate signal-to-noise ratio. Ambient excitation sources are provided by the surrounding environment, including high speed winds, traffic, pedestrians, ground motion, and waves (if applicable, as in the case of a pier) among other environmental loads, and while these excitation forces are difficult to accurately measure, they can often be assumed to be stochastic, or random, and broadband (Ren et al., 2004). Assumptions on the characteristics of these ambient excitations are then used to characterize the dynamic response of the structure and estimate the modal parameters using one or more output-only system identification techniques, such as frequency domain decomposition (Bendat and Piersol, 1993) or stochastic subspace state-space system identification (Peeters, 2000; Overschee and Moor, 1996).

Generally, distributed vibration measurements acquired at a limited number of sampling locations are used to record the output excitation in ambient vibration testing, and considerations about the duration of the tests, sensor placement, and measurement bandwidth are among the most important considerations for ensuring reliable and robust measurements (Whelan and Janoyan, 2009; Whelan et al., 2009). Single and dual-axis accelerometers are the most common types of accelerometers used during ambient vibration monitoring of bridges. Since traffic loading generally produces the most significant excitation during ambient vibration monitoring of a bridge, accelerometers are always oriented to measure vertical accelerations to capture transverse bending and torsional bending modes of the structure. In some studies, additional accelerometers are oriented in the transverse direction to measure lateral bending modes and to improve the identification of torsional modes. However,

longitudinal accelerometers are rarely employed in ambient vibration monitoring of bridges since accelerations in this direction are usually nominal.

Proper sensor placement on a structure plays an important role on the richness of the data set. Conventionally, accelerometers are distributed across the surface of the bridge deck due to ease of placement (Brownjohn et al., 2011; Wenzel and Pichler, 2005), although sensor placement is not restricted to the deck surface. In a study where OMA was performed on a concrete deck on steel girder bridge to assess the effects of sensor placement, ambient vibration monitoring was first performed using accelerometers placed on the concrete deck surface and then with the same number of accelerometers positioned on the steel girders (Whelan et al., 2011). It was concluded that placing accelerometers on the bridge deck limited the modal parameter estimation to only global bending modes, while placement of the accelerometers on the lower web of the girders resulted in richer datasets that additionally captured numerous well excited vibration modes associated with resonance of individual elements. It is also important to consider the density of the sensor network being employed during ambient vibration testing in order to anticipate spatial aliasing effects. Spatial aliasing refers to an effect produced by the experimental estimation of modes shapes at the limited number of discrete locations where the accelerometers are placed. Spatial aliasing results in the appearance of higher order bending mode shapes as similar in appearance to estimates of lower order mode shapes, which can lead to improper model correlation and challenges in correctly pairing experimental modes with analytical modes. Spatial aliasing can be anticipated by considering the highest order mode shape desired for reconstruction. In general, at least $n+1$ sensors should be

placed along the span of the bridge to reliably obtain an estimate of vertical bending modes up to the n-th order, while the grid must expand to include $n+1$ sensors across the width of the bridge to estimate torsional modes up to the n-th order (Whelan et al., 2011). In addition to sensor selection and placement, sampling rates and durations must be properly established to capture a sufficient frequency bandwidth with adequate frequency resolution and minimal spectral leakage. In ambient vibration monitoring, three minute sampling durations have been found to provide sufficient frequency resolution to perform operational modal analysis of highway bridges (Wenzel and Pichler, 2005). Sampling durations of over three minutes with an effective sampling rate of 128Sps were achieved with lossless data transmission during ambient vibration testing of an integral abutment highway bridge using a wireless sensor network (Whelan et al., 2009). This technological breakthrough established wireless sensing as a preferred alternative to cable-based instrumentation for ambient vibration monitoring due to the low-cost, ease of installation, and operation advantages offered by wireless sensors.

Following experimental testing of the structure, the fourth step identified by the ASCE Committee on Structural Identification of Constructed Systems is data processing and interpretation of measurements, which is the process of system identification when the monitoring is vibration-based. Before any data is processed, measurements need to be verified and checked for plausibility. Acceleration time histories and frequency spectra produced from the time histories are used to verify the plausibility of the measurements to detect and remove faulty sensors contributing inaccurate or corrupted data. Average normalized power spectral density (ANPSD) plots (Felber,

1993) can be used to assess the modal richness of the sampled data and identify likely resonance frequencies that are evident as clear peaks in the spectrum. Clear peaks with strong signal-to-noise ratios can then be used to verify the plausibility of the modal parameters obtained from system identification.

Among the many algorithms that have been developed for OMA, the two most widely used are the frequency-domain decomposition (FDD) method, also known as the peak picking (PP) method, and stochastic subspace identification (SSI), which is applied in time-domain. These two methods have gained extensive popularity in vibration-based structural health monitoring research due to their performance capabilities as well as the availability of software toolboxes that have facilitated the ease of their implementation for output-only system identification (Overschee and Moor, 1996). Although both the FDD and the SSI methods can be used for output-only system identification to extract modal parameter estimates of structures during ambient vibration testing, an important limitation of the FDD method is that it results in estimation of resonance frequencies and operational deflection shapes rather than true estimates of the undamped natural frequencies and mode shapes. However, since the FDD method is computationally swift and easy to apply, it can be used to complement the SSI method by validating estimates of natural frequencies and mode shapes yielded by SSI, provided that the damping ratios of the estimated modes are low and that the modes are not closely-spaced (Overschee and Moor, 1996). Peak picking techniques involve conversion of acceleration time histories to frequency domain plots (spectra) by using the Discrete Fourier Transform, followed by the selection of resonance frequencies associated with peaks in the average normalized power spectral

density. The frequency spectra are then used to determine the amplitude and relative phase angles with respect to a user-defined reference sensor to develop normalized operational deflection shapes. An operational deflection shape is defined as the actual deflection that the structure undergoes when excited at a resonance frequency by a pure sinusoidal force. These operational deflection shapes are not true estimates of mode shapes, but if the resonance frequencies are well spaced in the frequency spectrum, the operating deflection shapes closely approximate the mode shapes. However, when resonance frequencies are close to each other, the effect of modal superposition will be apparent in the operating deflection shapes, which renders the operational deflection shape an inaccurate estimate of the mode shape (Peeters, 2000).

Due to the previously described limitations of the FDD method, stochastic subspace identification is generally regarded as a more robust method for output-only system identification. SSI leads to estimates of the undamped natural frequencies, relative damping factors, and linear normal mode shapes of the structure. The method operates on the basis of fitting the measured data into a stochastic state-space model formed by casting the general equation of motion for linear time invariant structures with non-proportional or general damping into a recursive first-order differential equation. Eigenvalue decomposition of the state matrix of this model can then be used to extract estimates of the modal parameters, much in the way that this would be done for an analytical model. Additional details on the state-space representation and strategies for obtaining reliable modal parameter estimates using stabilization criteria and averages across different model orders will be covered in detail in Chapter 3. In several ambient vibration monitoring studies where operational modal analysis of

highway bridges were conducted, the SSI method has been shown to yield both more accurate and larger sets of modal parameter estimates than the FDD method (Whelan et al., 2009; Ren et al., 2004).

Following modal parameter estimation, the fifth step of structural identification involves the calibration of a preliminary idealized FE model through finite element model updating. The process of calibrating the FE model consists of selecting and modifying uncertain parameters within the model in order to achieve improved correlation between predictions produced by the model and the experimentally measured properties of the structure. This process of improving the model correlation to achieve the optimal parameter assignments is computationally challenging and much of the active research in the area of structural identification revolves around the use of optimization techniques to solve this problem. The most widely used uncertain parameters selected in model updating are the boundary condition restraints, connection rigidities, and material and section properties such as Young's modulus (E), axial stiffness (EA), and bending rigidity (EI) (E. Aktan, N. Çatbaş, A. Türer, and Z. Zhang, 1998; Ribeiro et al., 2012). An objective function is used in optimization schemes to aggregate the model correlation across all considered modes to describe the correlations as a single function that can be minimized. Different forms of objective functions have been formulated and used in the literature, although most incorporate some measure of the eigenvalue and eigenvector residuals between the experimental and analytical modal parameter estimates. One of the principal challenges of FE model updating is the computational time required to extract modal parameters from the parameterized analytical models. Since the objective function may be nonsmooth

and have local minima in addition to the globally optimal solution, the exploration of a large parameter search space with a large FE model can be time consuming. Furthermore, assuring the identification of the correct set of uncertain parameter assignments is difficult. One of the specific challenges explored within this thesis is the effect of the number of uncertain parameters and the number of modal parameters included in the objective function on the strength of the model correlation after FE model updating. Furthermore, the effect of these selections on the identified assignments for uncertain parameters in the calibrated model is also examined to investigate how data richness and choices made when implementing FE model updating affect the parameter identification. Since parameter identification is the primary objective of structural identification and since the results inform decision-making, the study of parameter variation and uncertainty is particularly important for advancing the practice of structural identification.

The final step identified by the ASCE Committee on Structural Identification of Constructed Systems is the assessment and decision-making that can be informed using the calibrated high fidelity FE model obtained and the values of the uncertain parameters identified. The following section includes summaries of several case study applications to illustrate the opportunities and challenges presented by the framework.

2.2 Approaches to Model Updating in Structural Identification

Within FE model updating, an idealized FE model is modified by assigning potential values within bounds to uncertain parameters like material and/or section properties within the FE model and assessing the correlation in the modal param-

eters between the measured and newly updated model by an objective function at each iteration. However, the calibrated model can lose its physical meaning due to idealization and discretization errors associated with the model that can not be corrected by the process of parameter identification. Idealization errors are introduced by inaccurate element selection, mass distribution, and mesh connectivity, while discretization errors are introduced by poor meshing, order reduction, and element convergence (Mottershead et al., 2011). Proper selection of uncertain parameters that can be corrected, followed by subsequent calibration of these parameters, results in a high fidelity calibrated FE model that can be used not only to predict the structural response due to new types of load cases and load combinations, but also use the values associated with the identified parameters to characterize material properties or performance of structural features described by the parameters.

An extensive list of case studies introducing numerous approaches utilized for structural identification of buildings and bridges can be found in ASCE SEI (2011). Among these approaches, heuristic or manual updating, sensitivity-based methods of optimization, and the use of genetic algorithms for global optimization will be discussed in the following sections. Each optimization approach presents unique challenges associated with achieving the optimal correlation between the model and experimental measurements as well as reliably identifying reasonable and accurate parameter assignments.

2.2.1 Heuristic Updating

Heuristic updating, also referred to as manual updating, is one of the most basic and oldest FE model updating approaches used for structural identification. This technique relies heavily on results from parametric analysis performed on uncertain parameters within the FE model to identify the most meaningful set of parameters and to approximate changes in the parameter assignments that will result in improved correlation between the analytical and measured modal parameter estimates. Calibration of the preliminary FE model is done by manually modifying parameter assignments one parameter at a time, performing modal analysis of the adjusted model to determine the change in model correlation, and iterating this process until satisfactory correlation is achieved. While heuristic updating is the simplest optimization scheme for model updating, the application can be very impractical and time consuming when updating several uncertain parameters in the model. Furthermore, manual approaches are prone to user errors since they require a significant amount of user interaction with the model. Most importantly, the iterations are very likely to converge on a local mimimum of the objective function rather than the global minimum due to the limited search space that can be covered by manual updating of the uncertain parameters. The correlation achieved in the updated model is largely dependent on the initial assumptions assigned to each uncertain parameters in the model. With advances in computational power, this approach has largely become outdated and, although it serves as a good introductory tool for model updating, it is not recommended for structural identification applications.

A heuristic model updating study was performed on an in-service steel-stringer highway bridge using vertical multireference impact testing data to calibrate a preliminary idealized three-dimensional finite element model of the structure. (E. Aktan, N. Çatbaş, A. Türer, and Z. Zhang, 1998). Uncertain parameters considered in the updating scheme included the rotational stiffnesses of the springs at the abutment, vertical stiffness of the springs at the bearing pads, and the flexural stiffness of link elements used to model the composite action between the concrete slab and steel girders among others. Multireference vertical impact testing was used to excite the bridge and accelerometers were used to measure the dynamic response for experimental modal analysis. Sixteen experimental modes were estimated from the test data and used for subsequent model correlation. Consequently, the manually calibrated model exhibited excellent correlations with the experimental data resulting in a minimum frequency error of less than 6% while the minimum modal assurance criteria (MAC) value was over 90%. Moreover, deformation of the bridge under a uniform load surface was simulated to verify plausibility and completeness of the calibrated FE model.

2.2.2 Sensitivity-Based Model Updating

The sensitivity-based model updating approach (Mottershead et al., 2011), also referred as the gradient-based method or sensitivity method, is an iterative FE model updating technique that has been extensively used for structural identification of large civil structures. This method is based on linearization, using a first order Taylor series expansion, of the commonly nonlinear relationship between the output response resid-

uals obtained by correlating the modal parameter estimates over a range of uncertain parameter fluctuations. Sensitivity-based updating approaches use gradient-based methods, such as the Newton-Raphson method, which establish a sensitivity matrix containing the eigenvalue and eigenvector derivatives with respect to changes in assignments of the uncertain parameters. This sensitivity matrix is used with the prediction errors in the model to iteratively inform the changes in parameter assignments as the optimization converges along a path. The greatest challenge associated with sensitivity-based methods is that the objective function is nonlinear and potentially nonsmooth over the search space. Consequently, sensitivity-based methods are highly prone to converging on a local minimum close to the initial guess assigned to the uncertain parameters (Adeli and Cheng, 1993; Bakir et al., 2007). Like the heuristic or manual updating approach, the quality of the correlation in the calibrated model and the identified parameter assignments often depends heavily on the accuracy of the engineering judgment used to assign the initial guesses for the parameter assignments. However, multiple parameters can be simultaneously and automatically calibrated, as opposed to the heuristic approach where the calibration of a large number of uncertain parameters becomes impractical. If the objective function is nonsmooth in the region where the sensitivity matrix is developed, the iterations in the optimization routine may become unstable. Another challenge associated with the use of the sensitivity method when calibrating numerous uncertain parameters is that it requires conditioning of the sensitivity matrix in order to ensure that the convergence of the objective function is not driven by a single uncertain parameter (Ahmadian et al., 1998). Another drawback of the sensitivity-based updating method is that more than

one local minimum may exist in the objective function, and the implementation of the method provides no information on how many might exist or if the global minimum was actually found.

Despite the limitations and challenges of sensitivity-based methods for model updating, it remains in widespread use for structural identification of bridges. In one study, structural identification of a concrete-filled steel tubular arch bridge was performed using sensitivity-based updating to calibrate a FE model of the span (Jaishi and Ren, 2005). Vibrations were induced during ambient vibration testing using a truck and the modal parameter estimates were obtained using the output-only system identification techniques of frequency domain decomposition and stochastic subspace state space system identification. The successful application of sensitivity-based model updating was attributed to the formulation of an objective function that aggregated contributions from the natural frequency residuals, a MAC relation function, and modal flexibility residuals. In another case study, structural identification was performed on a deteriorated reinforced concrete T-beam bridge using the sensitivity-based method to determine load rating factors to assess if the bridge could support loads from coal trucks (Zhou et al., 2012). An important extension of the sensitivity-based modeling updating technique is Modeling to Generate Alternatives (MGA). Zárate and Caicedo developed MGA as a way of exploring multiple local minima within the objective function and applied it to a cable-stayed bridge (Zárate and Caicedo, 2008). This approach, based on gradient information, searches for an initial solution by minimizing an objective function and then searches for other orthogonal solutions by minimizing a second objective function. This proposed method

provides multiple, alternative solutions to the model updating problem from which practitioner judgment is used to select the most plausible set of uncertain parameter assignments to use in the final calibrated model.

2.2.3 Genetic Algorithm

The genetic algorithm is a global optimization technique that is used to minimize a mathematical function. Genetic algorithm techniques rely on the Darwinian processes of evolution by natural selection by applying principles of survival of the fittest to individuals within a population to breed new generations of individuals that leverage the properties of the best parameter sets to encourage the convergence of the objective function on the optimal solution (Mitchell, 1996). An initial population is generated by randomly establishing assignments within lower and upper bounds for each uncertain parameter that is included in the optimization routine. Each combination of assignments for the uncertain parameters are referred to as an "individual" of the population and represent a potential solution of the system. The correctness of the solution is evaluated by the objective function to produce a scalar score for the model correlation. This score is called the fitness value of the individual and, at the end of each generation, the individuals are ranked in order according to their fitness values. Moreover, a percentage of the individuals with the best fitness scores, referred to as the "elite" set of individuals, are carried over into the subsequent population generated in a process known as survival. This ensures that the current best solution is retained and that each generation results in a best individual that is at least as good as the prior generation. In addition to the process of survival of the elites, new pop-

ulations at each generation are created using cross-over reproduction and mutation. Reproduction by cross-over is used to exchange characteristics (genetic information) between non-elite and elite parent individuals to produce intermediate points between these individuals in order to refine the search around the region of the current elites. Mutation is a way of introducing random parameter assignments into the population in order to diversify exploration of the search space. This encourages the optimization routine to keep searching for the global minimum, rather than quickly converging on a local minimum (Sivanandam and Deepa, 2007). The iterative process of evaluating and reproducing generations is performed until the objective function converges or until other stopping criteria are reached.

The genetic algorithm has been shown to be an effective optimization tool across a large number of industries (Jones et al., 1995; Dyer et al., 2012). Consequent to this success, many software packages for optimization support the implementation of genetic algorithms, including the widely utilized MATLAB computing environment (MathWorks, Inc., 2015). However, the use of genetic algorithms to solve the FE model updating problem within structural identification has been limited to a select number of studies and, furthermore, only a limited number of full-scale bridge case studies exist. A particularly relevant full-scale study of finite element model updating using genetic algorithms was performed on a bowstring-arch railway bridge (Ribeiro et al., 2012). This study used 24 experimentally measured modes in the objective function to calibrate 15 uncertain parameters in a finite element model of the structure. Moreover, four different initial populations within the genetic algorithm routine were randomly generated to explore the stability of the calibrated parameters with

respect to their bounds and identify the variability in the correlations between the experimentally measured model parameters and those predicted by the calibrated models. In all four cases, it was found that both the natural frequencies and the modes shapes experienced very little variability with errors associated with the frequencies of less than 5% and consistent MAC values greater than 85% respectively, with the exception of only one mode that exhibited a range of MAC values between 82% and 86%. Additionally, variability in parameter assignments for each parameter was explored by calculating the ratio of parameter assignments relative to their lower and upper bounds. In all four implementations of the genetic algorithm, ratios between assignments for each parameter were within less than 22%, while ratios less than or equal to 10% were exhibited for six of these parameters. An interesting aspect of this study was that the numerical model was validated by an ultrasonic testing program that independently determined the modulus of elasticity of the concrete as well as a dynamic test performed with railway traffic.

In addition to the use for structural identification of healthy structures, genetic algorithms have also been implemented for detecting and localizing damage in structures. In one of the earliest studies, damage was simulated in a FE model of a steel cantilever beam discretized into fifteen elements and a genetic algorithm was used to localize damage through model updating (Friswell et al., 1998). Damage was modeled as a reduction of the elastic modulus of individual elements while the elastic modulus of each element were treated as uncertain parameters in the model updating. Four damage scenarios were tested. First, the stiffness of an element located close to the free end condition was reduced. In the second scenario, the stiffness of an element

located near the fixed end condition was reduced, while in the third scenario simultaneous reductions in stiffness were introduced to both elements. Lastly, a systematic error was introduced to the model by introducing an additional mass at a given node such that the synthetic measurements were no longer exactly consistent with the underlying model used in the damage detection routine. For all scenarios, properties of the genetic algorithm remained the same including use of a population size of 10 individuals, a reproduction rate of 60%, and a mutation rate of 0.5%. The objective function that was minimized incorporated both natural frequencies and mode shapes residuals, but higher weighting was applied to the residuals between experimental and analytical natural frequencies due to the expectation of better measurement certainty and greater sensitivity to damage for the natural frequencies relative to the mode shapes. The implementation of the genetic algorithm for each scenario in this study concluded in successful damage detection and localization. Although it's common practice to set the mutation rate constant during the optimization of the objective function, one study exploring the use of genetic algorithms for damage detection proposed adaptively setting the mutation rate based on a diversity measurement (Zimmerman et al., 1999). In this study, a low mutation probability was suggested in early generations since the initially randomly distributed individuals are relatively diverse and mutation operations are likely to eliminate the benefits that are gained by crossover. However, as the elite solutions converge in later generations, higher degrees of mutation would be needed in order to ensure that the algorithm continues to sufficiently search over the entire solution space to avoid converging on a local minimum.

Experimental application of genetic algorithms for damage detection was presented in a study where damage was introduced to a one-span steel portal frame in the form of saw cuts (Hao and Xia, 2002). Scenarios of increasing damage, representing section width reduction of 10, 20, 30, and 40%, were introduced at four different locations. This study also evaluated the use of three different objective functions for determining the presence and location of damage. The first objective function incorporated only natural frequency residuals, the second objective function incorporated only mode shape residuals, and the third objective function incorporated weighted residuals from both. It was concluded that neither the first nor the second objective function formulations were able to reliably detect damage at the four locations and resulted in false positive indications of damage at undamaged locations. However, the objective function incorporating both weighted residuals from the natural frequencies and mode shapes successfully located the damage introduced at the four expected locations without misidentifying additional damage throughout the rest of the structure. Moreover, the assignment of the weighting factors applied to the residuals was found to have a significant effect on the damage detection routine. This effect was tested by exploring four mode shape residual weighting factor assignments, 10, 1.0, 0.1, and 0.001, while the residual natural frequency factor was fixed to one for all cases. It was determined that correct identification of damage at the four damaged locations was achieved only when the relative residual mode shape factor was assigned as 0.1. Principles from these foundational analytical and laboratory studies has since been applied successfully on full-scale building components subjected to damage in experiments (Kernicky et al., 2014).

2.3 Challenges Implementing Genetic Algorithm on Large Models

Challenges associated with the implementation of genetic algorithms on large FE models include the selection of several properties of the genetic algorithm that directly affect its performance in effectively exploring the search space and the speed of convergence of the objective function. Properties of the genetic algorithm include the population size, the elite survival rate, the number of generations, the reproduction rate, and the mutation rate, among several other properties associated with variations of the genetic algorithm that are beyond the scope of work of this thesis. However, reference to several variations of genetic algorithms along with their properties can be found in (Pandey et al., 2014; Chambers, 1995). The population size should reflect a fairly wide coverage of the search space which is dependent on the width of the bounds for each uncertain parameter and how many uncertain parameters are calibrated in the optimization scheme. While a population size that is too small may result in premature convergence of the objective function at a local minimum, a population size that is too large will slow down the speed of convergence. Similarly, use of a high percentage of the population for the survival of the elites can result in ineffective exploration of the search space as the elite dominance will reduce the diversity of the population and lead to premature convergence on a local minimum of the objective function. However, use of too low of a percentage of the population for elite survival will result in increased convergence time and require additional generations to arrive at the optimal solution. Likewise, while the rate of mutation used must be large enough to add diversity to encourage exploration of new regions of the search space

in order to avoid convergence on a local minimum, using a mutation rate too high will counteract the benefits acquired by cross-over reproduction (Zimmerman et al., 1999). Lastly, the number of generations evaluated, if used as the stopping criteria, also affects the performance of the genetic algorithm. It is important that enough generations are included in the optimization of the objective function and that convergence of the objective function has been reached before the genetic algorithm is ended. While all of these properties affect the performance of the genetic algorithm, they are problem dependent and require tuning at the early stages of the optimization routine (McCall, 2005).

Computationally, a challenge associated with the implementation of the genetic algorithm for model updating of large FE models is that it requires significant computational time to evaluate large population sizes over numerous generations for an effective coverage of the search space. However, genetic algorithms are highly-parallelizable since the individuals in each population can be evaluated by independent computational cores (Cantú-Paz, 2001). This allows the computational workload to be distributed among several computing cores in order to reduce the computational time of convergence of the objective function. Details on the parallel implementation of the genetic algorithm used in this thesis to perform model updating can be found in Whelan et al. (2016).

This thesis focuses primarily on an additional set of challenges within model updating that focus specifically on the richness of the data used and decisions made when selecting uncertain parameters in the model. Since an objective function is used within the genetic algorithm routine to aggregate all of the correlations between

the experimental measurements and the analytical model, properties of the objective function, such as the number of paired modes that are included in the objective function affect the performance of the genetic algorithm. Likewise, the number of uncertain parameters used increases the flexibility of the model to adjust to the measured data, but also increases the size of the search space which renders the optimization more challenging. Currently, published guidance on the number of modes suitable for an objective function developed with experimental data from a full-scale structure and the selection of uncertain parameters has not been developed. This thesis seeks to provide insight into developing an empirical formulation of such guidance as well as explores challenges associated with the variability of the calibrated uncertain parameters resulting from varying the number of modes and the number of uncertain parameters used in the objective function.

CHAPTER 3: VIBRATION TESTING AND SYSTEM IDENTIFICATION

Operational modal analysis performed on an in-service steel tied arch bridge is presented in this chapter. Details on the case study structure monitored under ambient vibration excitation and the instrumentation used for this field testing are described. Stochastic subspace state-space algorithms for output-only system identification and the theory behind operational modal analysis are reviewed and then applied to the experimental data set. Techniques for estimating the modal parameters of the structure, namely the natural frequencies, relative damping factors, and mode shapes are presented, including strategies to arrive at a final parameter set to use for structural identification. Within this process, an average normalized power spectral density (ANPSD) plot is produced from the experimental data to characterize the dynamic response of the Marquette-Joliet Bridge and verify the plausibility of the modal parameter estimates.

3.1 Details of Structure

The Marquette-Joliet Bridge, shown in Figure 3, is an in-service bridge located over the Mississippi River on U.S. Highway 18 that accommodates one lane of highway traffic in each direction and connects the States of Iowa and Wisconsin. This steel tied arch bridge was built in 1974 and was later recognized in 1976 with "the most beautiful bridge" award in the long span category by The American Institute of Steel

Construction (AISC).

Figure 3: Steel tied arch bridge serving as case study structure

The main span of the bridge is a simply supported span that is 140.8m in length. The primary superstructure components of the span are built-up steel arch ribs and built-up tie girders that are supported by rocker bearings at the western pier and fixed shoe bearings at the eastern pier. The tie girders are hollow rectangular sections, formed by welded plate steel, that are connected to one another by a system of floor beams and diagonal braces (Figure 4). The floor beams are built-up I-shaped sections that support five W24x55 steel stringers (not shown in the figure) that span longitudinally between adjacent floor beams and support a 20.3cm thick reinforced concrete deck slab. The bottom diagonal braces are WT7x39 sections that are connected at the ends and the midspan of the floor beams. Loads from the tie girder are shed to each arch rib by nine pairs of steel strand cable hangers that are evenly spaced along the span of the bridge. The arch ribs are also hollow rectangular sections formed by welded plate steel. Lateral bracing provided between the arch ribs consists of built-up rectangular sections used for both the top laterals and the top diagonal

braces. Lateral bracing members are provided at the same longitudinal spacing as the bridge hangers. Diagonal bracing of the arch ribs is provided at the two central panels of the arch rib framing plan as well as at the second panel from each end.

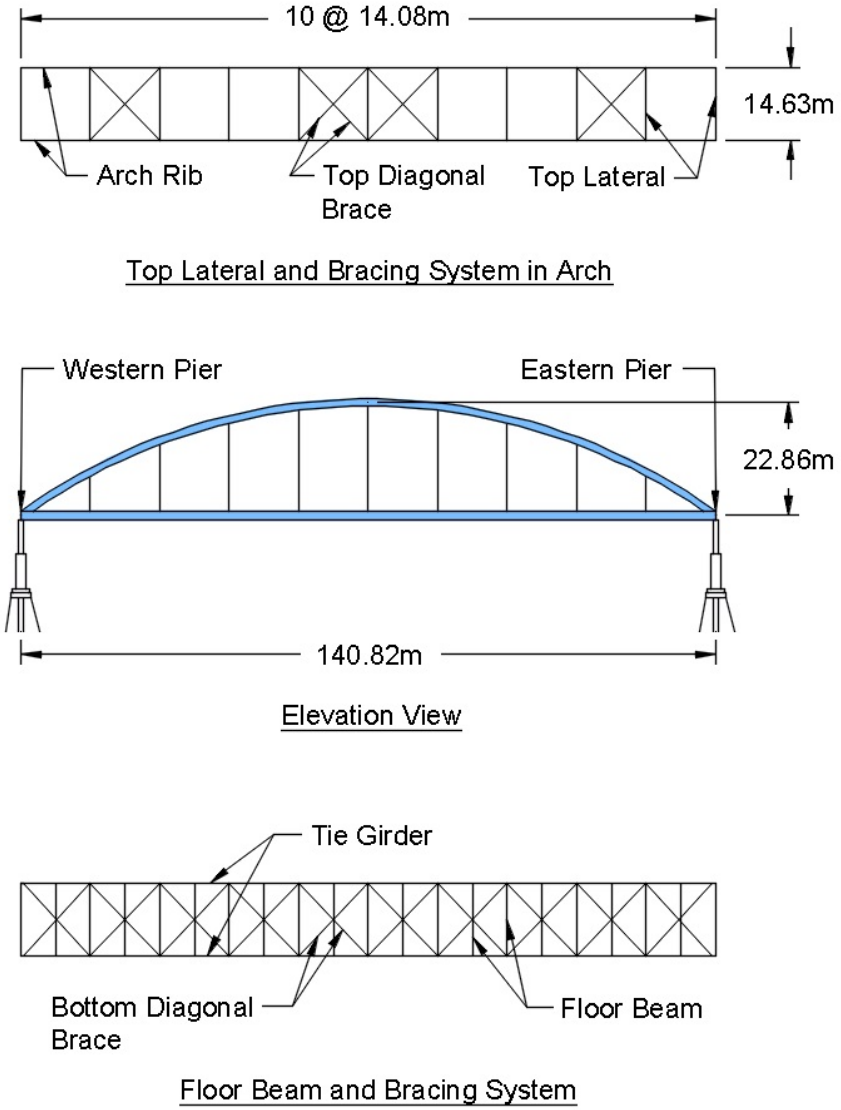

Figure 4: Details of case study structure: a) Plan view of arch framing plan; b) Elevation view of span: c) Plan view of tie girder framing plan.

Plate sections forming both the arch ribs and the tie girders are stiffened for out-of-plane deformations by transverse diaphragm plates. All stiffeners are interior diaphragm plates that match the inside dimensions of the girders for bearing at the top

and bottom flanges, while diaphragm plates in the tie girder were fabricated with an opening at the center that is large enough to allow inspection within the girders. Each arch rib is stiffened by 1.91cm thick transverse diaphragm plates along the interior of the rib girders at 28 different locations. Diaphragm stiffeners are placed on each side of the hanger assembly inside the arch rib, at the midspan between adjacent hanger assemblies, and halfway between the knuckle and the closest hanger. Diaphragm stiffeners of the same size are also provided throughout the span of each tie girder at 21 locations in a similar layout to that used in the arch ribs. A single 3.81cm thick bearing plate stiffener is also provided in the tie girders over the bearing supports.

3.2 Instrumentation for Ambient Vibration Monitoring

A customized wireless sensor network was developed by researchers at the University of North Carolina at Charlotte specifically to facilitate wireless real-time ambient vibration monitoring of moderately long span bridges, such as the tied arch instrumented in this study (Whelan, 2011). Six wireless data acquisition modules, which each permit simultaneous acquisition from 8 accelerometers, were used in the test program, thereby resulting in a total of 48 accelerometers distributed across the tie girders of the structure to record the dynamic response under ambient excitation. These modules were designed to achieve wireless real-time sampling measurements with low-noise, high resolution, and an ability to maintain continuous and lossless time synchronized sampling across the sensor network for at least 3 minutes (Whelan and Janoyan, 2009). In order to meet the sampling demands for operational modal analysis, the Texas Instruments ADS1178 was selected as the analog-to-digital con-

verter (ADC) within the modules. This device employs multiple 16-bit ADCs and allows for synchronous sampling from up to 8 channels at rates of up to 10kHz in the low-speed operating mode used, which consumes only 6mW/channel (Texas Instruments Incorporated, 2008). Its on-chip finite impulse response (FIR) digital low pass filter provides for anti-alias rejection, has a linear phase response, and is designed with a passband ripple of +/- 0.005dB and a stop band attenuation of 100dB. The computational core of each wireless sensor is a system-on-chip TI CC2530 wireless microcontroller and transceiver. Its radio frequency (RF) transceiver provides wireless communication within the 2.4GHz frequency range at data transfer rates of up to 256kbps. The microcontroller implements a radio transmission protocol developed in Whelan and Janoyan (2009) to achieve real-time data acquisition with no data loss. Additional features of the TI CC2530 tranceiver and microcontroller can be found in (Texas Instruments Incorporated, 2011).

The experimental test program interfaced Measurement Specialties, Inc. model 4000A accelerometers to the wireless sensor nodes to acquire the ambient vibration measurements. These accelerometers are relatively small in size and weigh only 7 grams each, which permitted application of a small amount of wax adhesive to temporarily adhere them to the tie girders during the testing. The wax adhesive also contributed to a fast and efficient placement process without compromising the measurement sensitivity of the sensor or leaving permanent alterations on the girders. The specifications of the model 4000A accelerometers include a sensitivity of 1000mV/g, full-scale dynamic range of +/- 2g, frequency bandwidth of 0-200Hz and a spectral noise floor of $35\mu g/\sqrt{Hz}$ (Measurement Specialties, Inc., 2010).

Real-time ambient vibration monitoring of the case study structure was performed by installing an array of 48 accelerometers along the two tie girders of the bridge at 24 uniformly spaced locations. To facilitate biaxial measurements, sensors were installed in pairs with one measuring vertical accelerations and the other measuring lateral accelerations. Longitudinal accelerations are typically small in magnitude and are generally not used to develop modal parameter estimates for highway bridges, so no sensors were positioned to measure longitudinal motion in the test program. The placement, orientation, and channel numbering of the accelerometers used within the specific ambient vibration monitoring program (to construct the modal parameter estimates developed in this research) are presented in Figure 5. In the channel numbering scheme, odd-numbered sensors correspond to those measuring vertical accelerations, which were oriented such that positive accelerations are in the direction opposite to gravitational acceleration, as indicated in Figure 6. Even-numbered sensors measured the lateral dynamic response of the tie girders and were all oriented in the same direction for consistency.

Monitoring of the structure was performed under ambient excitation provided by regular traffic serviced by the bridge and environmental loads. During this monitoring program, time windows of approximately three minutes were sampled at an effective sampling rate of 173.6Hz. The post-processing of measurement data described in this thesis used a subset of four of these windowed time histories that were each lossless and provided a generally strong amplitude of response.

As expected, vertical accelerations were larger in magnitude than the lateral ones due to direction of dynamic loading provided by the traffic excitation. However, sig-

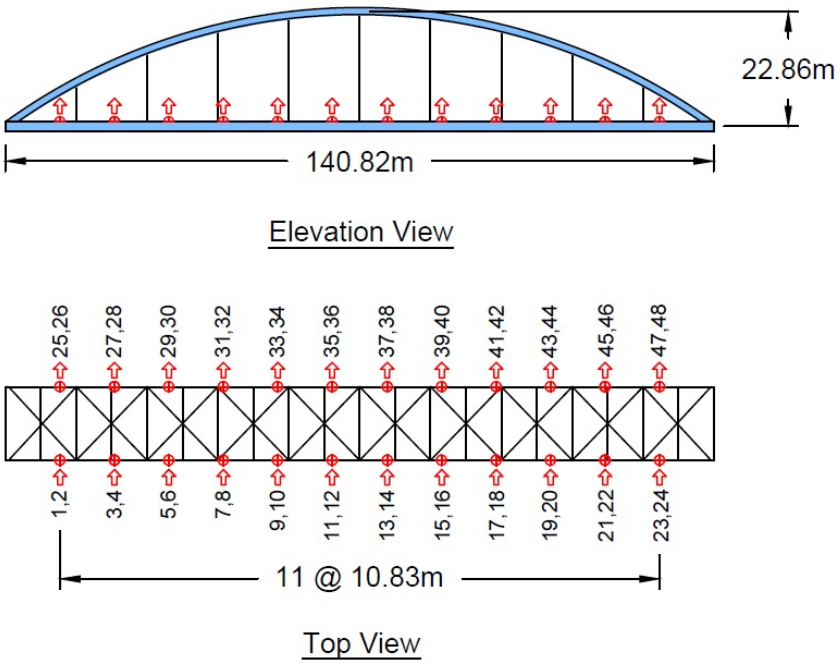

Figure 5: Distribution and orientation of accelerometers installed along the tie girders

Figure 6: Wireless sensor network powered by an external battery (left). Proximity of accelerometer to the top inner edge of the tie girders (middle). Accelerometers oriented to measure vertical and lateral accelerations (right).

nificant lateral accelerations were induced through torsional modes that were excited by the traffic loads. In addition to the time history analysis, an average normalized power spectral density (ANPSD) plot was developed to assess the modal richness of the measurements and, later, was used to verify the plausibility of modal parameter estimates (Figure 7). Clear peaks within the ANPSD indicate likely resonances asso-

ciated with well excited and well measured modes. An ANPSD plot can be produced by first computing a power spectrum estimate for each individual sensor, normalizing the individual power spectrum to a peak amplitude of one, and then averaging all of the normalized power spectrum estimates. By establishing the y-axis of the ANPSD as a logarithmic scale, resonance peaks are often more pronounced and easily identified. The ANPSD plot was produced within the MATLAB environment by first computing Welch's power spectral density estimates through the 'pwelch' function and using the Hamming window to reduce spectral leakage. Then, estimates were normalized and finally averaged over the 48 sensor channels and four recorded data sets.

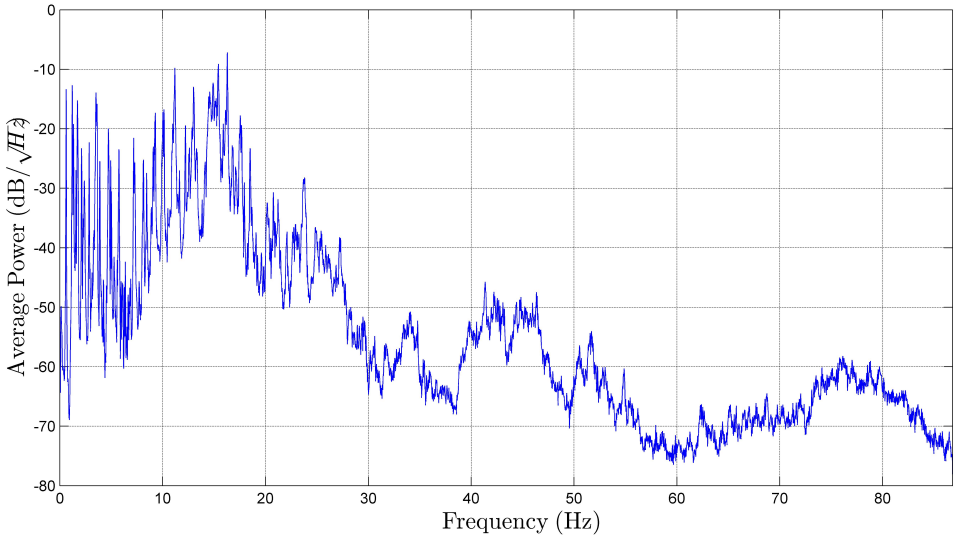

Figure 7: Full 0-86.8Hz bandwidth average normalized power spectral density

The ANPSD plot revealed a large set of resonance frequencies below 10Hz that suggested that at least 20 modes were well excited within this low frequency portion of the measurement bandwidth (Figure 8). Consequently, the measurement data

was filtered and downsampled during the system identification routine to emphasize analysis of this windowed frequency bandwidth. This downsampling approach aids in the system identification both in terms of estimation quality and computational requirements. However, it is important to establish the downsampling rate using the ANPSD to ensure a large enough set of modal parameter estimates to enable the subsequent structural identification research.

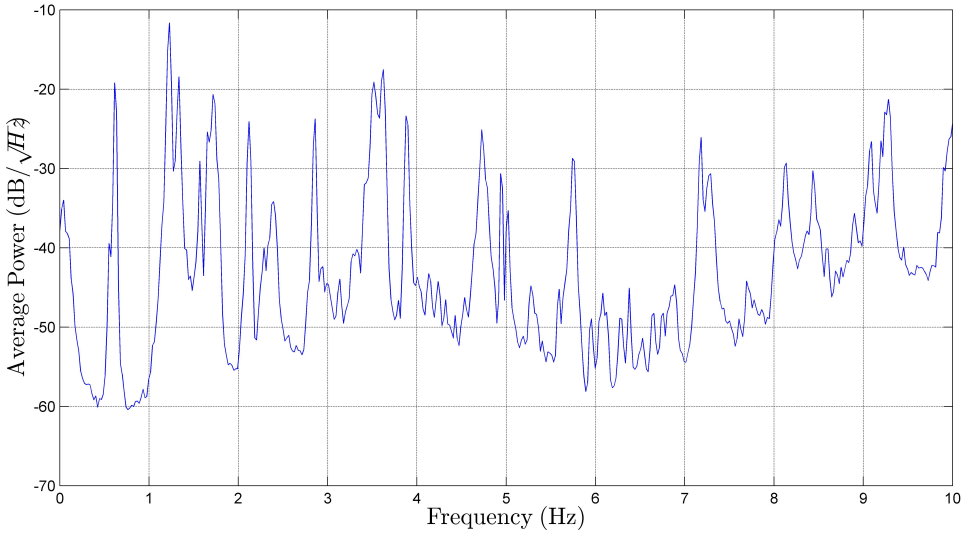

Figure 8: Average normalized power spectral density within 0-10Hz bandwidth

3.3 Operational Modal Analysis

Among the many algorithms that have been developed for structural identification, the SPICE V2.0 toolbox for MATLAB developed by Katholieke Universiteit Leuven (Overschee and Moor, 1996) provides two algorithms for operational modal analysis: frequency-domain decomposition and stochastic subspace state-space system identification (N4SID). However, frequency-domain decomposition does not perform well with closely spaced modes, provides fewer modal parameter estimates than

N4SID, and produces operational deflection shapes rather than proper mode shape estimates (Whelan et al., 2009). Consequently, SPICE V2.0 was only used to fit the experimental data to a stochastic state-space model and then to subsequently extract the experimental estimates of the modal parameters from this model.

As previously discussed during presentation of the ANPSD, a significant number of well excited modes were identified in each data set within the 0-10 Hz bandwidth to provide a sufficient number of experimental modal parameter estimates to facilitate structural identification. In order to improve the quality and speed of obtaining the experimental modal parameters, the four data sets were first pre-processed by deleting faulty sensor channels, detrending the data, and decimating data to a lower effective sampling rate. Due to the unreliable operation of accelerometers #3 and #22 during the ambient vibration monitoring test program, sensor channels #3 and #22 were deleted from each data set. However, interpolation between adjacent sensors to the ones that were not functioning permitted for presentation of generally smooth mode shape estimates. Detrending the sensor measurements ensures that any linear trend in the form of noise introduced by the data acquisition system and not from the actual acceleration measurements is eliminated prior to the system identification. Each data set was decimated by a factor of eight, thereby reducing the original sampling frequency from 173.6 Hz to an effective sampling rate of 21.7 Hz. This step provides the downsampling of the measured data and eliminates unnecessary spectral content above the bandwidth of interest that is associated with extra computational operations and memory requirements within the stochastic subspace algorithm. The effective sampling rate developed by the decimation routine permits for estimation of

modal parameters within the 0-10Hz frequency bandwidth.

3.3.1 State Space Representation

SPICE V2.0 was used to fit the measurement data to a stochastic state-space model constructed from the general equation of motion for linear time invariant structures with non-proportional, or general damping (Overschee and Moor, 1996). The continuous time form of the general equation of motion is a second-order ordinary differential equation (ODE) of the form

$$M\ddot{x}(t) + C\dot{x}(t) + Kx(t) = u(t) \tag{1}$$

where M, C, and K are the mass, damping, and stiffness matrices of a multiple degree of freedom system and $\ddot{x}(t)$, $\dot{x}(t)$, and $x(t)$ are the acceleration, velocity, and displacement vectors at time t. The excitation force vector is $u(t)$ and it can be expressed as an input function defined by location, orientation, and magnitude of the exciting forces. The idea of the state-space model is to cast a second-order ODE into a first-order ODE to solve for the modal properties of the system (Peeters, 2000). A new set of variables, called state variables, are defined by equating z_1 and z_2 to the displacement and velocity vectors respectively, as shown below in Equation 2 for a single degree of freedom (SDOF) system.

$$z(t) = \begin{Bmatrix} z_1(t) \\ \\ z_2(t) \end{Bmatrix} = \begin{Bmatrix} x(t) \\ \\ \dot{x}(t) \end{Bmatrix} \tag{2}$$

In addition, a new set of equations are formed by taking the derivatives of the state

variables and performing substitutions.

$$\dot{z}(t) = \begin{Bmatrix} \dot{z_1}(t) \\ \\ \dot{z_2}(t) \end{Bmatrix} = \begin{Bmatrix} \dot{x}(t) \\ \\ \ddot{x}(t) \end{Bmatrix} \tag{3}$$

$$\dot{z}(t) = \begin{Bmatrix} \dot{x}(t) \\ \\ -\frac{C}{M}\dot{x}(t) - \frac{K}{M}x(t) + \frac{u(t)}{M} \end{Bmatrix} = \begin{Bmatrix} z_2(t) \\ \\ -\frac{C}{M}z_2(t) - \frac{K}{M}z_1(t) + \frac{u(t)}{M} \end{Bmatrix} \tag{4}$$

Following this transformation, a first-order ODE referred to as the state equation is formed as

$$\dot{z}(t) = \begin{bmatrix} 0 & I \\ \\ -\frac{K}{M} & -\frac{C}{M} \end{bmatrix} \begin{Bmatrix} z_1(t) \\ \\ z_2(t) \end{Bmatrix} + \begin{Bmatrix} 0 \\ \\ \frac{I}{M} \end{Bmatrix} u(t) \tag{5}$$

where I is the identity matrix. Alternatively, the state equation can be expressed in matrix form as

$$\dot{z}(t) = \bar{A}z(t) + \bar{B}u(t) \tag{6}$$

where $\bar{A}$ is the state matrix and represents the dynamic properties of the system, as it contains the mass, damping, and stiffness matrices, and $\bar{B}$ is the input matrix that is associated with the excitation of the system.

For a multiple (n) degree of freedom system, $\bar{A}$ and $\bar{B}$ become

$$\bar{A} = \begin{bmatrix} 0_{nxn} & I_{nxn} \\ \\ -M^{-1}K & -M^{-1}C \end{bmatrix}; \bar{B} = \begin{Bmatrix} 0_{nxn} \\ \\ M^{-1} \end{Bmatrix} \tag{7}$$

Note that the eigenvalue decomposition of the state matrix contains the complex eigenvalues of the system that can be used to solve for the natural frequencies and relative damping factors of the structure. Likewise the eigenvectors of the structure are produced by eigenvalue decomposition of the state matrix. However, the eigenvalue

decomposition of the state matrix does not produce the eigenvectors of the system in the physical degrees of freedom, but rather in the coordinates of the state variables. In order to convert the eigenvectors to physical coordinates, a transformation equation of the form

$$\phi = \bar{C}\psi \tag{8}$$

is used. In this equation, ϕ is the eigenvector of the system in the physical coordinates (observed mode shapes), $\bar{C}$ is the output matrix that transforms the state variables to the desired degrees of freedom in the model, and ψ is the eigenvector of the system in the coordinates of the state variables (Peeters, 2000).

By converting to discrete-time, in order to accommodate the non-continuous sampling of measurement data, the state and observation equations can be approximated by

$$z_{k+1} = Az_k + Bu_k \tag{9}$$

$$y_k = Cz_k + Du_k \tag{10}$$

The developed model is purely deterministic as no random terms have been included to account for noise and error in the state-space model. A combined deterministic-stochastic state-space model can be obtained by introducing stochastic process noise and measurement noise (Peeters, 2000). In data-based applications, these sources of noise originate from measurement noise, unmeasured excitations, and computational noise. By accounting for these types of uncertainties and random errors, Equations 9 and 10 become

$$z_{k+1} = Az_k + Bu_k + w_k \tag{11}$$

$$y_k = Cz_k + Du_k + v_k \tag{12}$$

where w_k and v_k are the corresponding process and measurement noise. However, in most civil engineering applications of system identification, ambient excitation techniques are used since the application and measurement of controlled excitation can become costly, difficult, and time consuming. Within ambient vibration monitoring, input forces that develop from sources such as wind, ground motion, vehicular traffic, etc are assumed to be modeled with the same characteristics as the random noise. By considering the input forces to be part of the noise, the combined deterministic-stochastic state space model then becomes the stochastic state-space model

$$z_{k+1} = Az_k + w_k \tag{13}$$

$$y_k = Cz_k + v_k \tag{14}$$

where only the output (acceleration measurements) and noise are considered in the state-space model. The stochastic subspace state-space system identification routines use measurements data to construct estimates of the state matrix, A, and output matrix, C, associated with the underlying physical structure. As previously described, these two matrices can be used to estimate the natural frequencies, relative damping factors, and mode shapes of the structure through eigenvalue decomposition and transformation.

3.3.2 Application to Experimental Data

The SPICE V2.0 MATLAB toolbox was used to fit the measurement data to the stochastic subspace state-space model using the algorithm proposed by Van Overschee

and De Moor (Overschee and Moor, 1996). This system identification algorithm was implemented over each of the four data sets. However, the application of output-only system identification for the estimation of reliable modal parameter estimates is challenging and requires several strategies to ensure consistency and confidence in the final estimates. This is particularly important when the modal parameter estimates are to be used for structural identification. The following subsection details the process and strategies used to obtain reliable modal parameter estimates.

In application of the system identification routine, every channel was selected to serve as a reference channel, and the expected experience parameter, which defines the number of block rows in the Hankel matrix, was set as high as possible given the length of the measurement data. These decisions encourage the extraction of a large set of modal parameter estimates. One challenge encountered when performing system identification to estimate the state matrix and output matrix is that the size of these matrices, known as the model order, is unknown. By specifying too small of a size, the algorithm will produce less modal parameter estimates than present in the data and may not adequately separate closely spaced modes. Specifying a model order too high will cause the algorithm to overfit the noise and potentially corrupt the modal parameter estimates. To address this challenge, the system identification is performed over a range of model orders to determine the estimates by the way of stabilization criteria. A stabilization plot was generated for each data set in order to select sets of modal parameter estimates from stable poles.

Stabilization criteria of a 1% variation in frequency, 5% variation in relative damping, and 1% variation in mode shape were specified to identify stable poles. Stable

poles indicate model fitting where all stabilization criteria is satisfied and are represented by a "+" symbol in Figure 9. Poles represented by the "f" symbol indicate stable natural frequency estimates, while poles represented by the "d" symbol indicate both stable natural frequency estimates and stable damping estimates, and poles represented by the "v" symbol" indicate stable natural frequency estimates and mode shape estimates. In order to average uncertainties in the individual modal parameter estimates, five stable poles were selected for each potential mode shape by selecting estimates from groups of stable poles aligned vertically. The undamped natural frequency along with the relative damping factor and the mode shape were extracted for each stable pole that was selected.

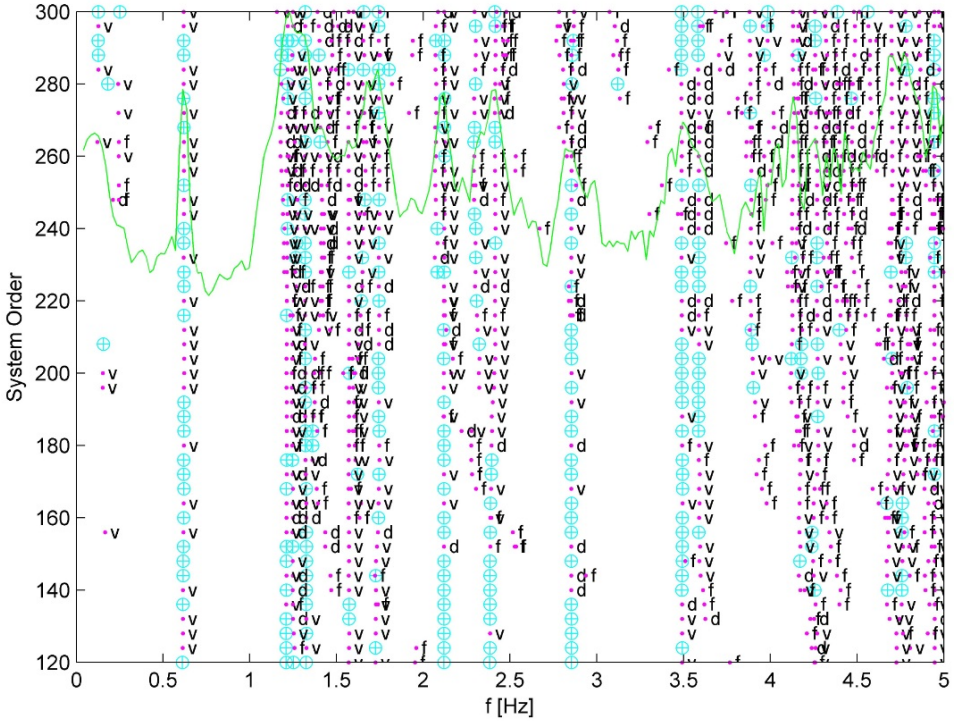

Figure 9: A typical stabilization plot

Since the underlying state-space model is based on non-proportional or general damping, the mode shapes are complex with a real part and an imaginary part.

The real part is the relative amplitude of the mode shape at the measured degree of freedom, and the imaginary part is the relative phase. Since the mode shapes are ultimately used for model updating of a finite element model that yields real-valued mode shape estimates, these complex modes needed to be transformed to real-valued normal modes to permit correlations with the finite element model. The complex mode shape estimates, ϕ_c, were converted to normalized undamped (real-valued) mode shape estimates, ϕ_r, using Niedbal's transformation (Niedbal, 1984), given by

$$\phi_r = Re(\phi_c) + Im(\phi_c)[Re(\phi_c)^T Re(\phi_c)]^{-1} Re(\phi_c)^T Im(\phi_c) \tag{15}$$

where $Re(\phi_c)$ is the real component of the complex mode shape and $Im(\phi_c)$ is the imaginary component of the complex mode shape.

A strategy for reducing uncertainties in the modal parameter estimates by averaging multiple estimates across the multiple data sets was employed to improve the reliability of the experimental modal parameters. As previously mentioned, five stable poles were selected for all potential natural frequencies identified by the system identification routine where there were more than four stable poles aligned vertically. These groups of natural frequency estimates along with their corresponding relative damping factor and real-valued mode shape estimates, were collected in separate tabs of a spreadsheet file established to database the individual experimental modal parameter estimates. Consistent natural frequency estimates obtained from applying the system identification routine to the four different data sets were added along with their relative damping factor and mode shape estimates to the same sheet within the spreadsheet database. By collecting repeated as well as unique sets of modal

parameter estimates across the four data sets, each sheet of the spreadsheet database consisted of anywhere from five estimates of the same potential mode shape, if it was expressed in only one data set, to as many as 20 estimates, if it was consistently expressed in all four time histories. This approach has the advantage of capturing modal parameters that were excited in only one of the data sets, which may occur if the mode is not well excited by typical traffic loads.

Prior to averaging the individual modal parameter estimates, the consistency of the estimates within each tab was assessed using the Modal Assurance Criterion (MAC). Additionally, each real-valued mode shape estimate was first normalized to a reference mode using the Modal Scale Factor (MSF). This scalar value was calculated for each individual mode shape estimate relative to the reference mode shape and was applied to all the mode shape estimates within each sheet in order to ensure that the relative amplitudes of the mode shape estimates were consistent to avoid potential biasing of individual estimates during averaging. The MSF also ensures consistent direction, or phase of the mode shapes. The modal scale factor is computed as

$$MSF_{cdr} = \frac{\{\phi_{dr}\}^H \{\phi_{cr}\}}{\{\phi_{dr}\}^H \{\phi_{dr}\}} \tag{16}$$

where ϕ_{dr} is the reference real-valued eigenvector to which the real-valued eigenvector subject to normalization ϕ_{cr} is compared to. Once all mode shapes were normalized, the MAC value for each normalized eigenvector was calculated using

$$MAC_{cdr} = \frac{\left|\{\phi_{dr}\}^H \{\phi_{cr}\}\right|^2}{\{\phi_{dr}\}^H \{\phi_{dr}\} \{\phi_{cr}\}^H \{\phi_{cr}\}} \tag{17}$$

where again ϕ_{dr} and ϕ_{cr} are different real-valued eigenvectors (Allemang, 2003). The

MAC serves to assess the consistency between mode shapes and assigns a scalar value that ranges between 0 and 1 (or 0% and 100%). MAC values that approach 1 (or 100%) indicate high levels of mutual consistency between estimates while MAC values that approach 0 (or 0%) indicate no correlation between the mode shape estimates. In this case study, MAC values between 0.70 to 1.00 were considered to be associated with consistent estimates of the same mode shape and were grouped together for averaging. Any estimates yielding a MAC value less than 0.70 were either eliminated from further consideration or explored as a potential unique mode shape estimate if additional estimates were found to be consistent with the mode shape. Natural frequencies, damping factors, and modes shapes associated with the groups of modal parameter estimates yielding MAC values greater than or equal to 0.70 were averaged together to minimize the effects of noise and uncertainty when yielding a single estimate for each mode.

In total, 47 candidate natural frequencies, ranging from 0.6186Hz to 9.3099Hz, were initially extracted through the stabilization plots and then averaged, as shown in Table 1. Due to the parameter estimation and consistency check strategies used, the number of estimates n that were included in the average for each final modal parameter estimate varied. While the calculation of some final modal parameter estimates included 20 estimates in the averaging, only 3 estimates were averaged in other cases. Additionally, the standard deviation σ was calculated to indicate the variance in the undamped natural frequencies that were averaged. Both the number of estimates included in the averaging and the standard deviation of the natural frequency averages serve as a measure of the overall confidence in the individual

modal parameter estimates.

Table 1: Averaging properties of the initial set of modal parameter estimates from system identification routine

#	f_n (Hz)	n	σ (Hz)	MAC* (%)	#	f_n (Hz)	n	σ (Hz)	MAC* (%)
1	0.6186	20	0.00255	99.99	25	4.9486	20	0.00731	98.50
2	1.2123	20	0.00604	99.25	26	5.0176	10	0.00379	99.30
3	1.2376	5	0.00084	99.25	27	5.2682	15	0.00567	98.31
4	1.3277	15	0.00638	99.14	28	5.3002	5	0.00467	99.08
5	1.3570	4	0.00274	99.61	29	5.5855	5	0.00034	99.92
6	1.5118	4	0.00632	98.63	30	5.7451	20	0.01667	99.85
7	1.5706	15	0.00247	95.03	31	6.0753	20	0.01028	94.37
8	1.6439	5	0.00749	95.97	32	6.2844	10	0.01195	96.26
9	1.7266	20	0.01410	99.73	33	6.3858	9	0.00230	98.32
10	1.8328	5	0.09563	90.65	34	6.7442	5	0.00623	97.93
11	2.1167	15	0.00785	99.61	35	7.1759	20	0.00650	98.26
12	2.2971	5	0.00433	99.94	36	7.2462	5	0.00611	87.29
13	2.3538	10	0.00447	99.67	37	7.2812	10	0.00528	93.04
14	2.4141	5	0.00153	99.97	38	7.7184	5	0.00614	96.85
15	2.8512	15	0.00317	99.84	39	8.1143	15	0.01149	99.02
16	3.4844	16	0.01679	99.65	40	8.4402	10	0.00920	89.53
17	3.5699	13	0.00710	87.04	41	8.8253	5	0.00716	96.24
18	3.6238	5	0.00148	99.97	42	8.8834	3	0.01060	93.00
19	3.8744	11	0.00830	88.34	43	8.9790	5	0.00623	98.14
20	4.1737	5	0.00773	91.81	44	9.0592	14	0.00557	96.16
21	4.2527	10	0.01252	94.30	45	9.2163	5	0.00728	99.80
22	4.7045	10	0.00846	99.77	46	9.2671	16	0.01162	99.25
23	4.7378	5	0.00082	100.00	47	9.3099	5	0.01675	99.17
24	4.7846	5	0.00314	99.96	-	-	-	-	-

Since the ultimate use of the developed modal parameter estimates was to direct structural identification of a model of the structure using finite element model updating, it was necessary that the final set of modal parameter estimates included only those estimates that expressed the highest confidence. Including an incorrect mode in the model updating could jeopardize the convergence of the optimal solution and physical meaning of the updated model. In the selection of the final set of modal parameter estimates, the objective was to select the set of 20 modes that provided the highest level of confidence. This was achieved by superimposing averaged natural frequency estimates obtained from the system identification routine on the 0-10Hz bandwidth ANPSD plot and comparing the modal parameter estimates with resonance frequencies, as shown in Figure 10.

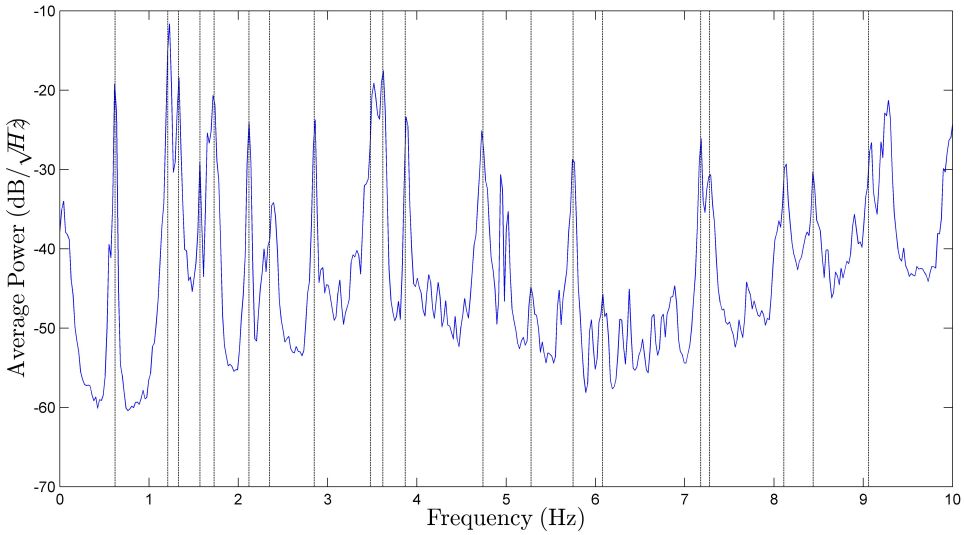

Figure 10: Average normalized power spectral density with the natural frequencies of the final set of modal parameter estimates identified

Modal parameter estimates without a corresponding clear resonance frequency in the ANPSD were excluded from the final set as they were considered to be unreliable estimates. On the contrary, modal parameter estimates that were associated with strong amplitude peaks in the ANPSD were considered to have the highest confidence level and were included in the final set of 20 modes. In addition, several instances of modal parameter estimates that had closely spaced natural frequencies and similar mode shapes were found. These estimates were averaged to yield a single modal parameter estimate when justified. Use of an initial finite element model of the structure, described in Chapter 4, was used to assist in assessing the likelihood of closely spaced modes with similar shapes. This was the case for two groups of closely spaced mode estimates. The first group consisted of the original modal parameter estimates #22, #23, and #24, while the second group consisted of the original modal parameter estimates #27 and #28. The similarities in estimated natural frequencies

and mode shapes, as well as the result of the averaging, are shown in Figure 11. The averaging characteristics of the final set of 20 modes ultimately used in the subsequent structural identification research are provided in Table 2.

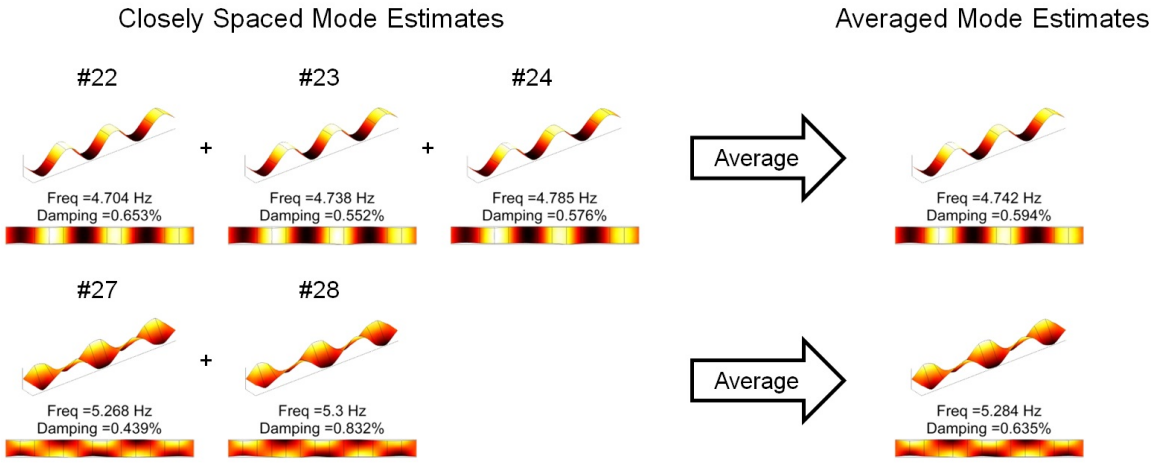

Figure 11: Averaged closely spaced modal parameters

Table 2: Averaging properties of the final set of modal parameter estimates used in study

f_n (Hz)	n	σ (Hz)	MAC* (%)
0.6186	20	0.00255	99.99
1.2123	20	0.00604	99.25
1.3277	15	0.00638	99.14
1.5706	15	0.00247	95.03
1.7266	20	0.01410	99.73
2.1167	15	0.00785	99.61
2.3538	10	0.00447	99.67
2.8512	15	0.00317	99.84
3.4844	16	0.01679	99.65
3.6238	5	0.00148	99.97
3.8744	11	0.00830	88.34
4.7423	10	0.0041	99.91
5.2842	15	0.0052	98.70
5.7451	20	0.01667	99.85
6.0753	20	0.01028	94.37
7.1759	20	0.00650	98.26
7.2812	13	0.00528	93.04
8.1143	15	0.01149	99.02
8.4402	10	0.00920	89.53
9.0592	14	0.00557	96.16

Renderings of the experimental mode shape estimates were developed using the MATLAB environment. The final set of 20 mode shapes along with their undamped natural frequencies and relative damping factors are presented in Figure 12. However, since sensor placement was limited to only the tie girders, the arches of the bridge were necessarily omitted from the renderings of the modes shapes. Consequently, modes that might look like repeated mode shapes (such as the modes at 1.328Hz and 1.571Hz) are likely distinguished by different responses in the arch ribs, which is not permitted to be identified by the sensor placement used. As previously noted, this was confirmed through use of an initial finite element model, described in Chapter 4. As expected by the nature of excitation provided by traffic, the developed mode shapes are either transverse bending modes or torsional modes, and there are no lateral bending modes in the extracted modal parameter estimates. The first mode shape is the expected fundamental mode shape of the structure and it occurs at a frequency of 0.619Hz. Second-order through eighth-order transverse bending mode shapes can also be identified, as well as numerous torsional bending modes. Relative damping factor estimates are provided along with each mode shape and indicate that the structure is lightly damped as the estimated relative damping ranges from 0.095% to 2.722% across the modal parameter estimates.

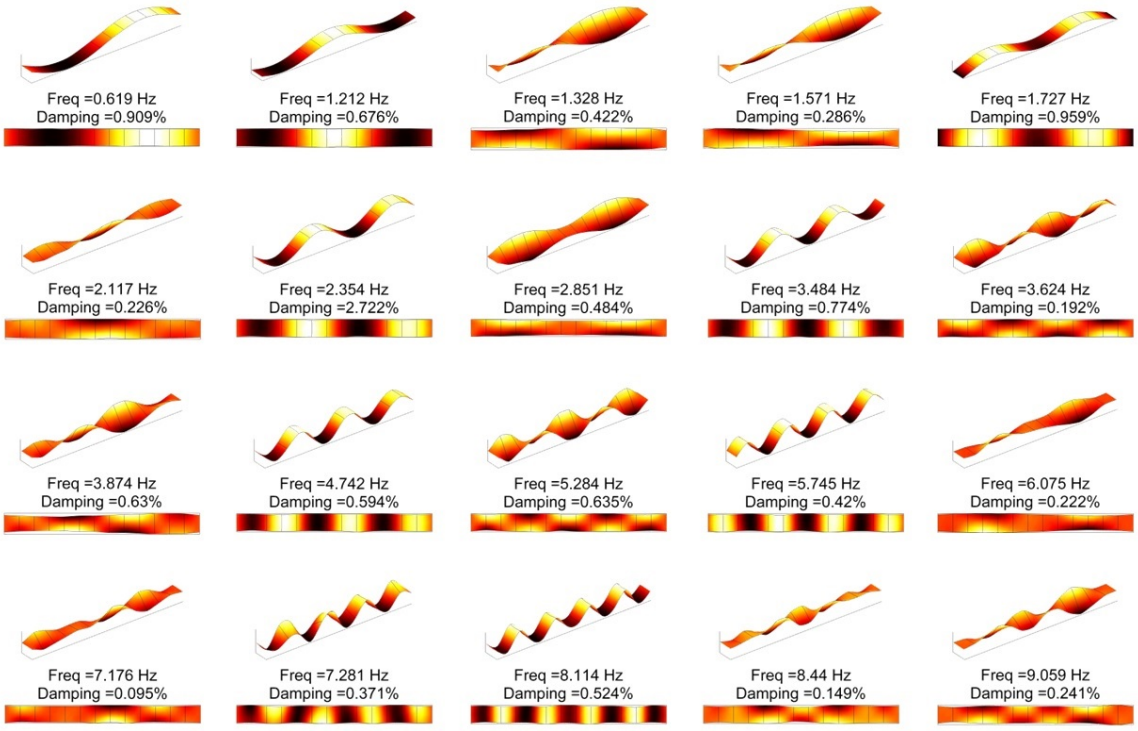

Figure 12: Final subset of 20 experimental modal parameter estimates obtained through operational modal analysis

CHAPTER 4: FINITE ELEMENT MODEL AND PARAMETERIZATION

In this chapter, a preliminary, idealized finite element (FE) model of the case study structure is described and the dynamic properties of the model are compared to the modal parameter estimates obtained from the operational modal analysis. The strategy for parameterization of the FE model to facilitate research on best practices for structural identification is presented with the techniques used for decomposition and reconstruction of the mass and stiffness matrices for the parameterized model. A sensitivity analysis of the analytical model is conducted across 19 candidate uncertain parameters to identify the most meaningful properties of the model affecting the modal properties and, consequently, the overall correlation with the field measurements. Ultimately, a subset of the 12 most significant uncertain parameters for the structural identification of the model is selected for the research effort.

4.1 Idealized FE Model

While structural identification provides a technique for improving model correlation through updating of uncertain parameters in the model, an idealized finite element model is typically first constructed and assessed to verify the plausibility of the modeling assumptions and serve as a benchmark for comparing the impact of the structural identification on the model correlation. In this study, an idealized three-dimensional linear elastic FE model of the tied arch bridge was developed within

the SAP2000 v15 commercial finite element analysis software (Figure 13). This FE model was developed using a total of 5,510 shell elements, 1,410 frame elements, and 18 cable elements. Four-node quadrilateral shell elements were used to model the arch ribs, the stiffeners, and the deck slab. Four-node quadrilateral shell elements were also predominantly used to model the tie girders, although some three-node triangular shell elements were used to mesh features around the knuckles of the arch. Moreover, three-node triangular shell elements were used along the bearing lines of the tie girders at the piers to discretize the area around the boundary conditions and knuckle of the arch. All shell elements in the model were thick-plate shell elements, which include transverse shear deformations (Mindlin/Reissner formulation). Frame elements were used to model the floor beams, stringers, the bottom diagonal braces within the bridge superstructure as well as the top laterals and diagonal braces of the arch. Lastly, cable elements, were used to model the stranded bridge cables serving as hangers in the tied arch. However, since the modal properties of the model are computed by linear elastic analysis, these cable elements are treated the same as pin connected frame elements in forming the stiffness and mass matrices. In total, the idealized three-dimensional FE model was composed of 6,938 elements and 4,603 nodes, which contributed 26,610 equilibrium equations and 850,125 non-zero terms to the stiffness matrix.

Boundary conditions, material properties, and connectivity between elements within the model were initially established using engineering judgment. Rocker bearings at the western pier were idealized by placing a line of roller restraints at the bottom nodes of the tie girder where the bearing was located. This restraint restricted vertical and

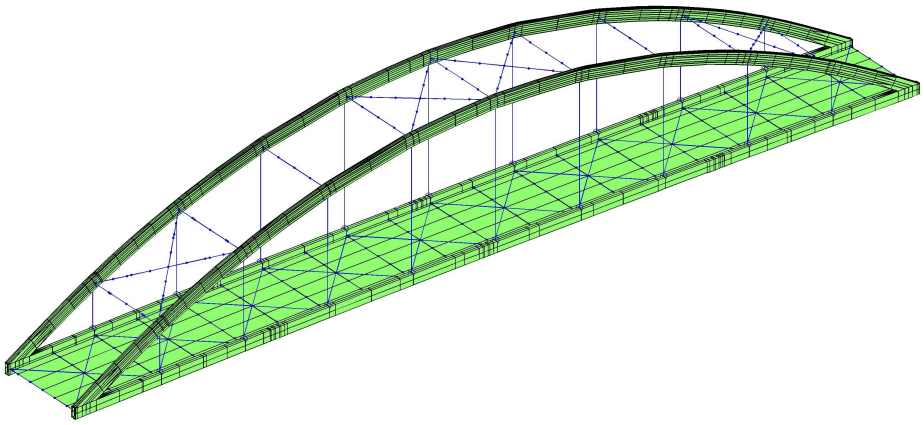

Figure 13: FE model of the tied arch bridge serving as the case study structure

lateral motion, but allowed for longitudinal translation as well as rotation about any axis. In the same manner, fixed shoe bearings at the eastern piers were idealized by introducing pin restraints along each bearing line, restricting local translation in all directions and permitting free rotation. The reinforced concrete of the slab was assumed to be normal weight and, consequently, the modulus of elasticity and unit weight for the shell elements representing the slab and parapets were assigned as 25GPa (3626ksi) and 2400kg/m^3 (150pcf), respectively. Lastly, connectivity between the floor beams and tie girders, arch laterals and ribs, and arch diagonal braces and ribs were idealized as fully restrained moment connections.

4.2 Correlation Between Idealized Model and Experimental Modal Parameter Estimates

Modal analysis of the idealized FE model was performed within the MATLAB environment through eigenvalue decomposition to extract the undamped natural frequencies and modes shapes of the model. The mass and stiffness matrices were first assembled in SAP2000 and then exported to MATLAB along with the geometry of the

idealized FE model. This approach permits for a more efficiently way of computing the eigenvalue decomposition of the model and, more importantly, allows for mode matching of the analytical modes with the experimentally measured modes, direct and automated assessment of the correlation between analytical and experimental modal parameters, and plotting of the idealized mode shapes, all within the MATLAB computing environment. While many approaches have been proposed to pair analytical and experimental modes, the modal assurance criteria (MAC) (Allemang, 2003) was determined to be adequate for this case study. In the matching process used in this study, the selection of potential analytical modes correlating with each experimental mode was first limited to only those analytical modes with a natural frequency, f_a, within +/- 25% of the measured natural frequency, f_e. This requirement that the natural frequencies of the paired modes are similar addresses potential issues in mode pairing arising from spatial aliasing on the limited instrumentation layout. Within this windowed search region, each experimental mode was paired with an analytical mode exhibiting strong MAC correlation with the experimental mode. However, to avoid selection of repeated analytical modes, the experimental modes were required to be paired with a unique analytical mode. Generally, experimental modes were paired with analytical modes that exhibited the highest MAC correlation. However, in cases where the analytical mode exhibiting the highest MAC correlation was already selected for another mode, the analytical mode exhibiting the second highest MAC correlation was selected.

All 20 experimental modal parameter estimates were paired to a unique analytical mode from the idealized finite element model and the results are presented in Figures

14 and 15. Model correlation between the experimental and analytical models was characterized using the percent error between natural frequencies (Δ), given by

$$\Delta = \left(\frac{f_a - f_e}{f_e}\right) \times 100 \tag{18}$$

where f_a and f_e are the corresponding predicted and measured undamped natural frequencies of the same paired mode. Besides the percent error between natural frequencies, model correlation was further characterized using the MAC value computed across all experimental and analytical mode shapes (Table 3). Discrepancies between the measured natural frequencies and those produced by the idealized model ranged from -5.54% to 18.6%, with an average absolute percent error of 7.52% (Table 3). In general, the mode shapes from the idealized model were well correlated to the experimental estimates as MAC values ranged from 34.69% to 99.95% and the average MAC was 80.26%. Upon closer inspection of the model correlation, it was observed that the idealized model exhibits consistently stronger agreement with the measured vertical bending modes than the torsional modes. Specifically, the average MAC correlation across the vertical bending modes is 93.12%, while the average MAC correlation across the torsional modes is 69.74%. Likewise, the average absolute percent frequency error between vertical bending modes is 4.81% while for the torsional modes the average absolute percent frequency error is 9.74%. However, much stronger model correlation, especially for the torsional modes, is sought in this research through the implementation of structural identification using Genetic Algorithms (GA). Overall, generally strong agreement between the model and the experimental estimate is indicated by an average MAC correlation across the modes shapes above 80% and an

average absolute percent error in natural frequencies below 8%.

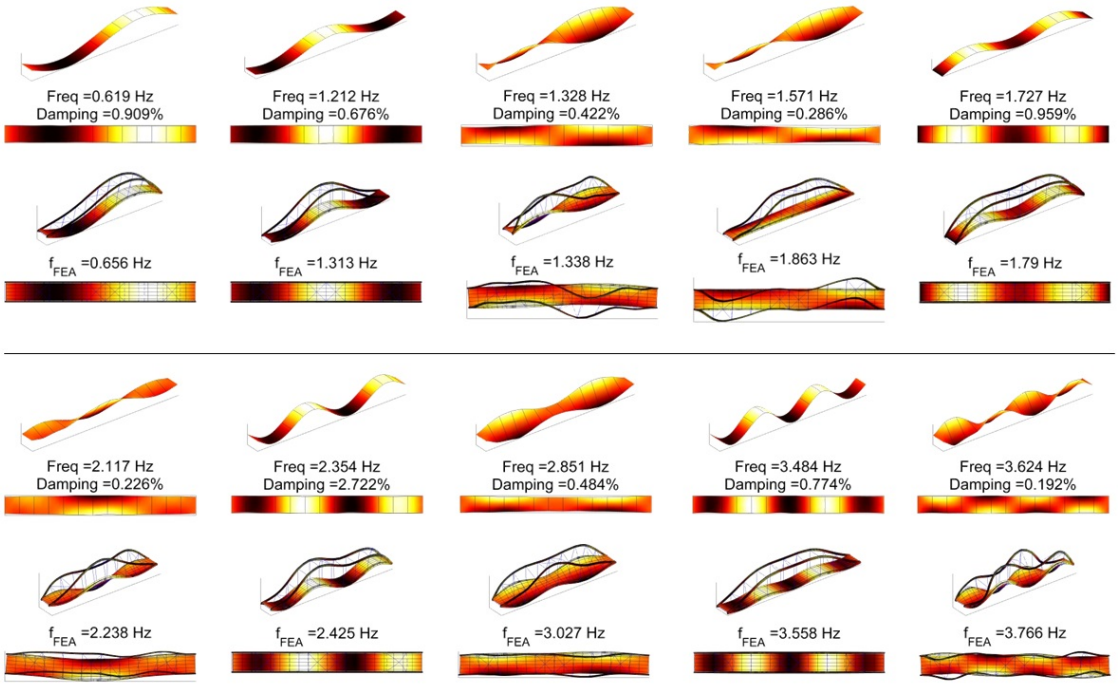

Figure 14: Modal parameters of the idealized finite element model corresponding to the first ten experimentally measured modes

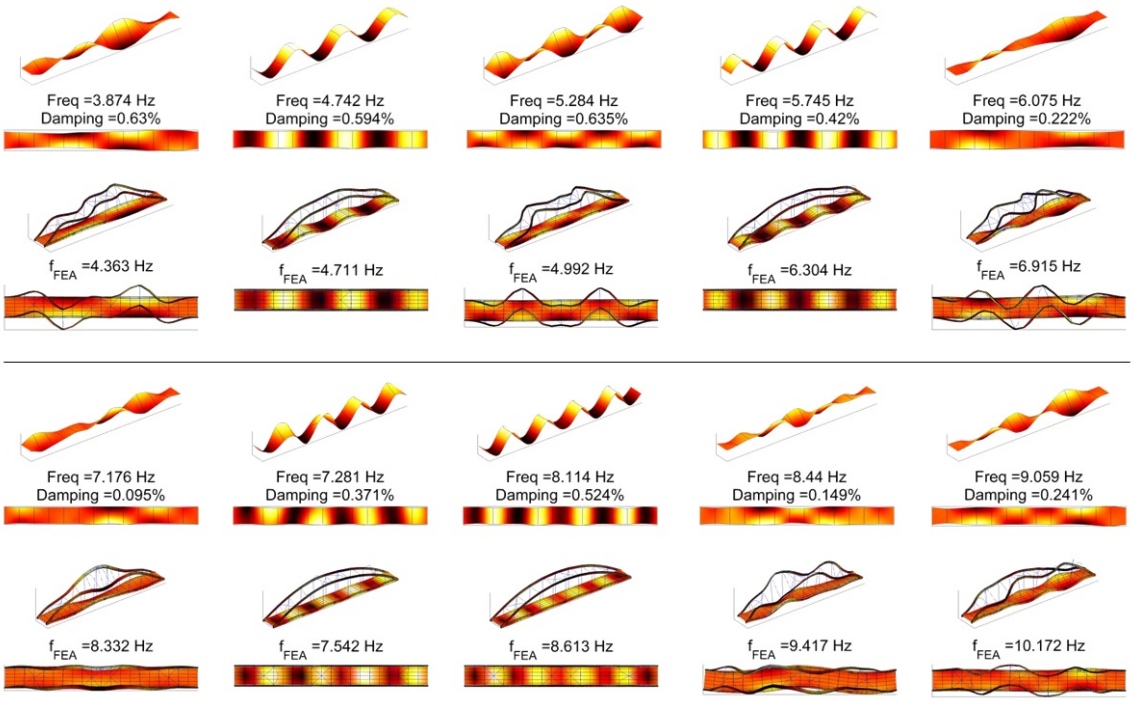

Figure 15: Modal parameters of the idealized finite element model corresponding to experimentally measured modes eleven through twenty

Table 3: Comparison between experimental modal parameter estimates and modal parameters of the idealized finite element model

Mode #	f_e (Hz)	f_a (Hz)	Δ (%)	MAC (%)	Behavior
1	0.619	0.656	6.07	99.95	Vertical
2	1.212	1.313	8.27	99.27	Vertical
3	1.328	1.338	0.77	82.16	Torsion
4	1.571	1.863	18.6	61.23	Torsion
5	1.727	1.790	3.67	99.28	Vertical
6	2.117	2.238	5.74	63.57	Torsion
7	2.354	2.425	3.04	97.75	Vertical
8	2.851	3.027	6.15	92.42	Torsion
9	3.484	3.558	2.12	97.88	Vertical
10	3.624	3.766	3.93	94.00	Torsion
11	3.874	4.363	12.6	64.40	Torsion
12	4.742	4.711	-0.65	79.35	Vertical
13	5.284	4.992	-5.54	82.52	Torsion
14	5.745	6.304	9.74	97.09	Vertical
15	6.075	6.915	13.8	77.74	Torsion
16	7.176	8.332	16.1	49.14	Torsion
17	7.281	7.542	3.58	83.54	Vertical
18	8.114	8.613	6.15	83.94	Vertical
19	8.440	9.417	11.6	34.69	Torsion
20	9.059	10.17	12.3	65.31	Torsion

4.3 Model Updating Technique and Parameterization of the FE Model

Structural identification of uncertain parameters within the FE model was performed within the MATLAB environment for 16 different scenarios. For each scenario, the number of modes included in the optimization and the number of uncertain parameters considered for structural identification were varied to investigate the influence of these factors on the structural identification. Scenarios included either 5, 10, 15, or 20 modes in the computation of the objective function and, for each of these scenarios, model updating was performed by calibrating sets of 3, 6, 9, and 12 uncertain parameters. For consistency purposes, the sets of 3, 6 , 9, or 12 uncertain parameters exhibiting the greatest influence on the modal parameters of the model were selected for the calibration of the model. This approach allows the investigator to examine the significance of the measured modal richness included in the structural identification and the number of uncertain parameters adapted on the consistency of estimated parameter assignments. In order to perform the structural optimization using a global optimization technique, an integer-constrained genetic algorithm was used to minimize the objective function formed with the eigenvalue residuals and modal assurance criterion. Due to the highly-parallelizable characteristics of genetic algorithms, a 125-core computing cluster was used instead of a single desktop computer to address the challenging computational workload associated with global optimization. Parallel computing allows for the use of larger population sizes, which more effectively explore the uncertain parameter search space to identify the optimal solution. In this study, a population size of 5,000 individuals per generation was used

over a fixed duration of 25 generations. Consequently, a total of 130,000 eigenanalyses were conducted on the finite element model for each scenario to facilitate the structural identification by genetic algorithm. Additional details on the implementation of the genetic algorithm for the structural identification performed in this study is presented in Chapter 5.

In order to facilitate the model updating process, specifically the generation of baseline models and parameterized mass and stiffness matrices, a MATLAB script was developed to interface with the finite element model using the Open Application Programming Interface (OAPI) provided by SAP2000 v15. The OAPI establishes a communication interface between the two softwares that allows MATLAB to execute commands in SAP2000 and share model information between the two softwares, making it a very powerful and useful tool for parametric analysis and model updating. Over this automated digital interface, MATLAB was used to access the FE model developed in SAP2000, adjust parameter assignments within the model, and import the corresponding mass and stiffness matrices of the model (Appendix A). The mass and stiffness matrices assembled in SAP2000 are written to files that can be imported into MATLAB and reassembled in sparse matrix format to generate parameterized mass and stiffness matrices (Figure 16). The script written to implement the parameterization of the model and assemble the matrix contributions is provided in Appendix A.

The benefits of this automated implementation are two-fold: first, scripted routines are faster and less error prone than manually manipulating the model to generate parameterized matrices and, second, the generalized eigenvalue solver in MATLAB

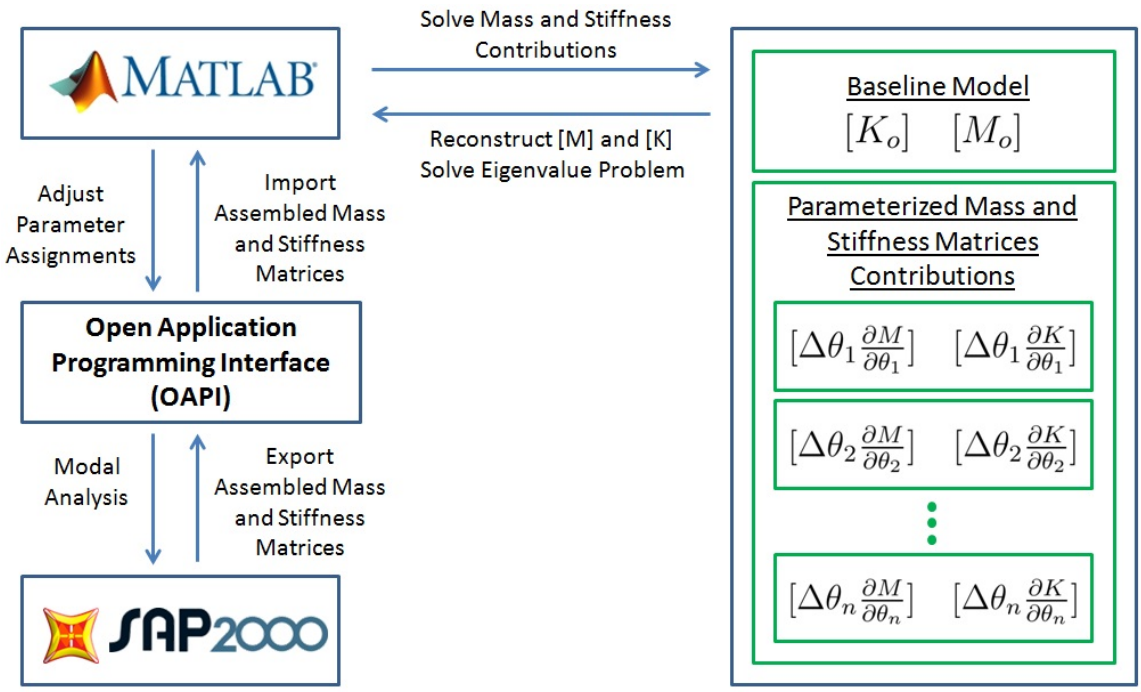

Figure 16: Schematic of Routines for the Parameterization of the FE Model and Reconstruction of the Mass and Stiffness Matrices

can be used to produce the eigenvalue analysis of the parameterized model more efficiently than SAP2000, leading to a faster optimization routine. Parameterization of the FE model was achieved by decomposition of both the mass and the stiffness matrices into the mass and stiffness matrices of a baseline model and the linear superposition of contributions from mass and stiffness changes for each uncertain parameter that is considered in the updating routine. Since linear superposition is leveraged, these uncertain parameters are necessarily restricted to only those that provide proportional, or linear, contributions to the mass and stiffness matrices with any change in the parameter assignments (Janter and Sas, 1990). This limitation precludes updating of parameters such as thickness of shell elements or geometries of frame elements, but does permit for use of many properties in the model as uncertain

parameters, such as the elastic modulus of elements, mass densities, spring stiffnesses, and fixity of connections. By linear superposition, reconstruction of the mass and stiffness matrices can be accomplished by the use of the following equations:

$$M = M_o + \Delta\theta_1 \frac{\partial M}{\partial \theta_1} + \Delta\theta_2 \frac{\partial M}{\partial \theta_2} + ... + \Delta\theta_n \frac{\partial M}{\partial \theta_n} \tag{19}$$

$$K = K_o + \Delta\theta_1 \frac{\partial K}{\partial \theta_1} + \Delta\theta_2 \frac{\partial K}{\partial \theta_2} + ... + \Delta\theta_n \frac{\partial K}{\partial \theta_n} \tag{20}$$

where M_o and K_o are the mass and stiffness matrices of the baseline model, $\Delta\theta_j$ is the difference between the j-th parameter assignment value and its lower bound, and $\frac{\partial K}{\partial \theta_j}$ and $\frac{\partial M}{\partial \theta_j}$ are the partial derivatives of the mass and stiffness with respect to the j-th parameter determined numerically. The mass and stiffness matrices of the baseline model are established by assigning each uncertain parameter in the model to its lower bound value. The partial derivatives of the mass and stiffness matrices are computed by linear perturbation of the model using the upper and lower bounds of individual parameter assignments.

4.4 Sensitivity Analysis

To facilitate decision making within the parameterization process, a sensitivity analysis was performed to identify the most meaningful uncertain parameters within the FE model to be included in the structural identification. Performing a sensitivity analysis is a fundamental step in identifying and ranking the most appropriate uncertain parameter choices for the calibration of the model, since the selection of the parameters that are updated directly affects the overall correlation between the modal parameters of the calibrated FE model and the measured modal parameter

estimates. Including a parameter within the model updating that the modal properties of the finite element model are insensitive to will result in negligible improvement in the model correlation after updating. Furthermore, the physical meaning of the updated parameter will lack confidence due to the insensitivity of the model to the updated parameter. Within the sensitivity analysis, a sensitivity index is calculated for each uncertain parameter based on a measure of the change in modal parameters exhibited by the model over the range of physically feasible assignments that the parameter could take. In this thesis, the sensitivity index, S_i, of each uncertain parameter, θ_i, was determined by evaluating change in the first twenty natural frequencies produced with the uncertain parameter set to its upper bound assignment, $(\bar{\theta}_i)$, and correspondingly at its lower bound assignment, $(\underline{\theta}_i)$. The sensitivity index is reduced to a scalar index by summing the absolute value of the changes in natural frequencies, as given by

$$S_i = \sum_{j=1}^{20} |f_j^{\bar{\theta}_i} - f_j^{\underline{\theta}_i}| \tag{21}$$

The sensitivity analysis was also used to establish upper and lower bounds on selected uncertain parameters in the model for which engineering judgment or knowledge of typical ranges of material properties could not be used to establish these limits. Common examples of where this is necessary are the cases of boundary condition spring assignments and rotational fixity of elements. In both instances, the feasible range of parameter assignments spans from the free condition, or zero stiffness, to the fully fixed condition, or infinite stiffness, which is handled by partitioning of the structural matrices. However, these parameters have practical limits when

the parameter assignment sufficiently replicates either idealized condition. In other words, a boundary spring does not need to be assigned infinite stiffness to sufficiently replicate the modal parameters associated with the fully fixed condition and, likewise, often does not need to be assigned zero stiffness to adequately replicate the modal parameters associated with the free condition. Establishing these practical limits is critical for structural identification using genetic algorithms since these practical limits reduce the size of the search space for the uncertain parameters and ensure that the parameter assignments produce some significant change in the modal parameters of the model over the region that optimization is conducted. Figure 17 provides results from the sensitivity analysis conducted on the boundary spring in the longitudinal direction (global X) parameter, where it is revealed that the full bounds associated with the effective extremes of the longitudinal boundary spring can be established as 0.2 MN/m to 2,000 MN/m. However, a smaller range was selected for the optimization scheme of this uncertain parameter as the longitudinal boundary spring was expected to behave closer to a free condition. Therefore, practical bounds on the longitudinal boundary spring assignment used later for the calibration of the preliminary FE model were established as 0.2 MN/m to 200 MN/m.

An initial set of 19 candidate uncertain parameters was identified for structural identification of the finite element model and the sensitivity index expressed in Equation 21 was calculated for each parameter. These candidate uncertain parameters were then ranked from highest to lowest sensitivity according to this index. Table 4 summarizes this analysis and identifies the subset of the top 12 most significant uncertain parameters for calibration of the finite element model. Subsequent structural

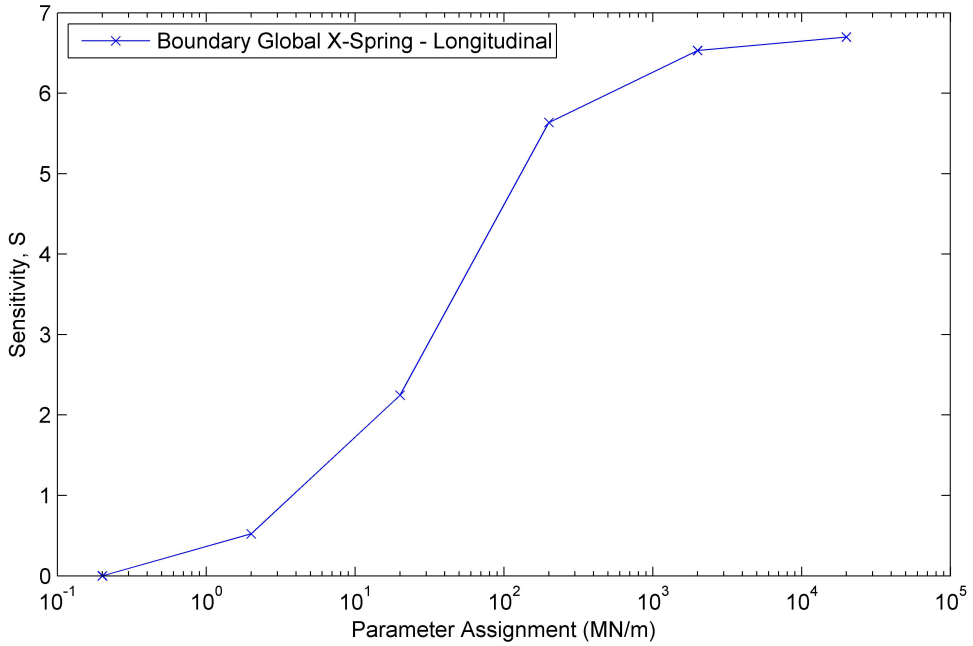

Figure 17: Sensitivity analysis performed on boundary global x-spring uncertain parameter

identification presented in the remainder of this thesis was limited to, at most, these 12 uncertain parameters, and the seven least sensitive parameters from the initial candidate set were reestablished in the finite element model to their assignment used in the idealized finite element model.

Uncertain parameters within the FE model that were considered in the sensitivity analysis included connection fixity assignments, boundary condition translational spring assignments, elastic modulus of the reinforced concrete deck, flexural stiffness property modifiers, and axial stiffness property modifiers. In the case of property modifiers, the uncertain parameter assignment is treated as a unitless multiplicative scale factor that is applied to the associated section properties of the elements in the model with that section assignment. Property modifiers were applied to the flexural stiffness of the webs and flanges of the arch ribs (θ_2 and θ_4, respectively), the webs

Table 4: Selection of final set of 12 uncertain parameters with highest sensitivity ($\underline{\theta}$ - lower bound, $\overline{\theta}$ - upper bound, S - sensitivity)

#	Parameter, θ	$\theta_{idealized}$	$\underline{\theta}$	$\bar{\theta}$	S
1	Rotational Fixity of Arch Laterals	1	0.01	1	17.43
2	Flexural Stiffness of Arch Rib Webs	1	0.5	1.5	6.37
3	Boundary Global X-Spring - Longitudinal (MN/m)	Pin/Roller	0.2	200	5.64
4	Flexural Stiffness of Arch Rib Flanges	1	0.5	1.5	3.64
5	Rotational Fixity of Arch Diagonals	1	0.01	1	2.64
6	Flexural Stiffness of Tie Girder Flanges	1	0.75	1.5	2.16
7	Flexural Stiffness of Parapet	1	0.5	1.5	2.14
8	Flexural Stiffness of Tie Girder Webs	1	0.5	1.5	1.58
9	Elastic Modulus of Deck Concrete (GPa)	25	14	34	1.54
10	Axial Stiffness of Stranded Bridge Cable	1	0.5	1.5	1.29
11	Boundary Global Z-Spring - Vertical (MN/m)	Fixed	200	20,000	1.17
12	Flexural Stiffness of Longitudinal Stiffeners	1	0.5	1.5	1.16
13	Flexural Stiffness of Knuckle Web	1	0.5	1.5	1.12
14	Flexural Stiffness of Diaphragm Plates	1	0.5	1.5	0.84
15	Axial Stiffness of Arch Diagonals and Laterals	1	0.5	1.5	0.82
16	Axial Stiffness of Deck Diagonal Bracing	1	0.5	1.5	0.55
17	Rotational Fixity of Floor Beams	1	0.01	2	0.13
18	Boundary Global Y-Spring - Lateral (MN/m)	Pin	200	200,000	0.05
19	Rotational Fixity of Deck Diagonal Bracing	1	0.01	1	0.01

and flanges of the tie girders (θ_8 and θ_6, respectively), parapets (θ_7), longitudinal stiffener plates (θ_{12}), the knuckle web (θ_{13}), and the diaphragm plates within the ribs and the tie girders (θ_{14}) in order to explore calibration of their effective stiffnesses to the structure. Axial stiffnesses that were expressed as uncertain parameters in the sensitivity analysis include the axial stiffness of the stranded bridge cables (θ_{10}), the arch diagonals and laterals (θ_{15}), and the deck diagonal bracing (θ_{16}). The rotational fixity of the arch laterals and diagonal bracing (θ_1 and θ_5), which refers to the degree of connection fixity between these structural elements and the arch, were also parameterized using a property modifier applied to the flexural stiffness of a single short element of each section type serving as a link between the arch and the member.

It is important to note that property modifiers applied to the axial or flexural stiffness of sections provide the optimization with the flexibility to adjust stiffness of elements in the model to improve the model correlation and effectively account for uncertainties in both material and geometric properties of the modeled elements. Con-

sequently, it is important to avoid including sets of parameters that do not produce independent effects on the properties of the model. For example, the elastic modulus of the shell elements representing the reinforced concrete deck was considered as an uncertain parameter (θ_9) in the sensitivity analysis, since this material property is both uncertain and known to vary across a significant range based on mix design, and since the stiffness of the deck should influence the flexural and torsional modes measured during the ambient vibration monitoring. However, the application of this parameter assignment for the elastic modulus of the reinforced concrete was limited to the deck and excluded the shell elements representing the parapet walls. This was done to maintain independence between this elastic modulus parameter with the uncertain parameter previously established to directly calibrate the flexural stiffness of the parapets. Since the flexural stiffness, EI, contains the elastic modulus, allowing the model to simultaneously optimize both parameters would lead to potential uniqueness issues that can render the identified parameter assignments meaningless.

Lastly, modal parameters of a structural system are often most sensitive to the boundary conditions of the structure (E. Aktan, N. Çatbaş, A. Türer, and Z. Zhang, 1998) (Zhou et al., 2012), so the idealized pin and roller boundary restraints used in the idealized finite element model were replaced by linear elastic translational springs in each of the three Cartesian axes. These springs in the longitudinal, vertical, and lateral directions (θ_3, θ_{11}, and θ_{18} respectively) were introduced to account for the non-ideal boundary conditions present in real-world structures. In this particular case, some degree of unknown stiffness is expected in each direction due to axial, shear, and flexural deformation of supporting elements, such as the bearings, piers,

and supporting foundation. The lower and upper bounds for each spring were established through the sensitivity analysis, as previously described. Since none of the 19 uncertain parameters selected introduced a change in the mass matrix of the model, the parameterization of the model was achieved using only Equation 20. This choice was intentional and was taken to alleviate uniqueness issues in the inverse eigenvalue problem associated with updating the mass and stiffness matrices simultaneously (Mottershead et al., 2011).

CHAPTER 5: STRUCTURAL IDENTIFICATION AND DISCUSSION OF RESULTS

The implementation of and results from application of genetic algorithm (GA) global optimization routines applied for structural parameter identification using the previously documented finite element model are discussed in detail within this chapter. Criteria used within the GA for global optimization along with the objective function used to evaluate the quality of the correlation between the experimental data and individual models within the populations are presented. The results of the implementation of the GA for sixteen different scenarios are summarized and compared to examine the influence of the number of modes included in the objective function and the number of uncertain parameters included in the model updating routine on the improvement in model correlation. Furthermore, the variability in the parameters identified across the structural identification analyses are analyzed. Lastly, modal analyses of the calibrated FE models are performed to quantify the improvement in agreement of the natural frequencies and mode shapes of the model with the experimental estimates relative to the preliminary idealized finite element model.

5.1 Details of Genetic Algorithm Applied for Structural Identification

The main goal of the genetic algorithm, as applied in this study, is to search for the global minimum discrepancy between modal parameter estimates extracted from

experimental measurements and the analytical predictions of a parameterized model offering many possible solutions to the eigenproblem. However, the genetic algorithm is associated with several properties or options that can influence its performance and affect its ability to explore a wide search space and subsequently reach global optimization in an efficient amount of time, rather than prematurely converge on a local minimum. The performance of genetic algorithms for global optimization depends on several properties of the genetic algorithm, as previously discussed in the literature review. For example, population size is widely recognized to have a significant effect on the performance of genetic algorithms. An insufficiently small population may prematurely converge on a local minimum before adequately exploring the search space, while an overly large population results in a longer time before convergence is achieved (Chambers, 1995). For the present study, a wide coverage of the search space was required to facilitate a higher probability of the optimization runs converging on the globally optimal solution. Consequently, a parallel implementation of the genetic algorithm was employed using a 125 core computing cluster to permit the use of a large population size, while maintaining a reasonable solution time. Complete details on the parallel implementation of the genetic algorithm on the computing cluster can be found in (Whelan et al., 2016).

For each of the 16 scenarios where the GA was applied, an initial population size of 5,000 individuals was generated by randomly distributing assignments for each uncertain parameter (θ) within their lower bounds ($\underline{\theta}$) and upper bounds ($\overline{\theta}$), indicated for each parameter in Table 5. An integer-constrained genetic algorithm was used to relax the computational burden associated with generation of real number

assignments, and thus integer value parameter assignments were scaled to prescribe the corresponding effective integer precision ($\delta\theta$) of each uncertain parameter, as discussed later in this section. At each generation, an elite count of 50 individuals, representing 1% of the population size, was allowed to survive and subsequent populations were generated by a 60% cross-over reproduction rate. The remaining 39% of the population was generated by mutation. The rate of cross-over is also widely recognized to influence the performance of the genetic algorithm in converging on the optimal parameter assignments (Chambers, 1995). The current study did not seek to study the influence of cross-over rates on the performance of the genetic algorithm but instead to focus on the influence of the structural properties of the model and robustness of the measurement. The 60% cross-over reproduction rate was selected for consistency with similar studies leveraging genetic algorithms for structural identification of civil structures with experimentally obtained modal parameter estimates (Kernicky, 2013; Moss, 2015). The genetic algorithm optimization routine was stopped after completion of a fixed number of 25 generations to maintain reasonable run times. Convergence of the objective function appeared to have been reached for all cases, although this convergence of the objective function is further discussed in the subsequent section.

In this study, an integer-constrained genetic algorithm was used to minimize the solution search space. An integer genetic algorithm constrains uncertain parameter assignments to integer values, rather than permitting them to take any real number value. The motivation behind adopting an integer constraint on the parameters is that there is a finite precision at which each parameter produces a quantifiable and

meaningful change in the modal properties of the model and therefore the computational burden associated with finding optimal real value parameter assignments can be relaxed. However, the uncertain parameters in the model must first be scaled to prescribe the effective precision desired for each parameter. In other words, a quantized real value scale can be mapped to integer values to effectively achieve the desired precision for each parameter during application of the genetic algorithm. Table 5 presents the effective integer precision $\delta\theta$ associated with each uncertain parameter included in the model. The same fixed scaling approach was also enforced to the lower and upper bounds of each parameter in order to generate lower and upper bounds on the corresponding integer scale.

Table 5: Parameter bounds and effective integer precision used within the structural identification analysis cases

#	Parameter, θ	$\underline{\theta}$	$\bar{\theta}$	$\delta\theta$
1	Rotational Fixity of Arch Laterals	0.01	1	0.01
2	Flexural Stiffness of Arch Rib Webs	0.5	1.5	0.01
3	Boundary Global X-Spring - Longitudinal (MN/m)	0.2	200	0.2
4	Flexural Stiffness of Arch Rib Flanges	0.5	1.5	0.01
5	Rotational Fixity of Arch Diagonals	0.01	1	0.01
6	Flexural Stiffness of Tie Girder Flanges	0.75	1.5	0.01
7	Flexural Stiffness of Parapet	0.5	1.5	0.01
8	Flexural Stiffness of Tie Girder Webs	0.5	1.5	0.01
9	Elastic Modulus of Deck Concrete (GPa)	14	34	0.01
10	Axial Stiffness of Stranded Bridge Cable	0.5	1.5	0.01
11	Boundary Global Z-Spring - Vertical (MN/m)	200	20,000	0.2
12	Flexural Stiffness of Longitudinal Stiffeners	0.5	1.5	0.01

While there are numerous forms of objective functions, the one used in this thesis has been specifically suggested for FE model updating routines based on the implementation of genetic algorithms (Caicedo and Yun, 2011; Ribeiro et al., 2012; Kernicky et al., 2014; Moss, 2015). This particular objective function incorporates the eigenvalue residuals as the absolute percent error between the predicted and the measured undamped natural frequencies and the eigenvector residual through the

MAC value computed across the mode shapes of the finite element model and those experimentally estimated, after mode pairing. The form of this objective function, computed over m total modes, is:

$$J(\vec{\theta}) = \sum_{i=1}^{m} \alpha_i \left(\frac{|f_{a_i} - f_{e_i}|}{f_{e_i}} \right) + \sum_{i=1}^{m} \beta_i \left(1 - MAC_{i,i}\right) \tag{22}$$

where f_{a_i} and f_{e_i} are the corresponding predicted and measured undamped natural frequencies associated with the i-th paired mode, α_i and β_i are weighting factors that are assigned to the measures of the eigenvalue and eigenvector residuals, respectively. In this study, fixed weighting factors across all modes, with α=1 and β=0.5, were used in the computation of the objective function for each individual. It is typical that less relative weighting is applied to the measure of the eigenvector residual since experimental mode shape estimates are considered to be more difficult to obtain with confidence than undamped natural frequency estimates (Friswell and Mottershead, 1995). It should be noted that the form of the objective function, like many of the other properties of the genetic algorithm, has a significant influence on the results of the structural identification since it serves as the single measure by which aggregate model correlation is assessed and optimized. In this study, the effect of the number of modal parameters included in the objective function is studied, but future research could examine the effect of the relative weighting of eigenvalue and eigenvector residuals or form of the objective function on the performance of the structural identification routine.

5.2 Comparison of Structural Identification Results

Structural identification using genetic algorithms was performed for sixteen different scenarios where either 5, 10, 15, or 20 modes were compared in the objective function while the number of uncertain parameters (from the final set of 12 identified by the sensitivity analysis) used in the updating routine included either 3, 6, 9, or 12 parameters. Objective scores and the influence of residuals developed from the average absolute percent error between the measured and the predicted undamped natural frequencies, and the MAC values associated with discrepancies in the predictions of modes included in the objective function, are further investigated. Additionally, the variation in parameter assignments obtained from the global minimization of the objective function for updating of the FE model is explored both across the different cases and within the elite individuals of the final generations.

Convergence plots showing the objective scores over the 25 generations obtained during the genetic algorithm optimization routine for all sixteen structural identification scenarios are presented in Figure 18. These convergence plots were produced as a means to examine the extent that the objective function improved over the genetic algorithm as well as whether or not convergence was generally achieved. These convergence plots show that as the number of uncertain parameters is increased for each set of modes included in the objective function, the initial objective score for the first generation consistently improves by a moderate amount. Furthermore, the relative improvement in the objective score over the 25 generations increases significantly as uncertain parameters are added. This relative improvement over the 25 generations

is generally less affected by including additional modes in the objective function. It is also interesting to note that the optimizations performed using only 3 uncertain parameters converged after less than 10 generations, while the remaining cases required at least 20 generations before exhibiting signs of convergence. Moreover, even though the final objective scores improve with additional parameters included in the optimization routine, the improvement generally occurs through infrequent, coarse steps rather than incrementally smooth steps. Although this has not been proven, larger steps are most likely associated with exploration of different local minima and it is possible that the optimizations performed with 9 or 12 uncertain parameters might not have fully converged on the global minimum. For the purposes of the following analysis, it is assumed that the genetic algorithm sufficiently converged after 25 generations for each case, as evidenced by the general exponential decay in the improvement in objective scores over each optimization run. Future research might consider exploration of the convergence function using genetic algorithms over a larger number of generations and the effects that this may produce on modal correlation and variability of the uncertain parameter estimates.

The influence of the number of uncertain parameters used and the number of modes included in the objective function on the objective score obtained after 25 generations of the genetic algorithm is presented in Figure 19. The reason for higher objective scores with more modes included in the objective function is simply that the objective function is a summation over the modes included in the model correlation. With the exception of the one objective score for the case of 9 uncertain parameters with 20 modes in the objective function, the addition of uncertain parameters in the optimiza-

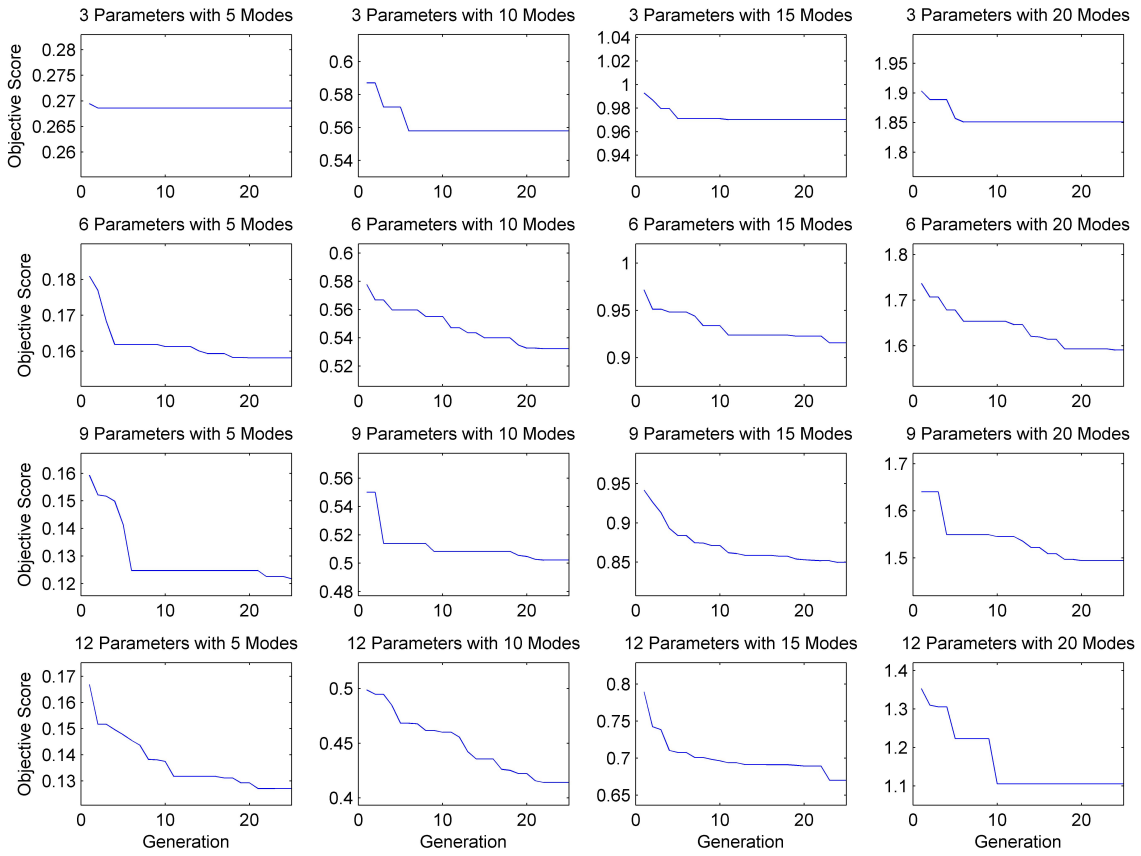

Figure 18: Objective scores obtained during the genetic algorithm optimization routine over the first 25 generations

tion consistently improved the objective score obtained. This is expected since the inclusion of additional parameters in the optimization provides greater flexibility to adjust the FE model to match the measured response. However, it was not expected that the improvement in the objective function would increase by larger increments as additional uncertain parameters were added. Since sensitivity analysis was used to first rank the uncertain parameters included, it was expected that the relative improvement obtained from increasing the number of uncertain parameters from 3 to 6 would be more significant than increasing from 9 to 12 uncertain parameters as the model was found to be less sensitive to these final parameters. This difference sug-

gests that the sensitivity index used may be too simplistic and alternative methods should be sought for future research adopting the approaches used in this thesis. The expected progression of relative improvements associated with the ranked sensitivities is exhibited for the cases using only 5 modes in the objective function.

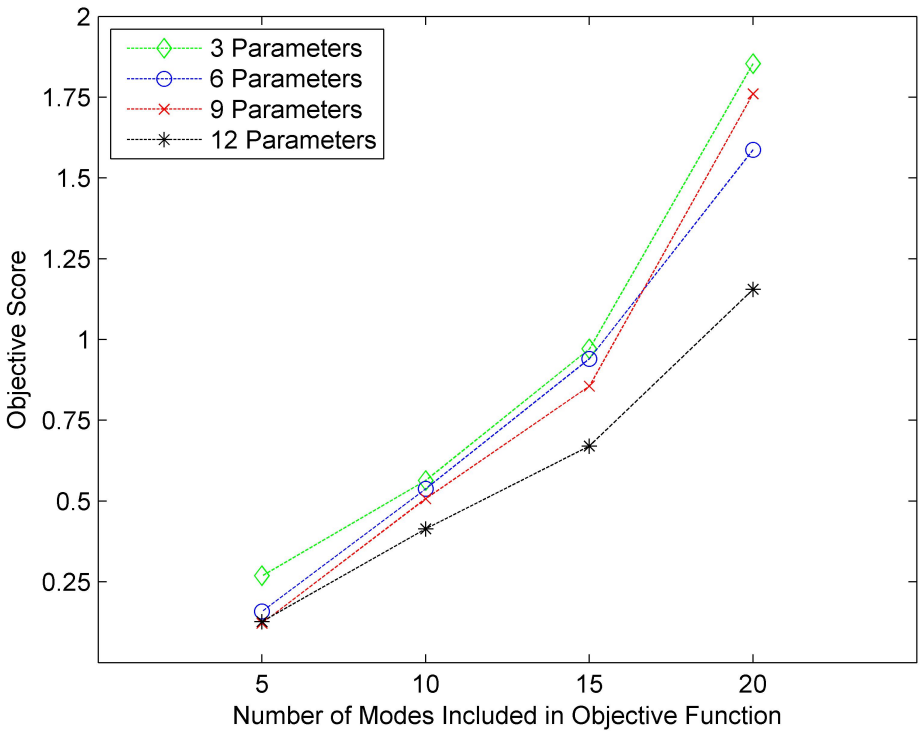

Figure 19: Objective scores achieved after 25 generations across all optimization cases

As a summary of the model correlations achieved for each optimization run, the average absolute percent error in natural frequencies and the average MAC values for each case is presented in Figure 20. For reference, the idealized FE model had an average absolute percent error in natural frequency of 7.52% and average MAC value of 80.26. Despite the number of uncertain parameters and modes included in the objective function, significant improvements relative to the idealized model in both the average absolute percent error in natural frequency and the MAC value correlations

were generated by all sixteen scenarios of the genetic algorithm implementation. In all but one scenario, an increase in the number of modes included in the objective function resulted in an increase in the natural frequency prediction error and a decrease in the mode shape correlations. Additionally, for most scenarios, increasing the number of uncertain parameters while keeping the number of modes in the objective function fixed resulted in an improvement in the natural frequency predictions. A similar trend was observed for the MAC values but the relative improvement in mode shape correlation was less significant than that of the natural frequency correlations. This is likely a reflection of the higher weighting factor applied to natural frequencies within the objective function in Equation 22.

As the main purpose of structural identification is to provide a technique for performance-based assessment of structures by model updating of FE model properties, the parameter assignments obtained by the optimization runs are of particular interest. Parameter assignments generated by the global optimization of the objective function for each of the sixteen scenarios are provided in Table 6. In addition to providing the parameter assignment for the optimal solution, the standard deviation calculated across the 50 elite individuals from the final generation of each optimization is also provided in parenthesis as a measure of parameter uncertainty. This will be discussed in more detail after discussing the variation in parameter assignments across the different scenarios.

Consistency within parameter assignments relative to the lower and upper bounds among all sixteen scenarios were identified for some parameters (θ_2, θ_5, θ_8, θ_{10}, and θ_{11}). As the number of uncertain parameters and the number of modes varied, the

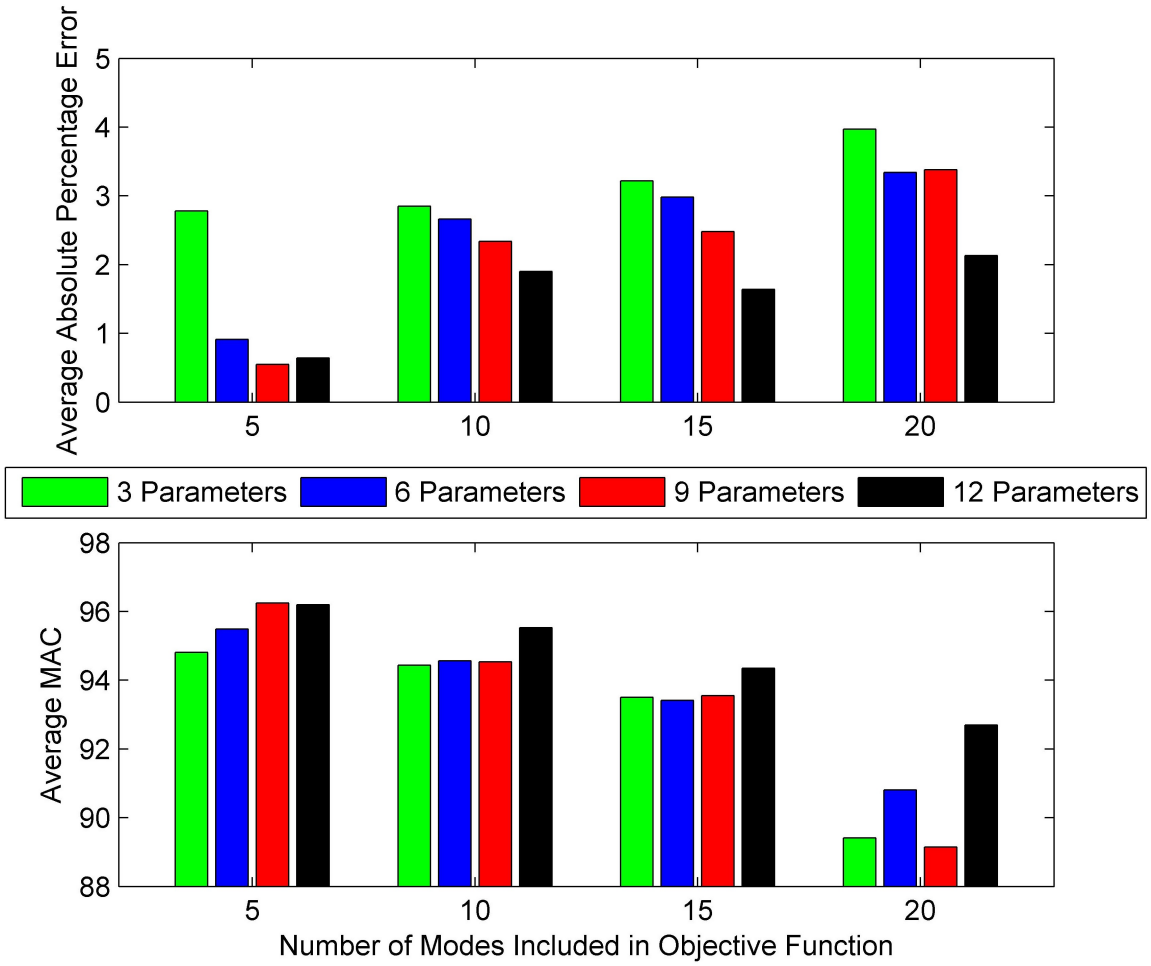

Figure 20: Average absolute percent error between the experimental and predicted undamped natural frequencies and average MAC values between mode shapes for all optimization cases

assignments of other parameters fluctuated between two consistent ranges of values (θ_1, θ_3, θ_9, and θ_{12}). The remaining parameters were assigned values that fluctuated between three ranges of assignments (θ_4, θ_6, and θ_7). However, the uncertain parameter assignments are generally much more consistent with a fixed number of modes included in the objective function than with changes in the number of uncertain parameters used. Consequently, while including additional uncertain parameters in the model can result in significant improvements in model correlation, the analysis sug-

Table 6: Uncertain parameter assignment predictions by genetic algorithm for each of the sixteen scenarios with standard deviation in values across final elites (n - number of calibrated parameters, m - number of modes included in the objective function)

n	m	Parameter Assignments											
		θ_1	θ_2	θ_3	θ_4	θ_5	θ_6	θ_7	θ_8	θ_9	θ_{10}	θ_{11}	θ_{12}
3	5	0.30	0.50	2.2	-	-	-	-	-	-	-	-	-
		(0.00)	(0.00)	(0.0)	-	-	-	-	-	-	-	-	-
6	5	0.29	0.54	33.4	0.50	0.08	1.20	-	-	-	-	-	-
		(0.02)	(0.01)	(1.3)	(0.01)	(0.03)	(0.01)	-	-	-	-	-	-
9	5	0.30	0.53	36.0	0.51	0.10	0.77	1.37	1.50	33.9	-	-	-
		(0.04)	(0.01)	(2.5)	(0.01)	(0.03)	(0.03)	(0.09)	(0.02)	(1.3)	-	-	-
12	5	0.28	0.55	47.0	0.58	0.04	0.75	1.44	1.39	33.5	0.56	3510.0	1.49
		(0.07)	(0.04)	(7.4)	(0.04)	(0.03)	(0.04)	(0.15)	(0.08)	(1.0)	(0.04)	(452.2)	(0.2)
3	10	0.02	0.55	2.2	-	-	-	-	-	-	-	-	-
		(0.00)	(0.00)	(0.1)	-	-	-	-	-	-	-	-	-
6	10	0.02	0.50	12.2	0.80	0.10	0.97	-	-	-	-	-	-
		(0.00)	(0.01)	(3.8)	(0.07)	(0.02)	(0.04)	-	-	-	-	-	-
9	10	0.02	0.50	2.6	0.76	0.05	0.96	0.85	1.43	31.4	-	-	-
		(0.00)	(0.02)	(3.6)	(0.09)	(0.03)	(0.07)	(0.19)	(0.06)	(5.4)	-	-	-
12	10	0.30	0.94	2.6	1.00	0.01	0.95	0.50	1.43	16.6	0.58	460.8	1.30
		(0.02)	(0.16)	(0.3)	(0.15)	(0.01)	(0.08)	(0.07)	(0.09)	(3.2)	(0.04)	(161.2)	(0.4)
3	15	0.30	0.59	2.2	-	-	-	-	-	-	-	-	-
		(0.00)	(0.00)	(0.0)	-	-	-	-	-	-	-	-	-
6	15	0.02	0.50	2.0	1.25	0.01	0.77	-	-	-	-	-	-
		(0.07)	(0.00)	(0.5)	(0.06)	(0.01)	(0.01)	-	-	-	-	-	-
9	15	0.02	0.50	3.2	1.32	0.10	0.78	0.53	1.50	15.1	-	-	-
		(0.08)	(0.01)	(1.1)	(0.07)	(0.04)	(0.03)	(0.09)	(0.03)	(0.4)	-	-	-
12	15	0.26	0.55	2.8	1.36	0.10	0.77	0.60	1.48	14.3	0.70	1802.6	0.85
		(0.01)	(0.01)	(0.1)	(0.01)	(0.01)	(0.00)	(0.02)	(0.00)	(0.0)	(0.01)	(571.8)	(0.1)
3	20	0.30	0.66	2.2	-	-	-	-	-	-	-	-	-
		(0.00)	(0.00)	(0.0)	-	-	-	-	-	-	-	-	-
6	20	0.30	0.60	6.2	0.78	0.02	0.92	-	-	-	-	-	-
		(0.02)	(0.01)	(3.5)	(0.07)	(0.03)	(0.05)	-	-	-	-	-	-
9	20	0.28	0.65	70.4	0.70	0.05	0.99	0.88	1.46	14.3	-	-	-
		(0.02)	(0.04)	(23.8)	(0.10)	(0.03)	(0.18)	(0.23)	(0.11)	(0.6)	-	-	-
12	20	0.24	0.67	55.4	0.81	0.06	1.17	0.66	1.38	14.9	0.73	1413.8	0.93
		(0.08)	(0.05)	(36.4)	(0.10)	(0.03)	(0.08)	(0.14)	(0.14)	(5.1)	(0.02)	(727.0)	(0.3)

gests that the parameter assignments are more significantly influenced by the richness of the measurement data included in the objective function.

As noted, the standard deviation associated with each parameter assignment was calculated across the 50 elites in the final generation and is also presented in Table 6 as a way to describe variability among the final elites. In addition to these standard deviations, histograms of the parameters associated with the final elites were prepared and are presented in Appendix B for all parameters. It is important to note that the x-axis of the histograms were set to the full range of the specified parameter bounds to present the variability in the identified parameters over the assigned search space.

The reader is reminded that the initial population is randomly seeded and therefore the histograms start out as uniform distributions before the optimization is run. One of the more interesting cases is found in the rotational fixity of the arch laterals, θ_1, which is presented in Figure 21. The optimization runs exhibited two general solutions for this parameter ($\theta_1 \approx 0.02$ and $\theta_1 \approx 0.28$). Some of the histograms, such as the one developed from the elites from the case with 12 parameters and 20 modes, have solutions containing both values in distinct distributions. This suggests the presence of a local minimum within the search space of the objective functions. These histograms also show that increased variability in the elites is present as the number of uncertain parameters is increased. This is attributed to a slower convergence rate of the objective function associated with the increased difficulty in finding the global minimum when additional parameters are being calibrated. This variability may also suggest that there is either inherently more uncertainty in the identified parameters as more are added to the optimization routine or that the optimization may not have fully converged for all cases and increased generations might have resulted in further improvements in model correlation. Variability among the elites for the flexural stiffness of the arch rib webs parameter, θ_2, are presented in Figure 22 as further evidence of the increased diversity, or variability, in parameter assignments for the elites as the number of uncertain parameters is increased. These histograms, as well as the optimal values presented in Table 6 for the remaining cases, also show that variability in the parameter assignments are generally more influenced by the number of modes included in the objective function than the number of uncertain parameters included in the optimization.

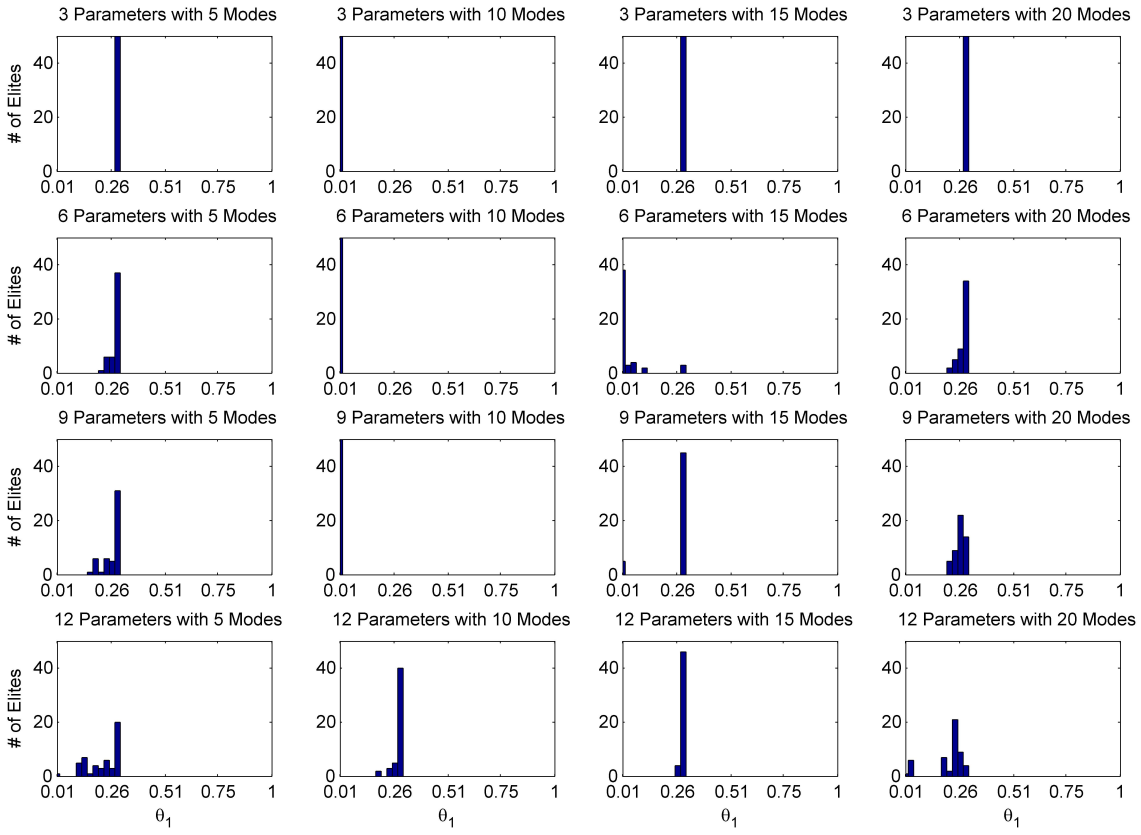

Figure 21: Parameter θ_1, rotational fixity of arch laterals, assignments associated with the 50 elites in the final generations of each structural identification case

In order to develop meaningful parameter assignments using genetic algorithms, it is important that the number of modes included in the optimization routines are allowed to vary in order to explore variations in the prediction of parameter assignment estimates. This allows the investigator to account for uncertainties and errors that are inherent to both the FE model and the optimization of the objective function since the global optimization solution might not physically represent the best solution (Zárate and Caicedo, 2008).

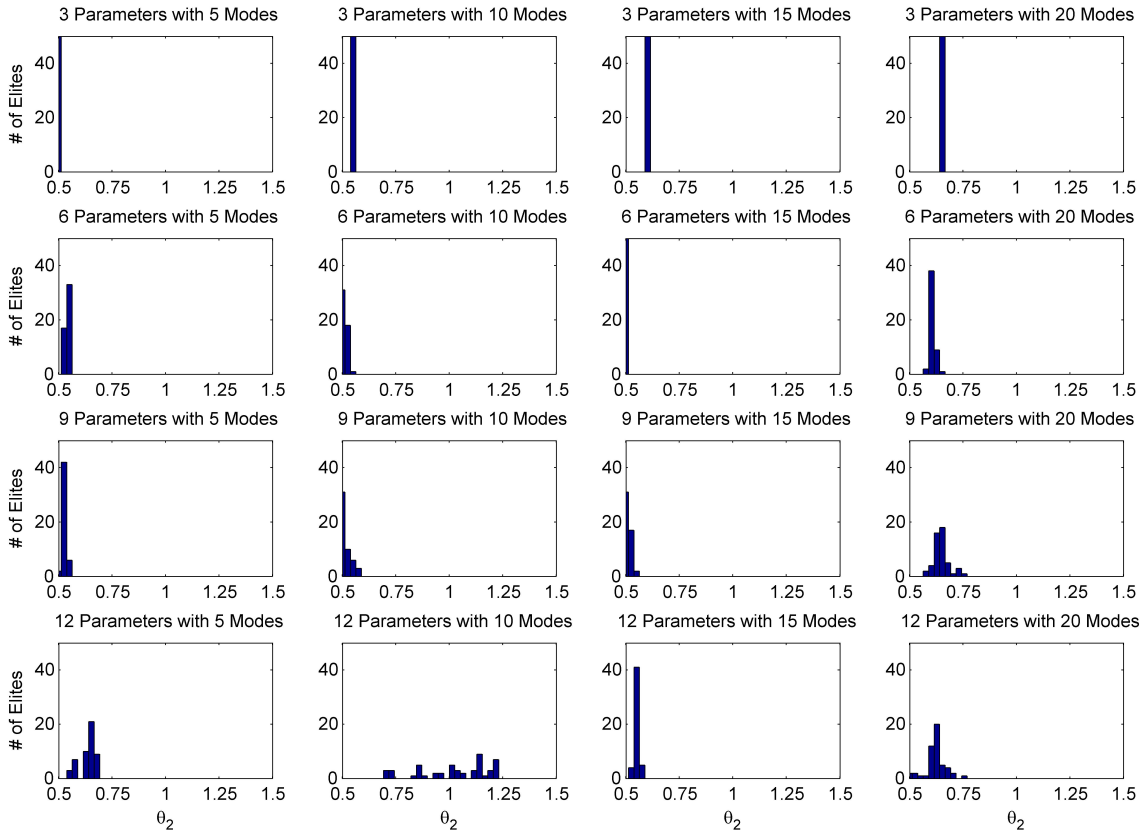

Figure 22: Parameter θ_2, flexural stiffness of arch rib webs, assignments associated with the 50 elites in the final generations of each structural identification case

5.3 Modal Parameter Comparison for Model Exhibiting Best Model Correlation

As detailed in the previous section, the field calibrated finite element model exhibiting the best correlation over the set of twenty experimental measured modes was developed using the full set of twelve uncertain parameters and all twenty sets of modal parameters within the computed objective function. This was expected since a greater number of uncertain parameters allows for greater flexibility in the optimization scheme to tune the model to the measured response and, likewise, including all modes in the objective function promotes calibration across all experimentally measured parameters. However, there was uncertainty as to whether or not the op-

timization would successfully produce a better solution with such a large number of uncertain parameters to be calibrated. In this study, the success of the optimization scheme with such a large number of uncertain parameters is attributed to the large population size used in the genetic algorithm and suggests that global minimums were successfully identified by the genetic algorithm, although this can not be definitely proven. The comparison between the analytical undamped natural frequencies and mode shapes of the calibrated model and those measured experimentally are presented to serve as an important case study for the growing field of structural identification applied to civil structures. Additionally, the relative improvement in model correlation from the idealized finite element model is quantified to demonstrate the benefit of model updating on the experimental agreement.

Consistent with the assessment of the idealized finite element model, the correlation between the measured and the calibrated modal parameter estimates was assessed by calculating the percentage error (Δ) between undamped natural frequency estimates and the MAC values computed across paired mode shapes. Discrepancies among all 20 experimental and calibrated undamped natural frequency estimate pairs ranged from -4.92% to 6.27%, with an average absolute percentage error of 2.13% (Table 7). Moreover, discrepancies among all 20 MAC values ranged from 70.52% to 99.95%, with an average MAC of 92.70%. This strong correlation between the properties of the calibrated model and the experimental measurements across all twenty modes is presented in Figures 23 and 24. The vertical modes exhibited an average MAC value of 97.49%, while the torsional bending modes exhibited an average MAC value of 88.78%. Likewise, a 2.82% average absolute percentage error in undamped natural

frequencies was calculated for the vertical bending modes, while for the torsional modes the average absolute percentage error in undamped natural frequencies was 1.56%. Overall, the average MAC above 92% and average absolute percent error in natural frequency below 2.2% indicates that the calibrated model exhibits exceptional dynamic consistency with the experimentally measured modal parameters.

Table 7: Modal parameter comparison between calibrated finite element model and operational modal analysis results

Mode #	f_e (Hz)	f_a (Hz)	Δ (%)	MAC (%)	Behavior
1	0.619	0.633	2.29	99.95	Vertical
2	1.212	1.239	2.16	99.33	Vertical
3	1.328	1.292	-2.69	95.76	Torsion
4	1.571	1.556	-0.93	85.25	Torsion
5	1.727	1.820	5.43	99.62	Vertical
6	2.117	2.053	-3.00	82.33	Torsion
7	2.354	2.332	-0.93	99.56	Vertical
8	2.851	2.711	-4.92	93.77	Torsion
9	3.484	3.408	-2.20	96.85	Vertical
10	3.624	3.570	-1.49	97.44	Torsion
11	3.874	3.831	-1.12	92.99	Torsion
12	4.742	4.938	4.13	98.26	Vertical
13	5.284	5.316	0.60	97.74	Torsion
14	5.745	6.105	6.27	98.69	Vertical
15	6.075	6.048	-0.45	81.51	Torsion
16	7.176	7.287	1.54	84.78	Torsion
17	7.281	7.296	0.21	89.36	Vertical
18	8.114	8.258	1.78	95.79	Vertical
19	8.440	8.472	0.38	70.52	Torsion
20	9.059	9.064	0.06	94.55	Torsion

Figure 23: Modal parameter estimates associated with modes one through ten extracted from the experimental measurements (row#1), idealized model (row#2), and calibrated model (row#3)

Graphical presentation of the percentage errors in undamped natural frequencies exhibited by the idealized and calibrated finite element models relative to the experimentally measured natural frequencies is presented in Figure 25. This bar plot demonstrates the significant changes in percent errors in undamped natural frequency produced through the model calibration relative to the measured undamped natural frequencies. In the idealized model, six modes were associated with an error in undamped natural frequency prediction greater than 10% and only eight modes were

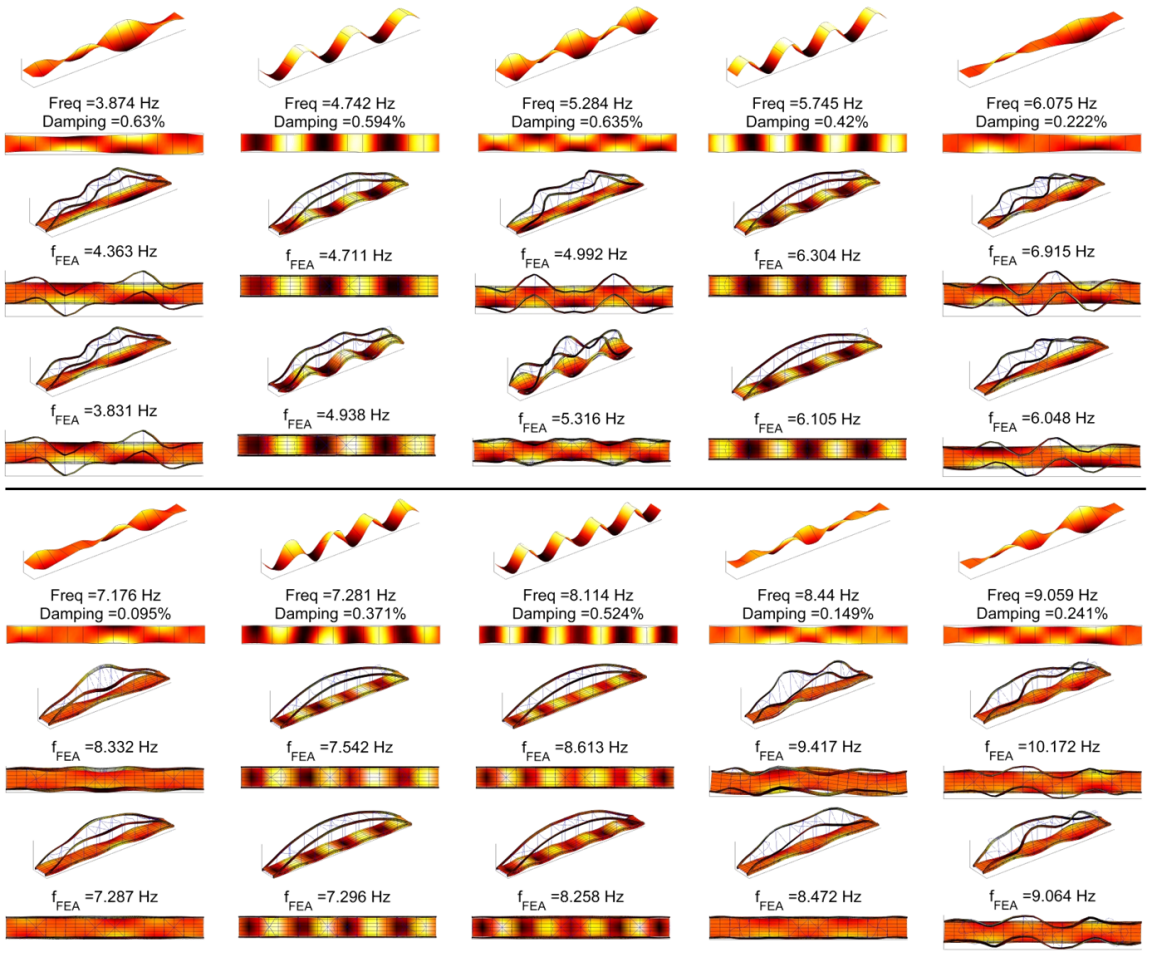

Figure 24: Modal parameter estimates associated with modes eleven through twenty extracted from the experimental measurements (row#1), idealized model (row#2), and calibrated model (row#3)

associated with percent frequency errors below 5%. Conversely, following application of the structural identification routine, eighteen of twenty modes in the model exhibited percentage errors in undamped natural frequency below 5%. Overall, the percentage error in natural frequency improved for sixteen of the twenty modes. The four exceptions correspond to cases where the error in undamped natural frequency in the initial model was less than 3.7%. This reflects the need for the model correlation to sacrifice some of the few instances of strong correlation in the initial model in

order to achieve a more balanced overall improvement in correlation across all of the measured modal parameters.

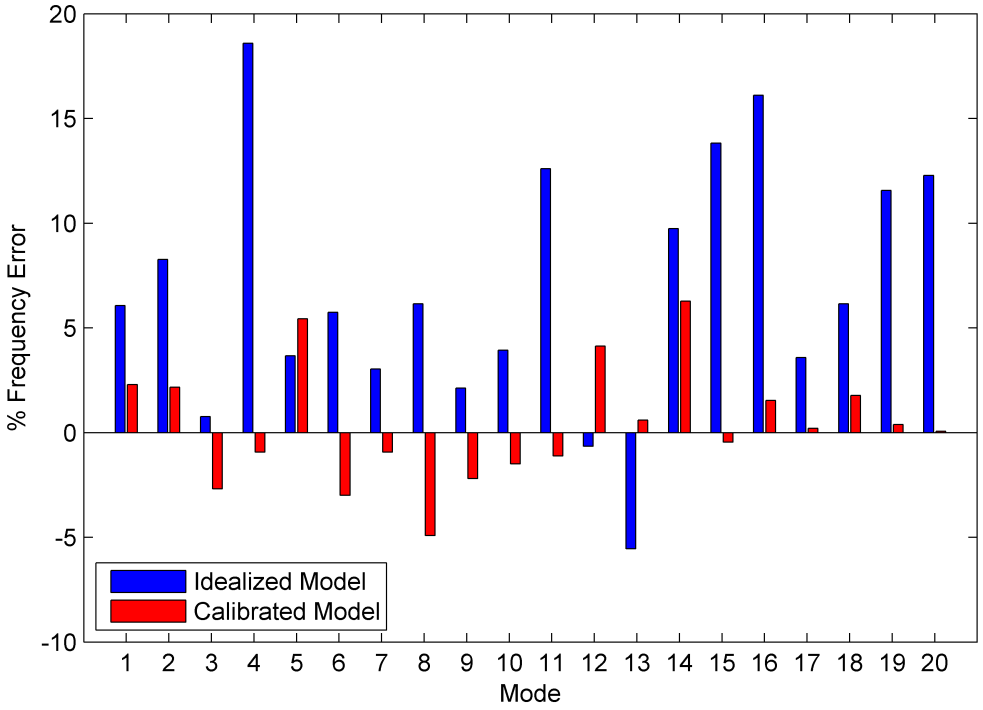

Figure 25: Percent error in frequency estimates before and after calibration of the FE model

Similarly, graphical representation of the correlation between analytical and experimental mode shapes, as quantified by the MAC measure of correlation, for the idealized and calibrated model is presented in Figure 26. As evidenced in this figure, only one mode (#9) reflected a decrease in MAC correlation, although the change did not exceed 1.1%, while the rest of the calibrated modes exhibited a moderate to significant increase in MAC correlations. Specifically, ten calibrated modes experienced a significant increased in MAC correlation over 10%, with five of these modes reaching over 20% improvement in MAC correlations, including two exceeding 35%

improvement. Such overall strong improvement associated with higher calculated MAC values between the experimental and calibrated modes is attributed to a large parameter selection with diverse sensitivity and a wider population size in the genetic algorithm.

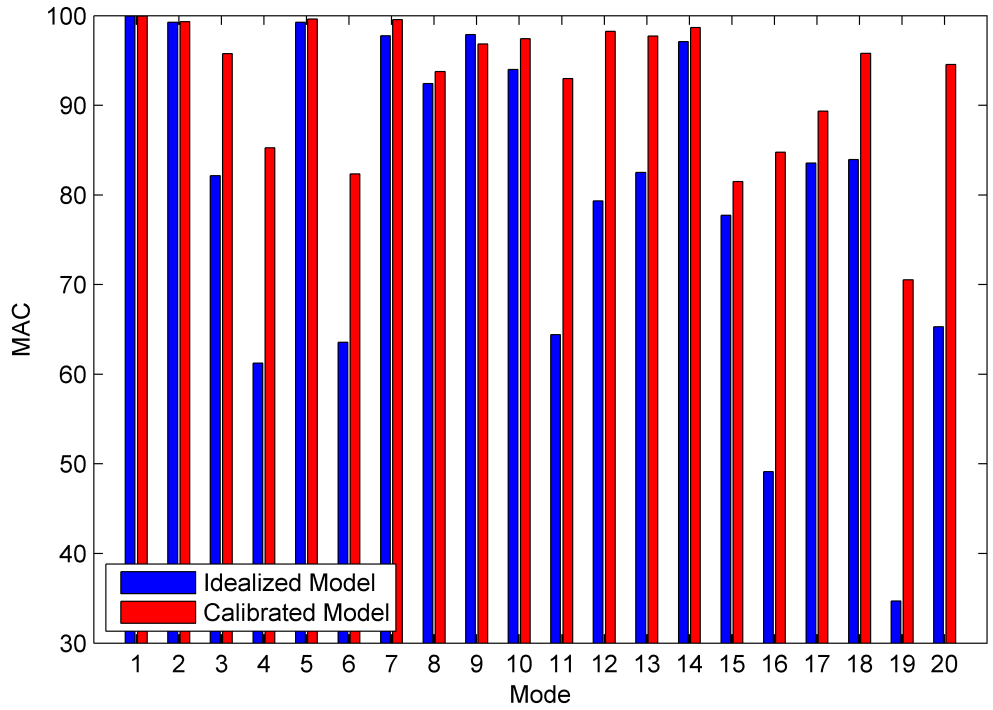

Figure 26: Modal correlation before and after calibration of the FE model

The improvement in model correlation exhibited from calibration of all 12 uncertain parameters is also presented in tabular form in order to assist in comparing and quantifying the relative improvement of the calibrated model over the idealized model across all 20 modes (Table 8). Overall, the average absolute percentage error in undamped natural frequencies from the idealized to the calibrated model was reduced from 7.52% to 2.13%, and the average MAC value for the mode shape estimates increased from 80.26% to 92.70%. The overall improvement in model correlation is

mainly reflected in significant improvements in the correlation of modal parameters for the torsional bending modes. For these modes, the average absolute percentage error in natural frequencies was reduced from 9.74% to 1.56% and the average MAC correlation across the mode shapes was increased from 69.74% to 88.78%. Although improvement in the correlation of modal parameters for the vertical bending modes is not as significant as the improvement for the torsional bending modes, vertical bending modes still contributed towards overall improvement in model correlation. Similarly, for the vertical bending modes, the average absolute percentage error in natural frequencies was reduced from 4.81% to 2.82% and the average MAC correlation across the mode shapes was increased from 93.12% to 97.49%. The overall exceptionally strong correlation between the experimental measurements and the calibrated model can be summarized by an average absolute percentage error improvement in natural frequency predictions of over 6.0% and an average MAC improvement of over 12%. Although the strongest model correlation was achieved when twelve parameters were calibrated within the finite element model and twenty modes shapes were used in the optimization routine, model correlation improvements between the measured and the calibrated modal parameters relative to the idealized model for all other 15 cases of the structural identification implementation are provided in Appendix C.

An additional graphical tool popular for presenting model correlation and improvement in model correlation is the "Modal Assurance Criterion with Frequency Scales" FMAC plot, which can be used to simultaneously present both the natural frequency errors and strength of the MAC correlation between experimental and analytical models (Fotsch and Ewins, 2000). Within FMAC plots, the degree of frequency correlation

Table 8: Model correlation improvement when 12 parameters within the finite element model were calibrated and 20 modes were compared in the model updating routine

Mode	f_{exp} (Hz)	Idealized Model			Calibrated Model			Improvement	
		f_{FE} (Hz)	Δ (%)	MAC (%)	f_{FE} (Hz)	Δ (%)	MAC (%)	Δ (%)	MAC (%)
1	0.619	0.656	6.07	99.95	0.633	2.29	99.95	3.78	0.00
2	1.212	1.313	8.27	99.27	1.239	2.16	99.33	6.11	0.06
3	1.328	1.338	0.77	82.16	1.292	-2.69	95.76	-1.92	13.6
4	1.571	1.863	18.6	61.23	1.556	-0.93	85.25	17.7	24.0
5	1.727	1.790	3.67	99.28	1.820	5.43	99.62	-1.76	0.34
6	2.117	2.238	5.74	63.57	2.053	-3.00	82.33	2.74	18.8
7	2.354	2.425	3.04	97.75	2.332	-0.93	99.56	2.11	1.82
8	2.851	3.027	6.15	92.42	2.711	-4.92	93.77	1.24	1.35
9	3.484	3.558	2.12	97.88	3.408	-2.20	96.85	-0.08	-1.03
10	3.624	3.766	3.93	94.00	3.570	-1.49	97.44	2.44	3.44
11	3.874	4.363	12.6	64.40	3.831	-1.12	92.99	11.5	28.6
12	4.742	4.711	-0.65	79.35	4.938	4.13	98.26	-3.48	18.9
13	5.284	4.992	-5.54	82.52	5.316	0.60	97.74	4.94	15.2
14	5.745	6.304	9.74	97.09	6.105	6.27	98.69	3.46	1.59
15	6.075	6.915	13.8	77.74	6.048	-0.45	81.51	13.4	3.77
16	7.176	8.332	16.1	49.14	7.287	1.54	84.78	14.6	35.6
17	7.281	7.542	3.58	83.54	7.296	0.21	89.36	3.37	5.82
18	8.114	8.613	6.15	83.94	8.258	1.78	95.79	4.37	11.8
19	8.440	9.417	11.6	34.69	8.472	0.38	70.52	11.2	35.8
20	9.059	10.17	12.3	65.31	9.064	0.06	94.55	12.2	29.2
Average	-	-	7.52	80.26	-	2.13	92.70	5.39	12.44

is represented by the location of circles with respect to a 45 degree line that indicates perfect prediction of the experimental natural frequency by the analytical model. Points above this line indicate that the natural frequency in the model is higher than experimentally measured and, conversely, points below the line are modes where the model underpredicts the natural frequency. The diameter of the circles corresponds to strength of the MAC correlation where the larger in diameter the circles are, the greater the strength of the MAC correlation is. FMAC plots were generated for both the idealized and the calibrated model in order to further explore overall improvement by taking into account the degree of frequency correlation as well as the strength of the MAC correlation among all 20 modes. In the plots, an additional feature has been introduced, which is to present the vertical modes in blue and the torsional modes in red. As shown in Figure 27, the FMAC for the idealized model clearly exhibits an overly stiff response, particularly for the higher frequency modes, and

the strength of the mode shape correlation is significantly weaker for the torsional modes. Following the application of the genetic algorithm for model updating, the discrepancies between measured and predicted natural frequencies were reduced and are more balanced about the 45 degree line that represents perfect model correlation. Likewise, both vertical and torsional modes exhibit strong MAC correlation with the experimental estimates following the model updating.

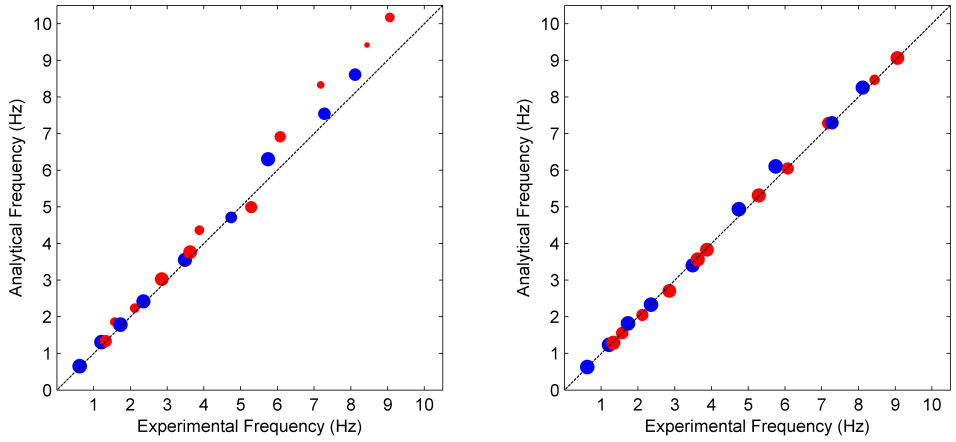

Figure 27: Model correlation between idealized (left FMAC plot) and calibrated (right FMAC plot) models with respect to the experimental measurements

CHAPTER 6: SUMMARY

6.1 Concluding Remarks

This thesis promotes the application of structural identification and seeks to expand the limited database of structural identification studies employing genetic algorithms for model updating by presenting a real-world case study using ambient vibration monitoring data. A series of FE model updating problems were structured around experimentally measured modal parameter estimates for a tied arch bridge span to investigate the influence of the problem setup on the results of the structural identification. Specifically, the study examined the effects on the model correlation and variability of parameter assignments resulting from varying both the number of modes included in the objective function and the number of uncertain parameters included in the model updating routine.

To characterize the dynamic properties of the structure, output-only system identification was applied to experimental measurements obtained from an in-service bridge using stochastic subspace identification and strategies to improve the experimental estimation of the modal parameters were presented in the application. A preliminary idealized finite element model of the structure was developed and linear modal analysis was performed to quantify the initial correlation between the experimentally measured and the analytically predicted natural frequencies and modes shapes.

To facilitate selection of the most meaningful uncertain parameters in the model for FE model updating, sensitivity analysis was conducted and the results were used to order the sets of uncertain parameters used in a series of FE model updating problems. Techniques including parallelization of the genetic algorithm and use of integer constraints were introduced within the optimization routine to facilitate accelerated convergence of the objective function and reduce the time associated with the exploration of large population sizes.

Across the 16 scenarios of FE model updating problems performed, the highest model correlation was achieved by including all 20 modes in the objective function and all 12 uncertain parameters in the model updating routine. For this scenario, the average absolute percent error in natural frequency prediction across the 20 modes was reduced from 7.52% to 2.13%. Additionally, the average MAC correlation computed across the 20 modes was improved from 80.26% to 92.70%. Results from the sixteen FE model updating scenarios were analyzed to examine the effects of varying both the number of modes included in the objective function and the number of uncertain parameters included in the model updating routine on the model correlation achieved through model updating as well as on the variability of parameter assignments identified. The results suggest that the parameter assignments identified through the structural identification framework are significantly influenced more by the number of modes included in the objective function than the number of uncertain parameters included. However, the inclusion of additional uncertain parameters can result in significant improvements in the model correlation achieved. Analysis of the elite individuals in the final generations of each application of the genetic algorithm

revealed that increased variability, or uncertainty, in the identified parameter assignments was generally present as the number of uncertain parameters included in the model updating was increased.

6.2 Future Research

Throughout this thesis, several recommendations for future research were suggested to improve, or provide improved insight into, the application of structural identification using genetic algorithms to solve the FE model updating problem. These recommendations are summarized below.

- The current study adopted an objective function that remained fixed throughout the analysis, although the number of modes included in the objective function was allowed to vary to investigate the effects resulting from 16 different scenarios of model updating. Exploration of the effects resulting from varying the relative weighting factors associated with the eigenvalue and eigenvector residuals in the objective function may provide additional insight into their effects on model correlation and variation in identified parameter assignments. Furthermore, a variety of different forms of objective functions for model updating have been proposed throughout the literature and these could be investigated to assess their impact on the performance of the structural identification routine.

- This study used a simple technique to perform sensitivity analysis for the uncertain parameters to rank the sensitivity ahead of the model updating. However, the results suggest that the sensitivity analysis was too simplistic and may not have considered important interactions between parameters and their effects on

model correlation. It is recommended that future research explore the use of more advanced sensitivity analysis routines to consider such potential interactions to improve the ranking of uncertain parameters.

- The study used a fixed number of generations as a stopping criteria of the genetic algorithm. Convergence plots for the objective function suggested that convergence had generally been achieved, but cases involving a large number of uncertain parameters exhibited more diversity in their elites. Future work could explore the influence of using a larger number of generations or alternative stopping criteria on the results of the analysis.

- This study generated conclusions based on results obtained from application to a single experimental case study. The conclusions drawn should be verified by applying the techniques described to numerical models with known solutions as well as validated by application across a large set of experimental studies.

REFERENCES

H. Adeli and N. Cheng. Integrated Genetic Algorithm for Optimization of Space Structures. *Journal of Aerospace Engineering*, 6(4):315–328, October 1993.

H. Ahmadian, J. Mottershead, and M. Friswell. Regularisation Methods for Finite Element Model Updating. *Mechanical Systems and Signal Processing*, 12(1):47–64, January 1998.

R. Allemang. The Modal Assurance Criterion (MAC): Twenty Years of Use and Abuse. *Sound and Vibration*, 37(8):14–23, 2003.

ASCE. 2013 Report Card for America's Infrastructure, March 2013.

ASCE SEI. Structural Identification of Constructed Facilities: Approaches, Methods and Technologies for Effective Practice of St-Id. A state-of-the-art report, ASCE, 2011.

P. Bakir, E. Reynders, and G. De Roeck. Sensitivity-Based Finite Element Model Updating Using Constrained Optimization with a Trust Region Algorithm. *Journal of Sound and Vibration*, 305(1-2):211–225, August 2007.

J. Bendat and A. Piersol. *Engineering Applications of Correlation and Spectral Analysis*. John Wiley & Sons, 2 edition, 1993.

J. Brownjohn, A. De Stefano, Y. Xu, H. Wenzel, and E. Aktan. Vibration-based Monitoring of Civil Infrastructure: Challenges and Successes. *Journal of Civil Structural Health Monitoring*, 1(3):79–95, December 2011.

J. Caicedo and G. Yun. A Novel Evolutionary Algorithm for Identifying Multiple Alternative Solutions in Model Updating. *Structural Health Monitoring*, 10(5): 491–501, September 2011.

E. Cantú-Paz. *Efficient and Accurate Parallel Genetic Algorithms*. Kluwer Academic Publishers, 1 edition, 2001.

L. Chambers. *Practical Handbook of Genetic Algorithms: Applications*, volume 1. CRC Press, 1995.

S. Doebling, C. Farrar, and M. Prime. A Summary Review of Vibration-Based Damage Identification Methods. *The Shock and Vibration Digest*, 30:91–105, March 1998.

J. Dyer, R. Hartfield, G. Dozier, and J. Burkhalter. Aerospace design optimization using a steady state real-coded genetic algorithm. *Applied Mathematics and Computation*, 218(9):4710–1730, January 2012.

E. Aktan, N. Çatbaş, A. Türer, and Z. Zhang. Structural Identification: Analytical Aspects. *Journal of Structural Engineering*, 124(7):817–829, July 1998.

A. Felber. *Development of a Hybrid Bridge Evaluation System*. PhD thesis, The University of British Columbia, Canada, December 1993.

FHWA. 2013 National Bridge Inventory. Technical Report, U.S. Federal Highway Administration, 2013.

D. Fotsch and D. Ewins. Applications of MAC in the Frequency Domain. In *Proceedings, International Modal Analysis Conference*, pages 1225–1231, 2000.

M. Friswell and J. Mottershead. *Finite Element Model Updating in Structural Dynamics*. Kluwer Academic Publishers, 1 edition, 1995.

M. Friswell, J. Penny, and S. Garvey. A Combined Genetic and Eigensensitivity Algorithm for the Location of Damage in Structures. *Computer and Structures*, 69 (5):547–556, December 1998.

C. Fritzen. Vibration-Based Structural Health Monitoring Concepts and Applications. *Key Engineering Materials*, 293-294:3–20, September 2005.

H. Hao and Y. Xia. Vibration-based Damage Detection of Structures by Genetic Algorithm. *Journal of Computing in Civil Engineering*, 16(3):222–229, 2002.

B. Jaishi and W. Ren. Structural Finite Element Model Updating Using Ambient Vibration Test Results. *Journal of Structural Engineering*, 131(4):617–628, April 2005.

T. Janter and P. Sas. Uniqueness Aspects of Model-updating Procedures. *AIAA Journal*, 28(3):538–543, 1990.

G. Jones, P. Willett, and R. Glen. Molecular Recognition of Receptor Sites Using a Genetic Algorithm with a Description of Desolvation. *Journal of Molecular Biology*, 245(1):43–53, 1995.

T. Kernicky. Structural Identification and Damage Characterization of a Full-scale Masonry Building Subject to Internal Blast Load. Master's thesis, The University of North Carolina at Charlotte, 2013.

T. Kernicky, M. Whelan, D. Weggel, and C. Rice. Structural Identification and Damage Characterization of a Masonry Infill Wall in a Full-Scale Building Subjected to Internal Blast Load. *Journal of Structural Engineering*, 141, September 2014.

MathWorks, Inc. *Global Optimization Toolbox User's Guide*. 3 Apple Hill Drive. Natick, MA 01760-2098, September 2015.

J. McCall. Genetic Algorithms for Modelling and Optimization. *Journal of Computational and Applied Mathematics*, 184(1):205–222, December 2005.

Measurement Specialties, Inc. *Model 4000A & 4001A Accelerometer*. 32 Journey Ste. 150 Aliso Viejo, CA 92656, January 2010.

M. Mitchell. *An introduction to genetic algorithms*. MIT Press, 1 edition, 1996.

J. Moss. Vibration Analysis of a Steel Twin I-girder Pedestrian Bridge: Structural Identification and Evaluation of Pedestrian Excitation Models. Master's thesis, The University of North Carolina at Charlotte, 2015.

J. Mottershead, M. Link, and M. Friswell. The Sensitivity Method in Finite Element Model Updating: A Tutorial. *Mechanical Systems and Signal Processing*, 25(7): 2275–2296, October 2011.

N. Niedbal. Analytical Determination of Real Normal Modes from Measured Complex Responses. In *Proceedings of the 25th Structures, Structural Dynamics and Materials Conference*, pages 292–295, Palm Springs, CA, May 1984.

P. Van Overschee and B. De Moor. *Subspace Identification for Linear Systems: Theory-Implementation-Applications*. Kluwer Academic Publishers, 1996.

H. Pandey, A. Chaudharya, and D. Mehrotra. A comparative Review of Approaches to Prevent Premature Convergence in GA. *Applied Soft Computing*, 24:1047–1077, November 2014.

B. Peeters. *System Identification and Damage Detection in Civil Engineering*. PhD thesis, Katholieke Universiteit Leuven, Belgium, December 2000.

W. Ren, T. Zhao, and I. Harik. Experimental and Analytical Modal Analysis of Steel Arch Bridge. *Journal of Structural Engineering*, 130(7):1022–1031, June 2004.

D. Ribeiro, R. Calçada, R. Delgado, M. Brehm, and V. Zabel. Finite Element Model Updating of a Bowstring-arch Railway Bridge Based on Experimental Modal Parameters. *Engineering Structures*, 40:413–435, July 2012.

A. Rytter. *Vibration Based Inspection of Civil Structures*. PhD thesis, Aalborg University, Denmark, May 1993.

S. Sivanandam and S. Deepa. *An introduction to genetic algorithms*. Springer, 1 edition, 2007.

Texas Instruments Incorporated. *Quad/Octal, Simultaneous Sampling, 16-Bit Analog-to-Digital Converters*, September 2008.

Texas Instruments Incorporated. *A True System-on-Chip Solution for 2.4-GHz IEEE 802.15.4 and ZigBee Applications*, February 2011.

U.S. Department of Transportation, Federal Highway Administration and Federal Transit Administration. 2013 Status of the Nation's Highways, Bridges, and Transit: Conditions & Performance, 2014.

H. Wenzel and D. Pichler. *Ambient Vibration Monitoring*. Wiley, 1 edition, 2005.

M. Whelan. Design and Application of a Wireless Sensor Network for Vibration-based Performance Assessment of a Tied Arch Bridge. In *Structural Health Monitoring 2011*, pages 709–716, September 2011.

M. Whelan and K. Janoyan. Design of a Robust, High-rate Wireless Sensor Network for Static and Dynamic Structural Monitoring. *Journal of Intelligent Material Systems and Structures*, 20(7):849–864, 2009.

M. Whelan and K. Janoyan. In-Service Diagnostics of a Highway Bridge from a Progressive Damage Case Study. *Journal of Bridge Engineering*, 15(5):597–607, September 2010.

M. Whelan, M. Gangone, K. Janoyan, and R. Jha. Real-time Wireless Vibration Monitoring for Operational Modal Analysis of an Integral Abutment Highway Bridge. *Engineering Structures*, 31(10):2224–2235, October 2009.

M. Whelan, M. Gangone, and K. Janoyan. Effect of Sensor Placement on Operational Modal Analysis of Steel Girder Bridges. *Smart Sensor Phenomena, Technology, Networks, and Systems 2011*, Proc. of SPIE Vol. 7982, April 2011.

M. Whelan, N. Salas Zamudio, and T. Kernicky. Structural Identification of a Tied Arch Bridge from Ambient Vibration Monitoring with a Wireless Sensor Network. *Engineering Structures*, 2016.

B. Zárate and J. Caicedo. Finite Element Model Updating: Multiple Alternatives. *Engineering Structures*, 30(12):3724–3730, December 2008.

Y. Zhou, J. Prader, J. Weidner, N. Dubbs, F. Moon, and E. Aktan. Structural Identification of a Deteriorated Reinforced Concrete Bridge. *Journal of Bridge Engineering*, 17(5):774–787, September 2012.

D. Zimmerman, K. Yap, and T. Hasselman. Evolutionary Approach for Model Refinement. *Mechanical Systems and Signal Processing*, 13(4):609–625, July 1999.

APPENDIX A: MATLAB ROUTINE USING OAPI TO COMMUNICATE WITH SAP2000

This section provides the MATLAB script used to interface with SAP2000 and build the parameterized mass and stiffness matrices.

```
clear all
%Define lower and upper bounds
lb=[1;50;1;50;1;75;50;50;1400;50;1000;50];
ub=[100;150;1000;150;100;150;150;150;3400;150;100000;150];
scale=[0.01;0.01;200;0.01;0.01;0.01;0.01;0.01;10;0.01;200;0.01];

Pop(1,:)=lb;
for k=1:numel(lb)
    Pop(k+1,:)=Pop(1,:);
    Pop(k+1,k)=ub(k);
end

for k=1:12
Pop(:,k)=Pop(:,k)*scale(k);
end

%Establish Model
root=strcat(cd,'\');
root='C:\Users\Matthew\Desktop\SAPNeal\2 Final IDEALIZED SAP MODEL 2\'

%Establish Global Optimization Problem
for k=1:numel(lb)+1
    params=Pop(k,:);
    clear SapObject SapModel
    feature('COM_SafeArraySingleDim',1);
    feature('COM_PassSafeArrayByRef',1);
    SapObject = actxserver('sap2000v15.SapObject');
    SapObject.ApplicationStart(6,'True');
    SapModel = SapObject.SapModel;
    ret = SapModel.InitializeNewModel(6); %#ok<*NASGU>
    ret = SapObject.SapModel.File.OpenFile(strcat(root...
        ,['/ORIGINAL MODEL - DO NOT MODIFY'...
        '/Matrix_012315_Updated_Z_X_springs_v15.sdb']));

%*****************************************************************
%****   INITIALIZING SAP WINDOW AND ESTABLISHING NEW MODEL     ****
%*****************************************************************
fprintf('Set Model Units to kN, m, C\n')
ret=SapObject.SapModel.SetPresentUnits(6)
%Delete Results
fprintf('Delete Results\n')
ret=SapObject.SapModel.Analyze.DeleteResults('MODAL',1)
%Unlock Model
fprintf('Unlock Model\n')
```

```
ret=SapObject.SapModel.SetModelIsLocked(false)
fprintf('Set Model Units to kN, m, C\n')
ret=SapObject.SapModel.SetPresentUnits(6)
fprintf('Set Gravity Load\n')
ret = SapObject.SapModel.AreaObj.SetLoadGravity('ALL'...
    ,'DEAD',0,0,1,true,'Global',1)

%params(9)=Elastic Modulus of Deck Concrete
fprintf('Set Concrete Modulus\n')
ret = SapObject.SapModel.PropMaterial.SetMPIsotropic('4000Psi'...
    ,params(9)*1000,0.2,0)

%params(NOT)=Concrete Unit Weight
fprintf('Set Concrete Mass Density\n')
ret = SapObject.SapModel.PropMaterial.SetWeightAndMass('4000Psi'...
    ,2,2.4)

%params(-17)=Rotational Fixity of Floor Beams
fprintf('Set Floor Beam Releases to Fixed\n')
ret = SapObject.SapModel.FrameObj.SetReleases('FloorBeamUpdate'...
    ,[false,false,false,false,false,false]'...
    ,[false,false,false,false,false,false]'...
    ,[0,0,0,0,0,0]',[0,0,0,0,0,0]',1)
fprintf('Set Floor Beam Modifier\n')
ret = SapObject.SapModel.FrameObj.SetModifiers('FloorBeamUpdate'...
    ,[1,1,1,1,1,1,1,1]',1)

%params(1)=Rotational Fixity of Arch Laterals
%params(5)=Rotational Fixity of Arch Diagonals
fprintf('Set Top Lateral Releases to Fixed\n')
ret = SapObject.SapModel.FrameObj.SetReleases('TopLateralUpdate'...
    ,[false,false,false,false,false,false]'...
    ,[false,false,false,false,false,false]'...
    ,[0,0,0,0,0,0]',[0,0,0,0,0,0]',1)
fprintf('Set Top Diagonal Releases to Fixed\n')
ret = SapObject.SapModel.FrameObj.SetReleases('TopDiagonalUpdate'...
    ,[false,false,false,false,false,false]'...
    ,[false,false,false,false,false,false]'...
    ,[0,0,0,0,0,0]',[0,0,0,0,0,0]',1)
fprintf('Set Top Lateral Modifiers\n')
ret = SapObject.SapModel.FrameObj.SetModifiers('TopLateralUpdate'...
    ,[1,1,1,1,1,params(1),1,1]',1)
fprintf('Set Top Diagonal Modifiers\n')
ret = SapObject.SapModel.FrameObj.SetModifiers('TopDiagonalUpdate'...
    ,[1,1,1,1,params(5),1,1,1]',1)

%params(-19)=Rotational Fixity of Deck Diagonal Bracing
fprintf('Set Bottom Diagonal Connection to Fixed\n')
ret = SapObject.SapModel.FrameObj.SetReleases...
    ('BottomDiagonalUpdate'...
    ,[false,false,false,false,false,false]'...
    ,[false,false,false,false,false,false]'...
    ,[0,0,0,0,0,0]',[0,0,0,0,0,0]',1);
fprintf('Set Bottom Diagonal Modifiers\n')
```

```
ret = SapObject.SapModel.FrameObj.SetModifiers...
    ('BottomDiagonalUpdate'...
    ,[1,1,1,1,1,1,1,1]',1)
% ret = SapObject.SapModel.FrameObj.SetInsertionPoint...
%     ('BottomDiagonalUpdate',10,false,true,[0,0,-params(11)]'...
%     ,[0,0,-params(11)]','GLOBAL',1)

%params(6)=Flexural Stiffness of Tie Girder Flanges
fprintf('Set Tie Top thickness to 1.5 in\n')
ret = SapObject.SapModel.PropArea.SetShell_1('Tie Top'...
    ,2,true,'A992Fy50',0,0.0381,0.0381)
fprintf('Set Tie Top Property Modifiers\n')
ret = SapObject.SapModel.PropArea.SetModifiers('Tie Top'...
    ,[params(6)*ones(1,8),1,1]')

%params(8)=Flexural Stiffness of Tie Girder Webs
fprintf('Set Tie Sides Property Modifiers\n')
ret = SapObject.SapModel.PropArea.SetModifiers('Tie Side'...
    ,[params(8)*ones(1,8),1,1]')
%params(4)=Flexural Stiffness of Arch Rib Flanges
fprintf('Set RG Top Property Modifiers\n')
ret = SapObject.SapModel.PropArea.SetModifiers('RG Top'...
    ,[params(4)*ones(1,8),1,1]')
%params(2)=Flexural Stiffness of Arch Rib Webs
fprintf('Set RG Sides Property Modifiers\n')
ret = SapObject.SapModel.PropArea.SetModifiers('RG Side'...
    ,[params(2)*ones(1,8),1,1]')

%params(-14)=Flexural Stiffness of Diaphragm Plates
fprintf('Set Diaphragm Plate Property Modifiers\n')
ret = SapObject.SapModel.PropArea.SetModifiers('Diaphram Plate'...
    ,[1*ones(1,8),1,1]')

%params(-13)=Flexural Stiffness of Knuckle Web
fprintf('Set Knuckle Sides Property Modifiers\n')
ret = SapObject.SapModel.PropArea.SetModifiers('KnuckleSides'...
    ,[1*ones(1,8),1,1]')

%params(10)=Axial Stiffness of Stranded Bridge Cable
fprintf('Set Knuckle Sides Property Modifiers\n')
ret = SapObject.SapModel.PropCable.SetModifiers('Cable'...
    ,[params(10),1,1]')

%params(12)=Flexural Stiffness of Longitudinal Stiffeners
fprintf('Set Longitudinal Stiffeners Property Modifiers\n')
ret = SapObject.SapModel.PropArea.SetModifiers('Long Stiffiners'...
    ,[params(12)*ones(1,8),1,1]')

%params(7)=Flexural Stiffness of Parapet
fprintf('Set Parapet Property Modifiers\n')
ret = SapObject.SapModel.PropArea.SetModifiers('Parapet'...
    ,[params(7)*ones(1,8),1,1]')

%params(-16)=Axial Stiffness of Deck Diagonal Bracing
```

```
153 fprintf('Set Bottom Diagonal Property Modifiers\n')
154 ret = SapObject.SapModel.PropFrame.SetModifiers('WT7X41'...
155     ,[1,1,1,1,1,1,1,1]')
156
157 %params(-15)=Axial Stiffness of Arch Diagonals and Laterals
158 fprintf('Set Top Bracing Axial Stiffness Property Modifiers\n')
159 ret = SapObject.SapModel.PropFrame.SetModifiers('RG Cross Bracing'...
160     ,[1,1,1,1,1,1,1,1]')
161
162 %params(NOT)=Knuckle Sides thickness
163 fprintf('Set Knuckle Side Thickness to 1.5in\n')
164 ret = SapObject.SapModel.PropArea.SetShell_1('KnuckleSides'...
165     ,2,true,'A992Fy50',0,0.0381,0.0381)
166
167 %params(3)=Boundary Global X- Spring - Longitudinal
168 %params(-18)=Boundary Global Y-Spring - Lateral
169 %params(11)=Boundary Global Z-Spring - Vertical
170 fprintf('Set BC Springs\n')
171 ret = SapObject.SapModel.PointObj.SetSpring('RollerSpring'...
172     ,[params(3),0,params(11),0,0,0]',1,false,true)
173 ret = SapObject.SapModel.PointObj.SetSpring('PinSpring'...
174     ,[params(3),0,params(11),0,0,0]',1,false,true)
175 ret = SapObject.SapModel.PointObj.SetRestraint('RollerSpring'...
176     ,[false,true,false,false,false,false]',1)
177 ret = SapObject.SapModel.PointObj.SetRestraint('PinSpring'...
178     ,[false,true,false,false,false,false]',1)
179
180 %********************************************************
181 %****          RUN THE INITIAL MODEL ANALYSIS          ****
182 %********************************************************
183 %Need to Save Model Before Analysis
184 ret = SapObject.SapModel.File.Save(strcat(root...
185     ,'MK',num2str(k-1),'.sdb'));
186 ret = SapObject.SapModel.Analyze.SetRunCaseFlag('Linear',1);
187 ret = SapObject.SapModel.Analyze.SetRunCaseFlag('MODAL',0);
188 ret = SapObject.SapModel.Analyze.RunAnalysis();
189 ret = SapObject.SapModel.Results.Setup.SetCaseSelectedForOutput...
190     ('MODAL',0);  %Set case and combo output selections
191 ret = SapObject.SapModel.Results.Setup.SetCaseSelectedForOutput...
192     ('Linear',1);
193 SapObject.ApplicationExit(true);
194 end
195
196 %%   Mass and Stiffness Matrix Assembly
197 for k=1:numel(lb)+1
198 %Import Stiffness Matrix file
199 TK=importdata(strcat(root,'MK',num2str(k-1),'.TXK'));
200 TK=TK.data;
201 %Import Mass Matrix file
202 TM=importdata(strcat(root,'MK',num2str(k-1),'.TXM'));
203 TM=TM.data;
204 n=max(TK(:,1)); %Determine full matrix size
205 %Populate other half of symmetric matrix
206 TK=[[TK(:,1);TK(:,2)],[TK(:,2);TK(:,1)],[TK(:,3);TK(:,3)]];
```

```
207 TK=unique(TK,'rows'); %Remove duplicate reference to diagonal entries
208 K{k}=sparse(TK(:,1),TK(:,2),TK(:,3),n,n);
209 clear TK;
210 TM=[[TM(:,1);TM(:,2)],[TM(:,2);TM(:,1)],[TM(:,3);TM(:,3)]];
211 TM=unique(TM,'rows');
212 M{k}=sparse(TM(:,1),TM(:,2),TM(:,3),n,n);
213 clear TM n;
214 end
215
216 for k=2:numel(lb)+1
217     delK{k-1}=K{k}-K{1};
218     delM{k-1}=M{k}-M{1};
219 end
220
221 %Equation Number Matrix
222 TE=importdata(strcat(root,'MK0.TXE')); %Import Mass Matrix filetk
223 TE=TE.data;
224
225 for k=10001:10024
226     I=find(TE(:,1)==k);
227     TES(k-10000,:)=TE(I,[1,4,3]); %Extract z,y-Coordinate Equation
228 end
229
230 K=K{1};
231 M=M{1};
232
233 %SAVE DATA
234 save(strcat(['\\Parallel17\Cluster\Cluster\'
235     'Cluster_WisconsinBridge\'...
236     'MK_WiscBridge_BEST_12params_01302015.mat']),...
237     ,'K','M','delK','delM','TES');
```

APPENDIX B: PARAMETER HISTOGRAMS

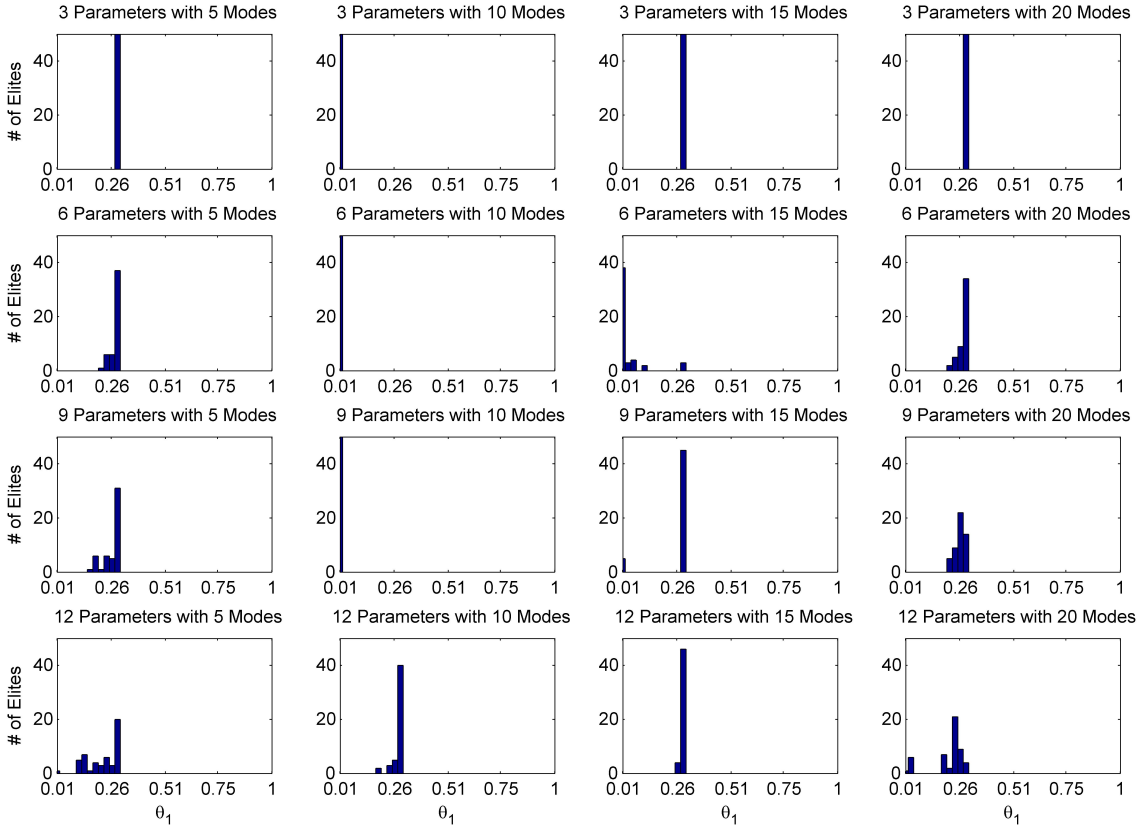

Figure 28: Parameter θ_1, rotational fixity of arch laterals, assignments associated with the 50 elites in the final generations of each structural identification case

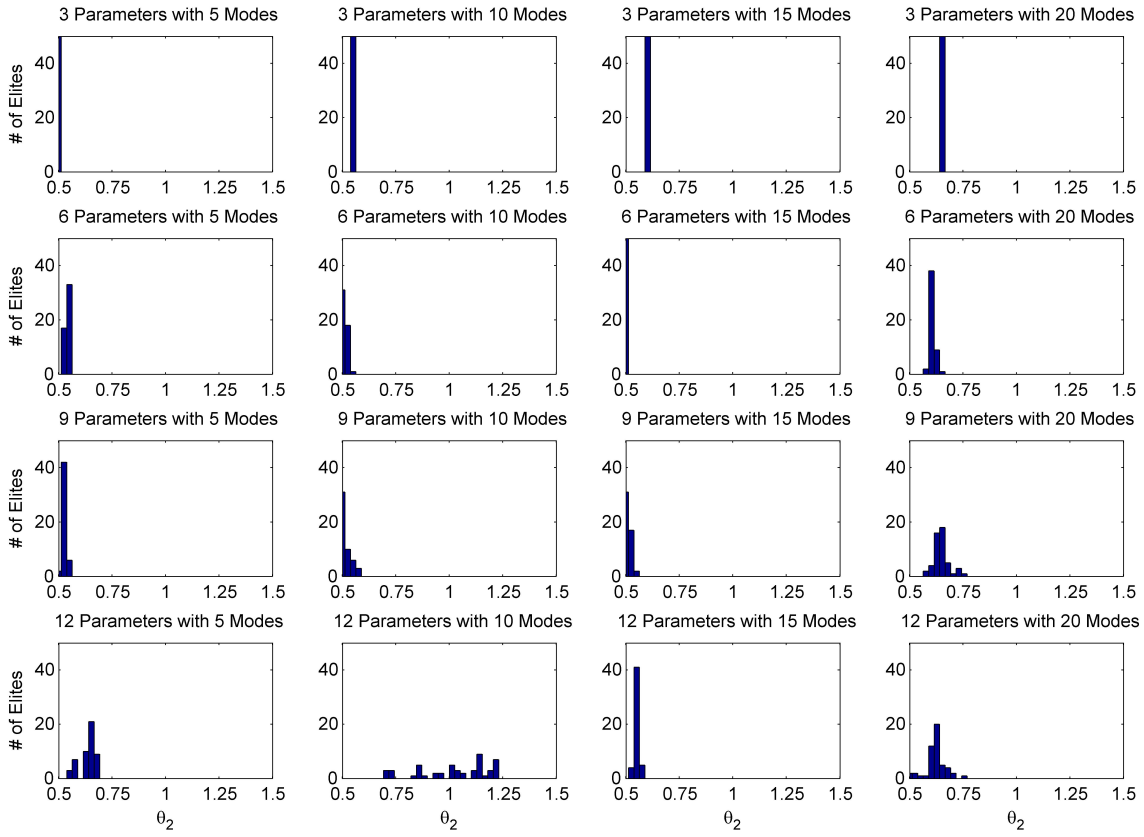

Figure 29: Parameter θ_2, flexural stiffness of arch rib webs, assignments associated with the 50 elites in the final generations of each structural identification case

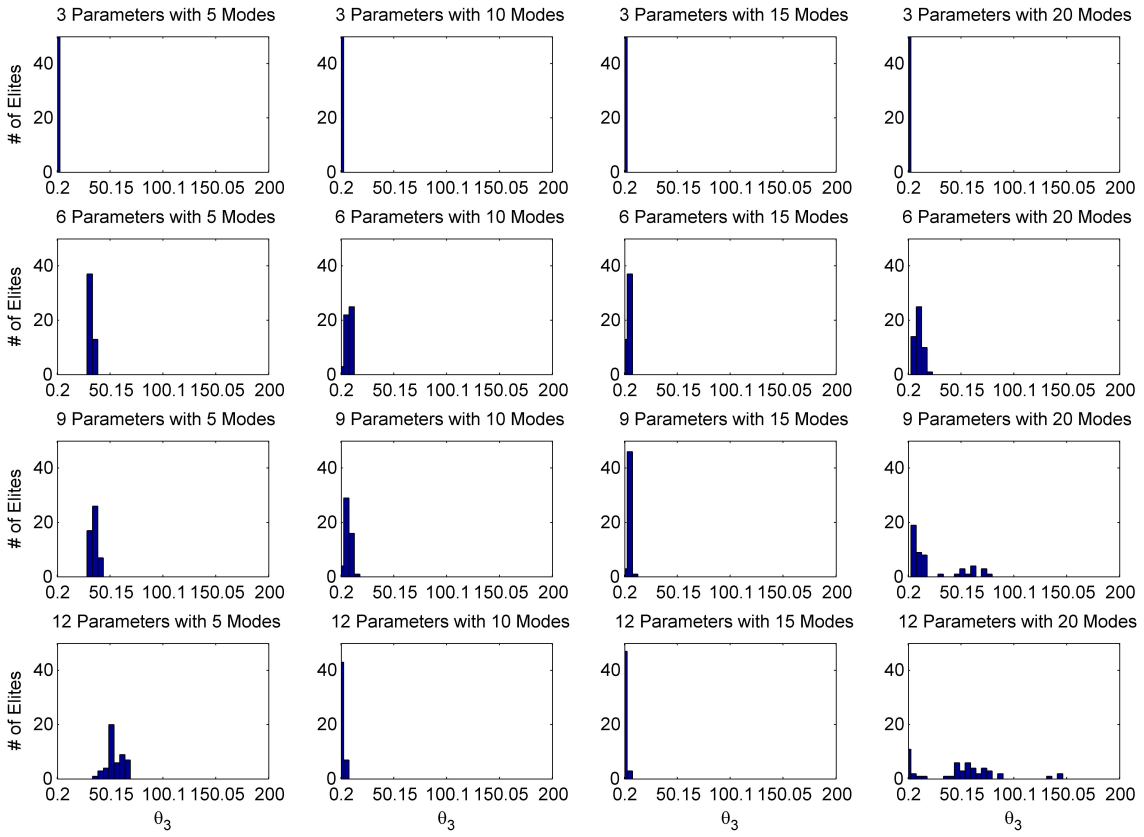

Figure 30: Parameter θ_3, boundary global x-spring - longitudinal, assignments associated with the 50 elites in the final generations of each structural identification case

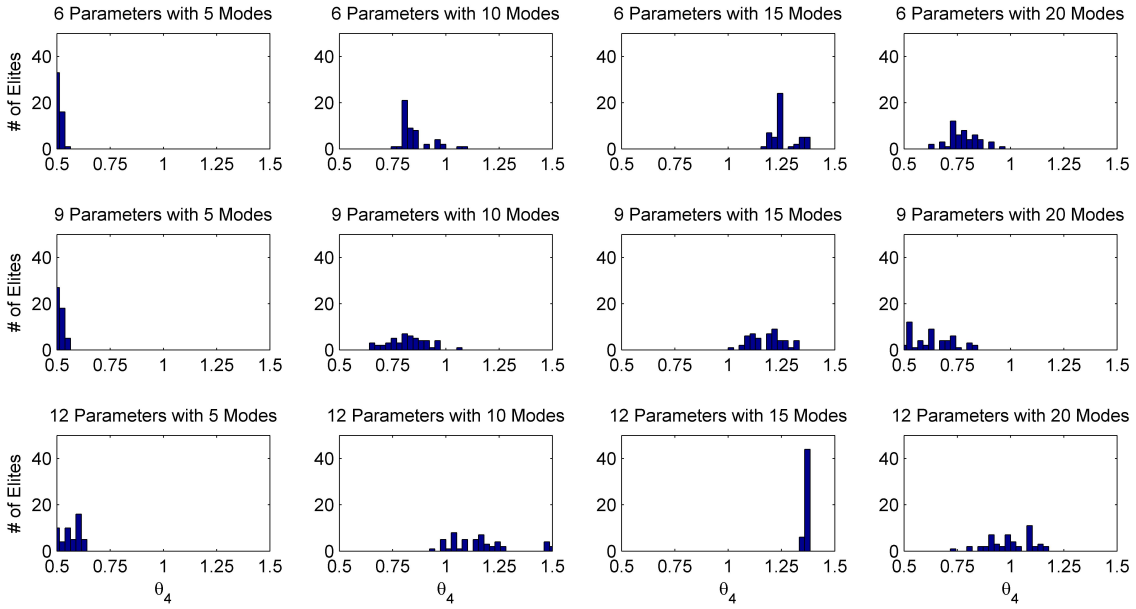

Figure 31: Parameter θ_4, flexural stiffness of arch rib flanges, assignments associated with the 50 elites in the final generations of each structural identification case

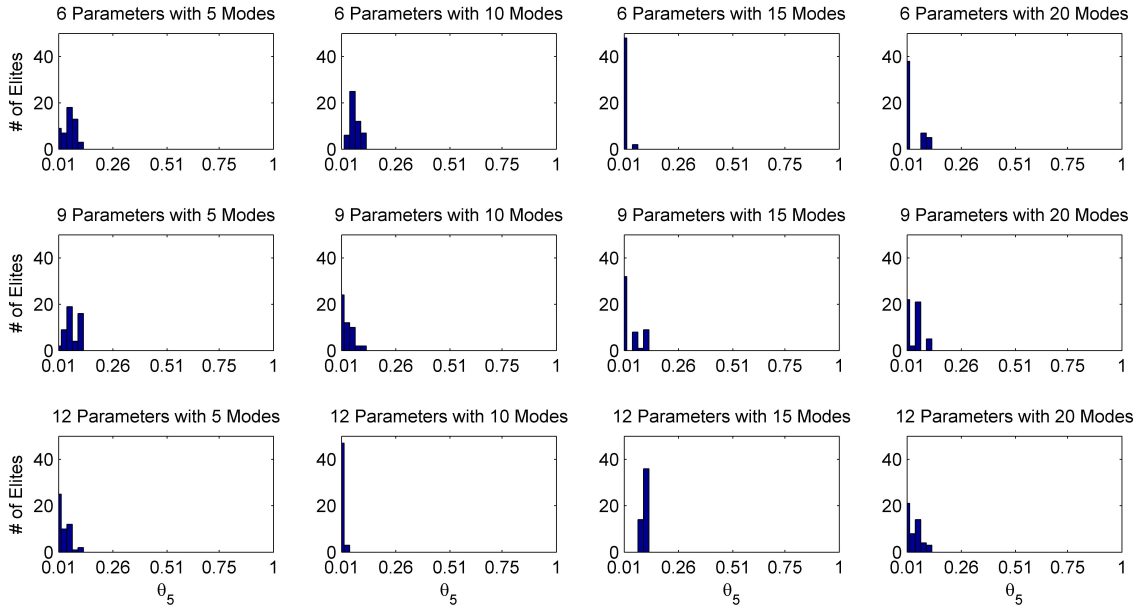

Figure 32: Parameter θ_5, rotational fixity of arch diagonals, assignments associated with the 50 elites in the final generations of each structural identification case

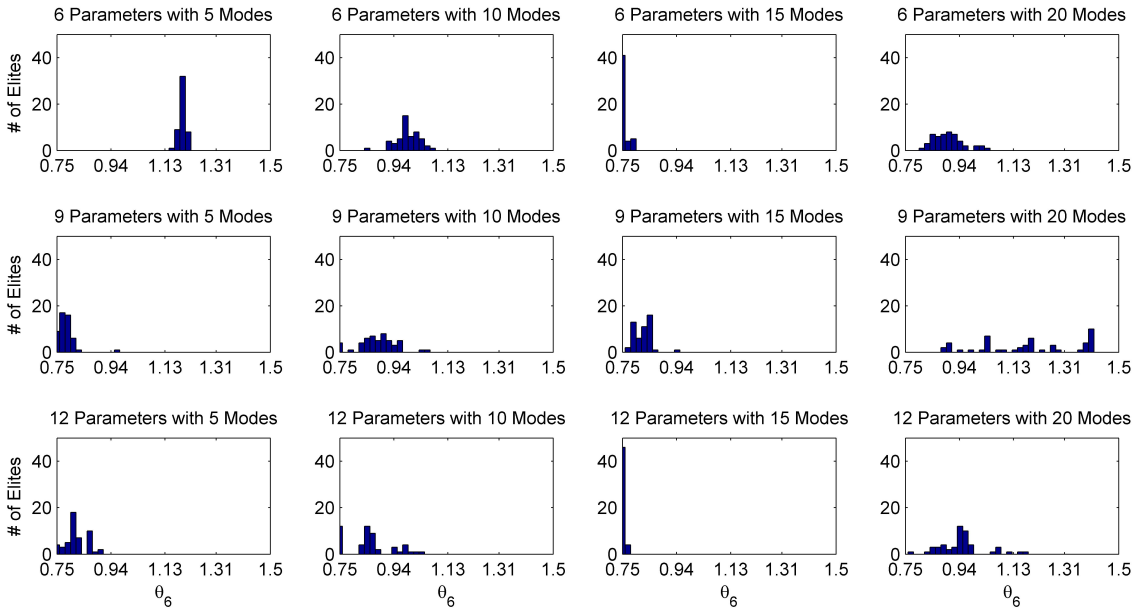

Figure 33: Parameter θ_6, flexural stiffness of tie girder flanges, assignments associated with the 50 elites in the final generations of each structural identification case

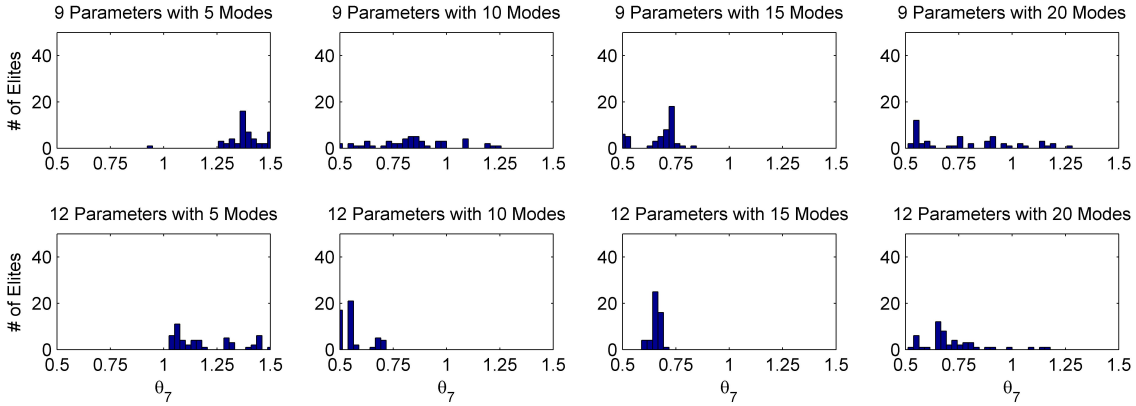

Figure 34: Parameter θ_7, flexural stiffness of parapet, assignments associated with the 50 elites in the final generations of each structural identification case

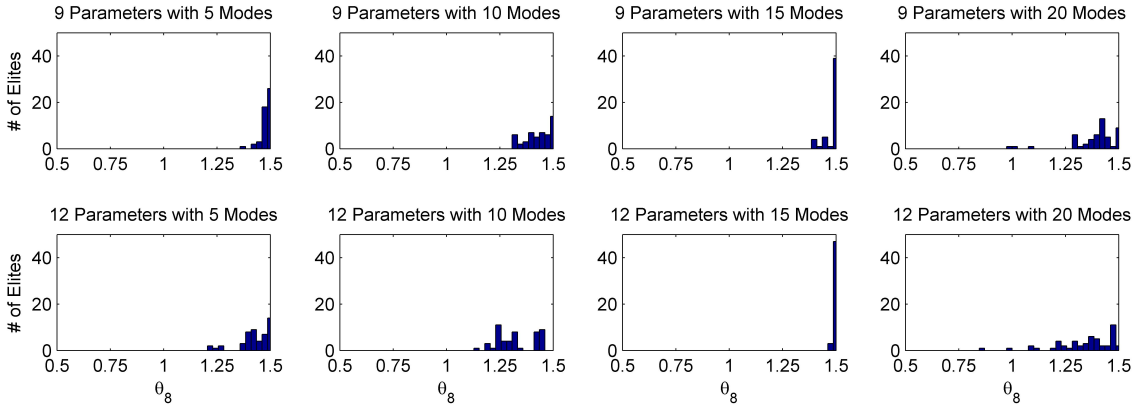

Figure 35: Parameter θ_8, flexural stiffness of tie girder webs, assignments associated with the 50 elites in the final generations of each structural identification case

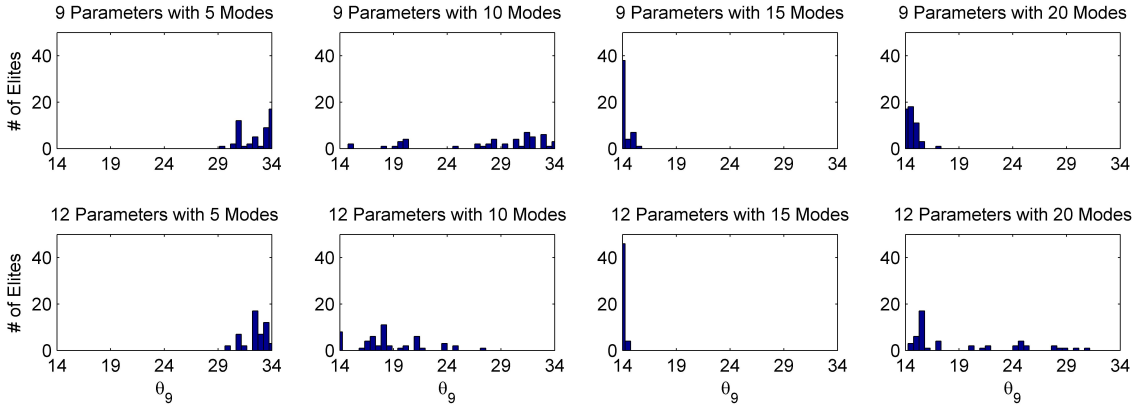

Figure 36: Parameter θ_9, elastic modulus of deck concrete, assignments associated with the 50 elites in the final generations of each structural identification case

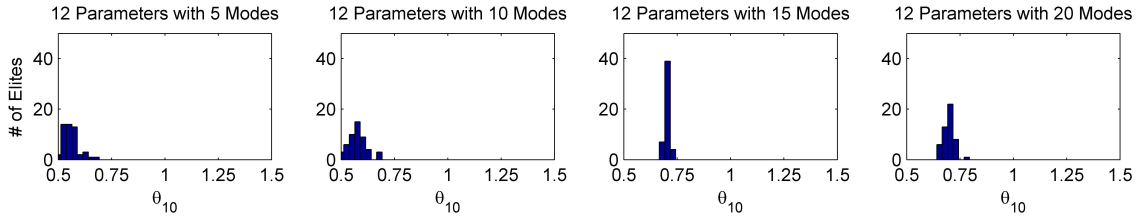

Figure 37: Parameter θ_{10}, axial stiffness of stranded bridge cable, assignments associated with the 50 elites in the final generations of each structural identification case

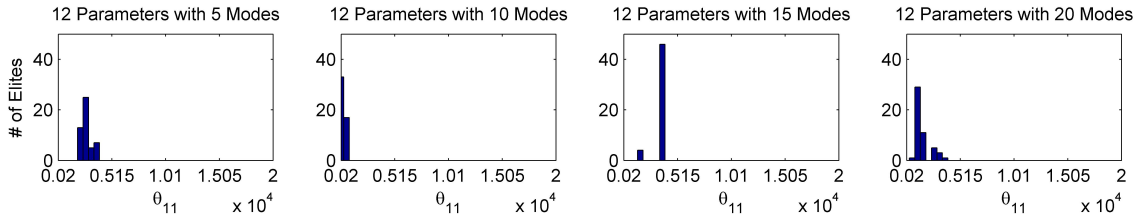

Figure 38: Parameter θ_{11}, boundary global z-spring - vertical, assignments associated with the 50 elites in the final generations of each structural identification case

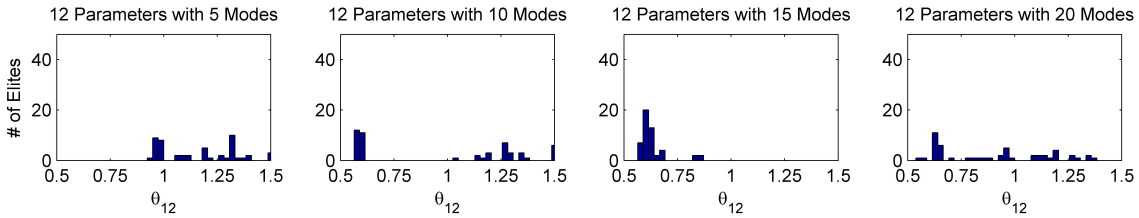

Figure 39: Parameter θ_{12}, flexural stiffness of longitudinal stiffeners, assignments associated with the 50 elites in the final generations of each structural identification case

APPENDIX C: SUMMARY OF MODEL CORRELATION IMPROVEMENT BETWEEN INITIAL IDEALIZED AND CALIBRATED FINITE ELEMENT MODELS

Table 9: Model correlation improvement when 3 parameters within the finite element model were calibrated and 5 modes were compared in the model updating routine

Mode	f_{exp} (Hz)	Idealized Model			Calibrated Model			Improvement	
		f_{FE} (Hz)	Δ (%)	MAC (%)	f_{FE} (Hz)	Δ (%)	MAC (%)	Δ (%)	MAC (%)
1	0.619	0.656	6.07	99.95	0.617	-0.30	99.95	5.77	0.00
2	1.212	1.313	8.27	99.27	1.264	4.29	99.45	3.98	0.18
3	1.328	1.338	0.77	82.16	1.274	-4.05	95.79	-3.28	13.6
4	1.571	1.863	18.6	61.23	1.634	4.06	79.24	14.5	18.0
5	1.727	1.790	3.67	99.28	1.747	1.18	99.63	2.49	0.34
6	2.117	2.238	5.74	63.57	2.058	-2.76	87.58	2.98	24.0
7	2.354	2.425	3.04	97.75	2.400	1.97	99.70	1.07	1.96
8	2.851	3.027	6.15	92.42	2.736	-4.06	88.96	2.10	-3.47
9	3.484	3.558	2.12	97.88	3.689	5.88	97.44	-3.76	-0.45
10	3.624	3.766	3.93	94.00	3.526	-2.69	97.90	1.24	3.90
11	3.874	4.363	12.6	64.40	3.716	-4.09	93.80	8.51	29.4
12	4.742	4.711	-0.65	79.35	4.893	3.17	99.00	-2.52	19.7
13	5.284	4.992	-5.54	82.52	5.273	-0.22	97.75	5.32	15.2
14	5.745	6.304	9.74	97.09	6.144	6.94	99.08	2.79	1.98
15	6.075	6.915	13.8	77.74	6.413	5.56	68.20	8.26	-9.54
16	7.176	8.332	16.1	49.14	8.188	14.10	61.56	2.01	12.4
17	7.281	7.542	3.58	83.54	7.389	1.48	87.03	2.10	3.49
18	8.114	8.613	6.15	83.94	8.444	4.06	94.83	2.09	10.9
19	8.440	9.417	11.6	34.69	9.231	9.37	51.08	2.20	16.4
20	9.059	10.17	12.3	65.31	9.771	7.86	80.89	4.42	15.6
Average	-	-	7.52	80.26	-	4.40	88.94	3.12	8.68

Table 10: Model correlation improvement when 3 parameters within the finite element model were calibrated and 10 modes were compared in the model updating routine

Mode	f_{exp} (Hz)	Idealized Model			Calibrated Model			Improvement	
		f_{FE} (Hz)	Δ (%)	MAC (%)	f_{FE} (Hz)	Δ (%)	MAC (%)	Δ (%)	MAC (%)
1	0.619	0.656	6.07	99.95	0.618	-0.09	99.95	5.98	0.00
2	1.212	1.313	8.27	99.27	1.269	4.67	99.45	3.60	0.18
3	1.328	1.338	0.77	82.16	1.275	-3.97	95.80	-3.20	13.6
4	1.571	1.863	18.6	61.23	1.659	5.63	77.33	13.0	16.1
5	1.727	1.790	3.67	99.28	1.757	1.75	99.64	1.92	0.35
6	2.117	2.238	5.74	63.57	2.065	-2.46	87.63	3.28	24.1
7	2.354	2.425	3.04	97.75	2.394	1.69	99.68	1.35	1.93
8	2.851	3.027	6.15	92.42	2.755	-3.36	88.72	2.79	-3.70
9	3.484	3.558	2.12	97.88	3.581	2.76	98.50	-0.64	0.62
10	3.624	3.766	3.93	94.00	3.546	-2.16	97.68	1.78	3.68
11	3.874	4.363	12.6	64.40	3.781	-2.42	95.03	10.2	30.6
12	4.742	4.711	-0.65	79.35	4.922	3.79	99.11	-3.14	19.8
13	5.284	4.992	-5.54	82.52	5.254	-0.56	97.82	4.97	15.3
14	5.745	6.304	9.74	97.09	6.221	8.28	99.27	1.45	2.17
15	6.075	6.915	13.8	77.74	6.473	6.54	68.51	7.28	-9.23
16	7.176	8.332	16.1	49.14	8.250	14.97	61.68	1.14	12.5
17	7.281	7.542	3.58	83.54	7.361	1.10	88.83	2.48	5.29
18	8.114	8.613	6.15	83.94	8.448	4.11	87.12	2.03	3.18
19	8.440	9.417	11.6	34.69	9.288	10.04	45.30	1.52	10.6
20	9.059	10.17	12.3	65.31	9.874	8.99	81.23	3.29	15.9
Average	-	-	7.52	80.26	-	4.47	88.41	3.05	8.15

Table 11: Model correlation improvement when 3 parameters within the finite element model were calibrated and 15 modes were compared in the model updating routine

Mode	f_{exp} (Hz)	Idealized Model			Calibrated Model			Improvement	
		f_{FE} (Hz)	Δ (%)	MAC (%)	f_{FE} (Hz)	Δ (%)	MAC (%)	Δ (%)	MAC (%)
1	0.619	0.656	6.07	99.95	0.619	0.09	99.95	5.98	0.00
2	1.212	1.313	8.27	99.27	1.274	5.09	99.45	3.18	0.18
3	1.328	1.338	0.77	82.16	1.285	-3.25	95.80	-2.48	13.6
4	1.571	1.863	18.6	61.23	1.680	6.98	77.58	11.6	16.3
5	1.727	1.790	3.67	99.28	1.768	2.40	99.63	1.27	0.35
6	2.117	2.238	5.74	63.57	2.073	-2.08	87.70	3.66	24.1
7	2.354	2.425	3.04	97.75	2.413	2.52	99.70	0.52	1.96
8	2.851	3.027	6.15	92.42	2.775	-2.67	88.67	3.48	-3.76
9	3.484	3.558	2.12	97.88	3.410	-2.14	96.07	-0.02	-1.82
10	3.624	3.766	3.93	94.00	3.564	-1.65	97.48	2.29	3.48
11	3.874	4.363	12.6	64.40	3.837	-0.97	94.40	11.6	30.0
12	4.742	4.711	-0.65	79.35	4.911	3.56	99.01	-2.91	19.7
13	5.284	4.992	-5.54	82.52	5.305	0.40	97.75	5.14	15.2
14	5.745	6.304	9.74	97.09	6.165	7.31	99.13	2.42	2.04
15	6.075	6.915	13.8	77.74	6.513	7.20	70.11	6.62	-7.64
16	7.176	8.332	16.1	49.14	8.215	14.48	61.78	1.63	12.6
17	7.281	7.542	3.58	83.54	7.394	1.55	88.51	2.03	4.98
18	8.114	8.613	6.15	83.94	8.435	3.95	97.47	2.19	13.5
19	8.440	9.417	11.6	34.69	9.270	9.84	47.56	1.73	12.9
20	9.059	10.17	12.3	65.31	9.849	8.72	82.02	3.56	16.7
Average	-	-	7.52	80.26	-	4.34	88.99	3.18	8.73

Table 12: Model correlation improvement when 3 parameters within the finite element model were calibrated and 20 modes were compared in the model updating routine

Mode	f_{exp} (Hz)	Idealized Model			Calibrated Model			Improvement	
		f_{FE} (Hz)	Δ (%)	MAC (%)	f_{FE} (Hz)	Δ (%)	MAC (%)	Δ (%)	MAC (%)
1	0.619	0.656	6.07	99.95	0.621	0.39	99.95	5.67	0.00
2	1.212	1.313	8.27	99.27	1.281	5.67	99.43	2.60	0.16
3	1.328	1.338	0.77	82.16	1.292	-2.66	95.80	-1.89	13.6
4	1.571	1.863	18.6	61.23	1.713	9.07	76.53	9.52	15.3
5	1.727	1.790	3.67	99.28	1.784	3.31	99.62	0.36	0.34
6	2.117	2.238	5.74	63.57	2.083	-1.58	87.78	4.16	24.2
7	2.354	2.425	3.04	97.75	2.423	2.94	99.70	0.10	1.95
8	2.851	3.027	6.15	92.42	2.805	-1.64	88.44	4.51	-3.98
9	3.484	3.558	2.12	97.88	3.442	-1.21	96.90	0.91	-0.98
10	3.624	3.766	3.93	94.00	3.585	-1.07	97.16	2.86	3.16
11	3.874	4.363	12.6	64.40	3.932	1.50	91.26	11.1	26.9
12	4.742	4.711	-0.65	79.35	4.925	3.84	99.02	-3.19	19.7
13	5.284	4.992	-5.54	82.52	5.330	0.86	97.74	4.68	15.2
14	5.745	6.304	9.74	97.09	6.180	7.57	99.17	2.17	2.07
15	6.075	6.915	13.8	77.74	6.585	8.39	71.33	5.43	-6.41
16	7.176	8.332	16.1	49.14	7.355	2.49	76.19	13.6	27.0
17	7.281	7.542	3.58	83.54	7.404	1.69	88.39	1.89	4.85
18	8.114	8.613	6.15	83.94	8.447	4.09	96.51	2.05	12.6
19	8.440	9.417	11.6	34.69	9.297	10.15	44.73	1.42	10.0
20	9.059	10.17	12.3	65.31	9.900	9.28	82.43	3.00	17.1
Average	-	-	7.52	80.26	-	3.97	89.41	3.55	9.14

Table 13: Model correlation improvement when 6 parameters within the finite element model were calibrated and 5 modes were compared in the model updating routine

Mode	f_{exp} (Hz)	Idealized Model			Calibrated Model			Improvement	
		f_{FE} (Hz)	Δ (%)	MAC (%)	f_{FE} (Hz)	Δ (%)	MAC (%)	Δ (%)	MAC (%)
1	0.619	0.656	6.07	99.95	0.620	0.22	99.95	5.85	0.00
2	1.212	1.313	8.27	99.27	1.210	-0.22	99.24	8.05	-0.03
3	1.328	1.338	0.77	82.16	1.273	-4.09	95.69	-3.32	13.5
4	1.571	1.863	18.6	61.23	1.571	-0.01	83.12	18.6	21.9
5	1.727	1.790	3.67	99.28	1.727	0.01	99.47	3.66	0.18
6	2.117	2.238	5.74	63.57	2.012	-4.93	78.98	0.80	15.4
7	2.354	2.425	3.04	97.75	2.236	-5.00	99.16	-1.96	1.41
8	2.851	3.027	6.15	92.42	2.584	-9.38	91.81	-3.22	-0.61
9	3.484	3.558	2.12	97.88	3.323	-4.64	96.61	-2.52	-1.28
10	3.624	3.766	3.93	94.00	3.401	-6.15	96.34	-2.21	2.35
11	3.874	4.363	12.6	64.40	3.559	-8.14	88.77	4.46	24.4
12	4.742	4.711	-0.65	79.35	4.874	2.77	98.38	-2.11	19.0
13	5.284	4.992	-5.54	82.52	5.093	-3.62	97.72	1.92	15.2
14	5.745	6.304	9.74	97.09	6.131	6.71	98.59	3.03	1.50
15	6.075	6.915	13.8	77.74	6.108	0.54	62.03	13.3	-15.7
16	7.176	8.332	16.1	49.14	8.079	12.59	60.04	3.53	10.9
17	7.281	7.542	3.58	83.54	7.495	2.93	88.41	0.65	4.87
18	8.114	8.613	6.15	83.94	8.591	5.88	82.27	0.27	-1.67
19	8.440	9.417	11.6	34.69	8.994	6.56	59.81	5.01	25.1
20	9.059	10.17	12.3	65.31	9.482	4.67	84.62	7.61	19.3
Average	-	-	7.52	80.26	-	4.45	88.05	3.07	7.79

Table 14: Model correlation improvement when 6 parameters within the finite element model were calibrated and 10 modes were compared in the model updating routine

Mode	f_{exp} (Hz)	Idealized Model			Calibrated Model			Improvement	
		f_{FE} (Hz)	Δ (%)	MAC (%)	f_{FE} (Hz)	Δ (%)	MAC (%)	Δ (%)	MAC (%)
1	0.619	0.656	6.07	99.95	0.619	0.02	99.95	6.05	0.00
2	1.212	1.313	8.27	99.27	1.225	1.06	99.44	7.21	0.17
3	1.328	1.338	0.77	82.16	1.257	-5.32	95.76	-4.55	13.6
4	1.571	1.863	18.6	61.23	1.598	1.74	79.22	16.8	18.0
5	1.727	1.790	3.67	99.28	1.724	-0.17	99.71	3.50	0.43
6	2.117	2.238	5.74	63.57	2.015	-4.79	85.47	0.95	21.9
7	2.354	2.425	3.04	97.75	2.357	0.12	99.27	2.92	1.52
8	2.851	3.027	6.15	92.42	2.656	-6.86	89.77	-0.71	-2.65
9	3.484	3.558	2.12	97.88	3.529	1.27	99.08	0.85	1.20
10	3.624	3.766	3.93	94.00	3.435	-5.22	97.93	-1.29	3.93
11	3.874	4.363	12.6	64.40	3.616	-6.68	93.63	5.92	29.2
12	4.742	4.711	-0.65	79.35	4.826	1.76	98.98	-1.11	19.6
13	5.284	4.992	-5.54	82.52	5.101	-3.46	97.84	2.07	15.3
14	5.745	6.304	9.74	97.09	6.129	6.69	99.21	3.05	2.12
15	6.075	6.915	13.8	77.74	6.278	3.33	65.49	10.5	-12.3
16	7.176	8.332	16.1	49.14	8.181	14.01	61.01	2.10	11.9
17	7.281	7.542	3.58	83.54	7.291	0.14	85.24	3.44	1.70
18	8.114	8.613	6.15	83.94	8.399	3.51	85.45	2.64	1.51
19	8.440	9.417	11.6	34.69	9.151	8.42	61.25	3.15	26.6
20	9.059	10.17	12.3	65.31	9.680	6.85	81.45	5.43	16.1
Average	-	-	7.52	80.26	-	4.07	88.76	3.45	8.49

Table 15: Model correlation improvement when 6 parameters within the finite element model were calibrated and 15 modes were compared in the model updating routine

Mode	f_{exp} (Hz)	Idealized Model			Calibrated Model			Improvement	
		f_{FE} (Hz)	Δ (%)	MAC (%)	f_{FE} (Hz)	Δ (%)	MAC (%)	Δ (%)	MAC (%)
1	0.619	0.656	6.07	99.95	0.608	-1.76	99.95	4.31	0.00
2	1.212	1.313	8.27	99.27	1.268	4.59	99.38	3.68	0.12
3	1.328	1.338	0.77	82.16	1.268	-4.53	95.76	-3.76	13.6
4	1.571	1.863	18.6	61.23	1.664	5.94	75.87	12.6	14.6
5	1.727	1.790	3.67	99.28	1.768	2.40	99.57	1.27	0.29
6	2.117	2.238	5.74	63.57	2.063	-2.55	87.33	3.18	23.8
7	2.354	2.425	3.04	97.75	2.368	0.62	99.68	2.42	1.93
8	2.851	3.027	6.15	92.42	2.799	-1.85	87.89	4.31	-4.54
9	3.484	3.558	2.12	97.88	3.544	1.71	98.88	0.41	0.99
10	3.624	3.766	3.93	94.00	3.530	-2.58	97.49	1.35	3.49
11	3.874	4.363	12.6	64.40	3.802	-1.86	94.12	10.7	29.7
12	4.742	4.711	-0.65	79.35	4.800	1.22	99.12	-0.57	19.8
13	5.284	4.992	-5.54	82.52	5.221	-1.20	97.83	4.34	15.3
14	5.745	6.304	9.74	97.09	6.042	5.18	99.32	4.56	2.22
15	6.075	6.915	13.8	77.74	6.480	6.66	69.05	7.16	-8.69
16	7.176	8.332	16.1	49.14	7.256	1.11	27.87	15.0	-21.3
17	7.281	7.542	3.58	83.54	7.144	-1.89	87.94	1.69	4.40
18	8.114	8.613	6.15	83.94	8.216	1.25	98.09	4.89	14.1
19	8.440	9.417	11.6	34.69	9.229	9.35	39.41	2.22	4.72
20	9.059	10.17	12.3	65.31	9.955	9.89	72.49	2.39	7.2
Average	-	-	7.52	80.26	-	3.41	86.35	4.11	6.09

Table 16: Model correlation improvement when 6 parameters within the finite element model were calibrated and 20 modes were compared in the model updating routine

Mode	f_{exp} (Hz)	Idealized Model			Calibrated Model			Improvement	
		f_{FE} (Hz)	Δ (%)	MAC (%)	f_{FE} (Hz)	Δ (%)	MAC (%)	Δ (%)	MAC (%)
1	0.619	0.656	6.07	99.95	0.614	-0.80	99.95	5.27	0.00
2	1.212	1.313	8.27	99.27	1.226	1.13	99.41	7.14	0.14
3	1.328	1.338	0.77	82.16	1.263	-4.90	95.79	-4.13	13.6
4	1.571	1.863	18.6	61.23	1.647	4.84	77.83	13.7	16.6
5	1.727	1.790	3.67	99.28	1.724	-0.17	99.61	3.50	0.33
6	2.117	2.238	5.74	63.57	2.016	-4.78	86.65	0.96	23.1
7	2.354	2.425	3.04	97.75	2.328	-1.08	99.62	1.96	1.87
8	2.851	3.027	6.15	92.42	2.688	-5.74	88.86	0.41	-3.56
9	3.484	3.558	2.12	97.88	3.357	-3.66	98.44	-1.54	0.56
10	3.624	3.766	3.93	94.00	3.446	-4.91	97.43	-0.98	3.43
11	3.874	4.363	12.6	64.40	3.743	-3.39	93.64	9.22	29.2
12	4.742	4.711	-0.65	79.35	4.776	0.70	98.90	-0.05	19.5
13	5.284	4.992	-5.54	82.52	5.114	-3.22	97.79	2.32	15.3
14	5.745	6.304	9.74	97.09	6.036	5.06	99.06	4.67	1.97
15	6.075	6.915	13.8	77.74	6.431	5.86	70.95	7.96	-6.79
16	7.176	8.332	16.1	49.14	7.064	-1.56	73.20	14.6	24.1
17	7.281	7.542	3.58	83.54	7.275	-0.09	88.22	3.49	4.68
18	8.114	8.613	6.15	83.94	8.343	2.81	97.24	3.33	13.3
19	8.440	9.417	11.6	34.69	8.837	4.70	67.35	6.87	32.7
20	9.059	10.17	12.3	65.31	9.734	7.45	86.31	4.83	21.0
Average	-	-	7.52	80.26	-	3.34	90.81	4.18	10.55

Table 17: Model correlation improvement when 9 parameters within the finite element model were calibrated and 5 modes were compared in the model updating routine

Mode	f_{exp} (Hz)	Idealized Model			Calibrated Model			Improvement	
		f_{FE} (Hz)	Δ (%)	MAC (%)	f_{FE} (Hz)	Δ (%)	MAC (%)	Δ (%)	MAC (%)
1	0.619	0.656	6.07	99.95	0.619	0.09	99.95	5.98	0.00
2	1.212	1.313	8.27	99.27	1.213	0.02	99.32	8.25	0.05
3	1.328	1.338	0.77	82.16	1.299	-2.15	95.69	-1.38	13.5
4	1.571	1.863	18.6	61.23	1.565	-0.34	86.66	18.2	25.4
5	1.727	1.790	3.67	99.28	1.729	0.15	99.56	3.52	0.27
6	2.117	2.238	5.74	63.57	2.061	-2.62	71.61	3.11	8.04
7	2.354	2.425	3.04	97.75	2.222	-5.59	99.28	-2.55	1.53
8	2.851	3.027	6.15	92.42	2.596	-8.95	90.61	-2.80	-1.81
9	3.484	3.558	2.12	97.88	3.314	-4.90	97.38	-2.78	-0.51
10	3.624	3.766	3.93	94.00	3.395	-6.31	95.72	-2.38	1.72
11	3.874	4.363	12.6	64.40	3.556	-8.21	87.90	4.39	23.5
12	4.742	4.711	-0.65	79.35	4.850	2.26	98.27	-1.61	18.9
13	5.284	4.992	-5.54	82.52	5.078	-3.91	97.84	1.63	15.3
14	5.745	6.304	9.74	97.09	6.127	6.64	98.56	3.09	1.46
15	6.075	6.915	13.8	77.74	6.190	1.89	44.19	11.9	-33.6
16	7.176	8.332	16.1	49.14	8.092	12.77	60.88	3.34	11.7
17	7.281	7.542	3.58	83.54	7.540	3.55	88.40	0.03	4.87
18	8.114	8.613	6.15	83.94	8.722	7.49	90.31	-1.34	6.37
19	8.440	9.417	11.6	34.69	8.991	6.53	55.23	5.04	20.5
20	9.059	10.17	12.3	65.31	9.690	6.96	89.35	5.32	24.0
Average	-	-	7.52	80.26	-	4.57	87.33	2.95	7.07

Table 18: Model correlation improvement when 9 parameters within the finite element model were calibrated and 10 modes were compared in the model updating routine

Mode	f_{exp} (Hz)	Idealized Model			Calibrated Model			Improvement	
		f_{FE} (Hz)	Δ (%)	MAC (%)	f_{FE} (Hz)	Δ (%)	MAC (%)	Δ (%)	MAC (%)
1	0.619	0.656	6.07	99.95	0.619	-0.01	99.95	6.06	0.00
2	1.212	1.313	8.27	99.27	1.242	2.42	99.41	5.85	0.14
3	1.328	1.338	0.77	82.16	1.286	-3.15	95.66	-2.38	13.5
4	1.571	1.863	18.6	61.23	1.596	1.60	82.11	17.0	20.9
5	1.727	1.790	3.67	99.28	1.715	-0.66	99.61	3.02	0.32
6	2.117	2.238	5.74	63.57	2.053	-3.01	85.28	2.73	21.7
7	2.354	2.425	3.04	97.75	2.354	0.00	99.68	3.04	1.93
8	2.851	3.027	6.15	92.42	2.672	-6.29	88.57	-0.13	-3.85
9	3.484	3.558	2.12	97.88	3.545	1.74	98.24	0.38	0.36
10	3.624	3.766	3.93	94.00	3.462	-4.47	96.77	-0.54	2.77
11	3.874	4.363	12.6	64.40	3.630	-6.31	89.19	6.29	24.8
12	4.742	4.711	-0.65	79.35	4.916	3.65	99.03	-3.00	19.7
13	5.284	4.992	-5.54	82.52	5.176	-2.05	97.67	3.49	15.1
14	5.745	6.304	9.74	97.09	6.274	9.21	99.15	0.52	2.05
15	6.075	6.915	13.8	77.74	5.833	-3.98	61.43	9.84	-16.3
16	7.176	8.332	16.1	49.14	7.197	0.29	27.94	15.8	-21.2
17	7.281	7.542	3.58	83.54	7.488	2.84	88.53	0.74	4.99
18	8.114	8.613	6.15	83.94	8.622	6.25	92.74	-0.10	8.80
19	8.440	9.417	11.6	34.69	9.283	9.99	76.86	1.58	42.2
20	9.059	10.17	12.3	65.31	9.678	6.84	84.04	5.45	18.7
Average	-	-	7.52	80.26	-	3.74	88.09	3.78	7.83

Table 19: Model correlation improvement when 9 parameters within the finite element model were calibrated and 15 modes were compared in the model updating routine

Mode	f_{exp} (Hz)	Idealized Model			Calibrated Model			Improvement	
		f_{FE} (Hz)	Δ (%)	MAC (%)	f_{FE} (Hz)	Δ (%)	MAC (%)	Δ (%)	MAC (%)
1	0.619	0.656	6.07	99.95	0.620	0.30	99.95	5.77	0.00
2	1.212	1.313	8.27	99.27	1.252	3.25	99.29	5.02	0.02
3	1.328	1.338	0.77	82.16	1.287	-3.06	95.44	-2.29	13.3
4	1.571	1.863	18.6	61.23	1.674	6.60	70.92	12.0	9.69
5	1.727	1.790	3.67	99.28	1.792	3.77	99.54	-0.10	0.26
6	2.117	2.238	5.74	63.57	2.061	-2.61	89.09	3.13	25.5
7	2.354	2.425	3.04	97.75	2.353	-0.05	99.67	2.99	1.92
8	2.851	3.027	6.15	92.42	2.834	-0.62	89.30	5.54	-3.12
9	3.484	3.558	2.12	97.88	3.538	1.53	99.28	0.59	1.39
10	3.624	3.766	3.93	94.00	3.543	-2.23	96.78	1.70	2.78
11	3.874	4.363	12.6	64.40	3.830	-1.14	92.31	11.5	27.9
12	4.742	4.711	-0.65	79.35	4.752	0.19	99.12	0.46	19.8
13	5.284	4.992	-5.54	82.52	5.236	-0.91	97.52	4.63	15.0
14	5.745	6.304	9.74	97.09	5.961	3.76	99.31	5.97	2.22
15	6.075	6.915	13.8	77.74	6.510	7.16	75.73	6.66	-2.01
16	7.176	8.332	16.1	49.14	7.273	1.35	27.89	14.8	-21.3
17	7.281	7.542	3.58	83.54	6.999	-3.88	87.87	-0.30	4.33
18	8.114	8.613	6.15	83.94	7.996	-1.46	97.26	4.69	13.3
19	8.440	9.417	11.6	34.69	9.332	10.57	56.44	1.00	21.8
20	9.059	10.17	12.3	65.31	9.987	10.25	70.42	2.03	5.11
Average	-	-	7.52	80.26	-	3.23	87.16	4.29	6.89

Table 20: Model correlation improvement when 9 parameters within the finite element model were calibrated and 20 modes were compared in the model updating routine

Mode	f_{exp} (Hz)	Idealized Model			Calibrated Model			Improvement	
		f_{FE} (Hz)	Δ (%)	MAC (%)	f_{FE} (Hz)	Δ (%)	MAC (%)	Δ (%)	MAC (%)
1	0.619	0.656	6.07	99.95	0.620	0.22	99.95	5.85	0.00
2	1.212	1.313	8.27	99.27	1.225	1.07	99.41	7.20	0.14
3	1.328	1.338	0.77	82.16	1.320	-0.61	95.54	0.16	13.4
4	1.571	1.863	18.6	61.23	1.661	5.75	76.79	12.8	15.6
5	1.727	1.790	3.67	99.28	1.861	7.81	99.61	-4.14	0.32
6	2.117	2.238	5.74	63.57	2.057	-2.84	80.48	2.90	16.9
7	2.354	2.425	3.04	97.75	2.286	-2.88	99.65	0.16	1.90
8	2.851	3.027	6.15	92.42	2.740	-3.91	93.89	2.25	1.47
9	3.484	3.558	2.12	97.88	3.391	-2.68	98.53	-0.56	0.64
10	3.624	3.766	3.93	94.00	3.517	-2.94	97.20	0.99	3.20
11	3.874	4.363	12.6	64.40	3.783	-2.37	92.96	10.2	28.6
12	4.742	4.711	-0.65	79.35	4.918	3.70	97.60	-3.05	18.2
13	5.284	4.992	-5.54	82.52	5.219	-1.24	97.78	4.30	15.3
14	5.745	6.304	9.74	97.09	6.086	5.94	99.01	3.80	1.91
15	6.075	6.915	13.8	77.74	6.324	4.10	78.77	9.72	1.03
16	7.176	8.332	16.1	49.14	7.165	-0.16	28.52	16.0	-20.6
17	7.281	7.542	3.58	83.54	7.303	0.30	88.17	3.28	4.63
18	8.114	8.613	6.15	83.94	8.272	1.94	94.01	4.20	10.1
19	8.440	9.417	11.6	34.69	9.300	10.2	76.54	1.38	41.9
20	9.059	10.17	12.3	65.31	9.713	7.22	88.55	5.07	23.2
Average	-	-	7.52	80.26	-	3.39	89.15	4.13	8.89

Table 21: Model correlation improvement when 12 parameters within the finite element model were calibrated and 5 modes were compared in the model updating routine

Mode	f_{exp} (Hz)	Idealized Model			Calibrated Model			Improvement	
		f_{FE} (Hz)	Δ (%)	MAC (%)	f_{FE} (Hz)	Δ (%)	MAC (%)	Δ (%)	MAC (%)
1	0.619	0.656	6.07	99.95	0.623	0.72	99.95	5.35	0.00
2	1.212	1.313	8.27	99.27	1.213	0.06	98.88	8.21	-0.39
3	1.328	1.338	0.77	82.16	1.300	-2.11	95.80	-1.35	13.6
4	1.571	1.863	18.6	61.23	1.574	0.19	86.98	18.4	25.8
5	1.727	1.790	3.67	99.28	1.725	-0.12	99.37	3.55	0.08
6	2.117	2.238	5.74	63.57	2.072	-2.13	68.91	3.60	5.35
7	2.354	2.425	3.04	97.75	2.255	-4.21	99.43	-1.17	1.68
8	2.851	3.027	6.15	92.42	2.593	-9.06	92.05	-2.91	-0.37
9	3.484	3.558	2.12	97.88	3.337	-4.23	97.41	-2.11	-0.47
10	3.624	3.766	3.93	94.00	3.465	-4.39	98.08	-0.45	4.08
11	3.874	4.363	12.6	64.40	3.695	-4.63	94.91	7.97	30.5
12	4.742	4.711	-0.65	79.35	4.851	2.29	97.44	-1.64	18.1
13	5.284	4.992	-5.54	82.52	5.119	-3.12	98.03	2.41	15.5
14	5.745	6.304	9.74	97.09	6.091	6.02	97.64	3.71	0.55
15	6.075	6.915	13.8	77.74	6.606	8.74	66.16	5.08	-11.6
16	7.176	8.332	16.1	49.14	6.459	-9.99	66.10	6.12	17.0
17	7.281	7.542	3.58	83.54	7.498	2.98	83.71	0.60	0.17
18	8.114	8.613	6.15	83.94	8.784	8.25	89.33	-2.10	5.39
19	8.440	9.417	11.6	34.69	7.662	-9.22	72.02	2.34	37.3
20	9.059	10.17	12.3	65.31	8.485	-6.33	92.73	5.95	27.4
Average	-	-	7.52	80.26	-	4.44	89.75	3.08	9.49

Table 22: Model correlation improvement when 12 parameters within the finite element model were calibrated and 10 modes were compared in the model updating routine

Mode	f_{exp} (Hz)	Idealized Model			Calibrated Model			Improvement	
		f_{FE} (Hz)	Δ (%)	MAC (%)	f_{FE} (Hz)	Δ (%)	MAC (%)	Δ (%)	MAC (%)
1	0.619	0.656	6.07	99.95	0.620	0.28	99.95	5.79	0.00
2	1.212	1.313	8.27	99.27	1.249	2.98	99.39	5.29	0.12
3	1.328	1.338	0.77	82.16	1.253	-5.59	95.57	-4.82	13.4
4	1.571	1.863	18.6	61.23	1.579	0.56	86.11	18.0	24.9
5	1.727	1.790	3.67	99.28	1.735	0.51	99.65	3.16	0.36
6	2.117	2.238	5.74	63.57	2.060	-2.70	88.87	3.04	25.3
7	2.354	2.425	3.04	97.75	2.379	1.07	99.71	1.98	1.96
8	2.851	3.027	6.15	92.42	2.750	-3.56	90.10	2.59	-2.32
9	3.484	3.558	2.12	97.88	3.469	-0.45	99.38	1.67	1.50
10	3.624	3.766	3.93	94.00	3.575	-1.35	96.57	2.58	2.57
11	3.874	4.363	12.6	64.40	3.588	-7.40	79.08	5.20	14.7
12	4.742	4.711	-0.65	79.35	4.747	0.11	99.17	0.55	19.8
13	5.284	4.992	-5.54	82.52	5.335	0.96	97.11	4.57	14.6
14	5.745	6.304	9.74	97.09	5.911	2.90	96.32	6.84	-0.77
15	6.075	6.915	13.8	77.74	5.990	-1.41	80.72	12.4	2.97
16	7.176	8.332	16.1	49.14	6.681	-6.90	57.41	9.21	8.27
17	7.281	7.542	3.58	83.54	7.082	-2.74	86.83	0.84	3.29
18	8.114	8.613	6.15	83.94	8.050	-0.79	97.25	5.36	13.3
19	8.440	9.417	11.6	34.69	8.015	-5.04	32.42	6.53	-2.27
20	9.059	10.17	12.3	65.31	8.800	-2.86	65.52	9.42	0.20
Average	-	-	7.52	80.26	-	2.51	87.36	5.01	7.09

Table 23: Model correlation improvement when 12 parameters within the finite element model were calibrated and 15 modes were compared in the model updating routine

Mode	f_{exp} (Hz)	Idealized Model			Calibrated Model			Improvement	
		f_{FE} (Hz)	Δ (%)	MAC (%)	f_{FE} (Hz)	Δ (%)	MAC (%)	Δ (%)	MAC (%)
1	0.619	0.656	6.07	99.95	0.622	0.60	99.95	5.46	0.00
2	1.212	1.313	8.27	99.27	1.248	2.93	99.41	5.34	0.14
3	1.328	1.338	0.77	82.16	1.273	-4.10	95.53	-3.33	13.4
4	1.571	1.863	18.6	61.23	1.573	0.13	81.28	18.5	20.0
5	1.727	1.790	3.67	99.28	1.740	0.79	99.64	2.88	0.36
6	2.117	2.238	5.74	63.57	2.050	-3.14	89.71	2.59	26.1
7	2.354	2.425	3.04	97.75	2.370	0.67	99.69	2.37	1.94
8	2.851	3.027	6.15	92.42	2.752	-3.48	90.44	2.67	-1.98
9	3.484	3.558	2.12	97.88	3.361	-3.53	97.83	-1.41	-0.06
10	3.624	3.766	3.93	94.00	3.564	-1.66	96.73	2.27	2.73
11	3.874	4.363	12.6	64.40	3.858	-0.42	89.97	12.2	25.6
12	4.742	4.711	-0.65	79.35	4.687	-1.17	99.15	-0.52	19.8
13	5.284	4.992	-5.54	82.52	5.282	-0.04	97.46	5.50	14.9
14	5.745	6.304	9.74	97.09	5.853	1.88	99.02	7.86	1.93
15	6.075	6.915	13.8	77.74	6.080	0.08	79.42	13.7	1.68
16	7.176	8.332	16.1	49.14	7.223	0.66	72.84	15.5	23.7
17	7.281	7.542	3.58	83.54	6.974	-4.22	87.43	-0.64	3.89
18	8.114	8.613	6.15	83.94	7.922	-2.37	97.72	3.77	13.8
19	8.440	9.417	11.6	34.69	8.528	1.04	74.01	10.5	39.3
20	9.059	10.17	12.3	65.31	9.207	1.64	81.03	10.6	15.7
Average	-	-	7.52	80.26	-	1.73	91.41	5.79	11.15

Table 24: Model correlation improvement when 12 parameters within the finite element model were calibrated and 20 modes were compared in the model updating routine

Mode	f_{exp} (Hz)	Idealized Model			Calibrated Model			Improvement	
		f_{FE} (Hz)	Δ (%)	MAC (%)	f_{FE} (Hz)	Δ (%)	MAC (%)	Δ (%)	MAC (%)
1	0.619	0.656	6.07	99.95	0.633	2.29	99.95	3.78	0.00
2	1.212	1.313	8.27	99.27	1.239	2.16	99.33	6.11	0.06
3	1.328	1.338	0.77	82.16	1.292	-2.69	95.76	-1.92	13.6
4	1.571	1.863	18.6	61.23	1.556	-0.93	85.25	17.7	24.0
5	1.727	1.790	3.67	99.28	1.820	5.43	99.62	-1.76	0.34
6	2.117	2.238	5.74	63.57	2.053	-3.00	82.33	2.74	18.8
7	2.354	2.425	3.04	97.75	2.332	-0.93	99.56	2.11	1.82
8	2.851	3.027	6.15	92.42	2.711	-4.92	93.77	1.24	1.35
9	3.484	3.558	2.12	97.88	3.408	-2.20	96.85	-0.08	-1.03
10	3.624	3.766	3.93	94.00	3.570	-1.49	97.44	2.44	3.44
11	3.874	4.363	12.6	64.40	3.831	-1.12	92.99	11.5	28.6
12	4.742	4.711	-0.65	79.35	4.938	4.13	98.26	-3.48	18.9
13	5.284	4.992	-5.54	82.52	5.316	0.60	97.74	4.94	15.2
14	5.745	6.304	9.74	97.09	6.105	6.27	98.69	3.46	1.59
15	6.075	6.915	13.8	77.74	6.048	-0.45	81.51	13.4	3.77
16	7.176	8.332	16.1	49.14	7.287	1.54	84.78	14.6	35.6
17	7.281	7.542	3.58	83.54	7.296	0.21	89.36	3.37	5.82
18	8.114	8.613	6.15	83.94	8.258	1.78	95.79	4.37	11.8
19	8.440	9.417	11.6	34.69	8.472	0.38	70.52	11.2	35.8
20	9.059	10.17	12.3	65.31	9.064	0.06	94.55	12.2	29.2
Average	-	-	7.52	80.26	-	2.13	92.70	5.39	12.44